
PHOTOINDUCED ELECTRON TRANSFER
ACROSS *ortho*-OLIGO-PHENYLENES AND
NOVEL LUMINOPHORES BASED ON
EARTH-ABUNDANT METALS

Inauguraldissertation

zur Erlangung der Würde eines Doktors der Philosophie
vorgelegt der
Philosophisch-Naturwissenschaftlichen Fakultät
der Universität Basel

von

Sabine Marie Malzkuhn

aus Hamburg

Basel 2018

Originaldokument gespeichert auf dem Dokumentenserver der Universität Basel
edoc.unibas.ch

Genehmigt von der Philosophisch-Naturwissenschaftlichen Fakultät auf Antrag von

Fakultätsverantwortlicher: Prof. Oliver S. Wenger

Korreferent: Prof. Silvio Decurtins

Basel, 18.09.2018

Prof. Dr. Martin Spiess, Dekan

Wissen ist Nacht!

Prof. Dr. Abdul Nachtigaller

The electron you want to go
a photon you need, that you know
the ruthenium waits for it to hit
and the electron can go, that's how it is

Chemist made in the past
molecular dyads, slow and fast
where electron transfer can take place
depending on the environment, the electron has to face

The flatter the better, that's what they say
para-phenylenes maybe nearly flat as a tray
measured charge transfer rates for this system
revealed low β -values, that's now wisdom

Xylenes however, with methyl groups on the side
force the rings out of plane, that's not to fight
a less conjugated π -system, that's the result
so the slope is steeper, as you can see on the slide

I told you some old stuff, now comes the new
I gave the electron a new bridge to go through
the connection is different, so are the results
If you want to know more, you need to read the following slides

Abstract

LONG-range electron-transfer is of high interest for many fields, such as artificial photosynthesis and molecular electronics. Donor – bridge – Acceptor compounds, wherein photoinduced electron transfer takes place were thoroughly investigated in this regard. Especially *para*-phenylene systems were chosen due to their rigid, rod-like wire behaviour. Depending on the electronic coupling of the bridge, *para*-phenylenes reveal β -values ranging from 0.2 to 0.8 \AA^{-1} . Their *ortho*-connected relatives are completely unexplored until now. In **chapter I** of this thesis the motivation for this work and the theoretical background for electron transfer will be given. This will be followed by a few examples of electron transfers across *para*-phenylenes, to put the herein presented work into perspective. In **chapter II** photoinduced electron-transfer across an *ortho*-phenylene wire consisting of 2 to 6 phenyl units will be presented. A Ru(II)-photosensitiser and a triarylamine electron donor were chosen to investigate the kinetics of the charge-shift reaction. The photoinduced forward, as well as the thermal back-reaction, were explored with time resolved measurements. Due to the flexibility of the bridge and slowly interconverting conformers in solution, analysis of charge-separation remains turbid, but a coherent analysis can be made for charge-recombination. The main discovery is that *ortho*-phenylenes possess very low β -values for charge-transfer, with a β -value in acetonitrile of 0.04 \AA^{-1} . The mechanism for the hole transfer is coherent tunnelling and a relevant aspect seems to be the σ -pathway, which is shorter for *ortho*-phenylenes than for *para*-phenylenes. *Ortho*-phenylenes can therefore be considered as a new class of molecular wires.

Chapter III will then present the results of photoinduced long-range electron transfer through *ortho*-naphthalenes, which can form different atropisomers and electron transfer is studied in these systems for the first time.

Photoinduced electron transfer would not be possible without photosensitisers, which allow for an enough long living excited state with enough reducing or oxidising power, that electron transfer reactions can take place. Most photosensitisers today which reach the photophysical goals for being applied, for example in photoredox catalysis or in long-range electron transfer, rely on noble metals, such as Ru(II) or Ir(III). Therefore it would be desirable, to shift from noble metals as centres to more earth abundant metals. Nickel(0) allows for an MLCT transition when the ligand orbitals are of the right energy. In **chapter IV** first preliminary results of a nickel(0)-bis(diphenylphosphino)naphthalene complex will be presented, which were accompanied by DFT calculations.

Following this approach of using more earth-abundant metals, in **chapter V** the possibility of titanium(IV) complexes is considered, which could possibly undergo LMCT emission transitions. Different possible approaches towards a titanium-based luminophore will be given.

Contents

1	Introduction	1
1.1	Motivation - Here comes the sun	1
1.2	Natural photosynthesis	2
1.3	Artificial photosynthesis and theoretical background	5
1.4	Distance dependence of electron transfer	6
1.5	Electron transfer across <i>para</i> -connected phenylene bridges	8
1.6	<i>Ortho</i> -oligo-phenylenes	10
1.7	Luminophores based on <i>3d</i> -transition metals	11
2	Electron transfer across <i>ortho</i>-oligo-phenylenes	12
2.1	Synthesis	12
2.2	Electrochemistry and reaction free energies	13
2.3	Optical spectroscopy	16
2.4	Steady state luminescence	16
2.5	Transient absorption spectroscopy	18
2.5.1	Photoinduced forward charge shift reaction	18
2.5.2	Distance dependence of the forward charge shift reaction	19
2.5.3	Thermal reverse electron transfer	21
2.6	Flash-quench experiments with the dyads	23
2.7	Distance dependence for thermal back electron transfer and activation energies	24
2.8	Conformational analysis of the molecular dyads	31
2.9	Summary and Outlook	35
3	Electron transfer through oligo-<i>ortho</i>-naphthalenes	36
3.1	Optical spectroscopy	37
3.2	Steady state luminescence	37
3.3	Transient absorption spectroscopy	37
3.3.1	Photoinduced forward charge shift reaction	38
3.3.2	Thermal back electron transfer	39
3.4	Summary and outlook	40
4	Luminescent Ni(0) complexes	41
4.1	Ligand design	47
4.1.1	Density Functional Theory (DFT) calculations	47
4.2	Synthesis	49
4.3	UV-Vis and steady-state luminescence spectroscopy	51
4.4	Transient emission spectroscopy	53

CONTENTS

4.5	Summary and Outlook	54
4.5.1	Phosphite ligand	55
5	New luminescent Titanium-complexes	56
5.1	Pyrrol-based ligands	57
5.1.1	Ligand design	57
5.1.2	Synthesis	57
5.2	Scorpionate ligands	58
5.2.1	Ligand design	58
5.2.2	Synthesis	59
5.2.3	Spectroscopy	60
5.2.4	Summary and Outlook	61
6	Experimental	62
6.1	General	62
6.2	Reagents	62
6.3	Chromatography	62
6.4	Nuclear Magnetic Resonance Spectroscopy	62
6.5	Mass Spectrometry	63
6.6	Elemental Analysis	63
6.7	UVvis spectroscopy	63
6.8	Cyclic Voltammetry	63
6.9	Transient UVvis absorption measurements	63
6.10	Luminescence Spectroscopy	64
7	Syntheses	65
7.1	Synthesis of the oligo- <i>ortho</i> -phenylene dyads	65
7.2	Synthesis of the Nickel-(2,3-bis-diphenylphosphino naphthalene) complex	98
7.3	Synthesis of the [Ti(MeIm ₃) ₂](OTf) ₂ -complex	101
8	References	103
A	Appendix	113
B	Acknowledgement	124
C	Curriculum Vitae	125

1 Introduction

1.1 Motivation - Here comes the sun

”THERE’S one issue that will define the contours of this century more dramatically than any other, and that is the urgent threat of a changing climate.”^[1]

This statement was made by Barack Obama, the former president of the United States concerning climate change. A major challenge for mankind nowadays is to balance the demand for energy against the ejection of green house gases as well as using up resources like fossil fuels too fast.^[2] The generation of energy is still closely related to the combustion of fossil fuels.^[3] The search for alternatives is not only a political, but also a scientific endeavour. In 2014 it was estimated that alternative energy sources like solar, wind, biomass etc. have the potential to provide more than 3000 times the energy that is actually demanded by the world (Figure 1.1).^[4] Shifting from the combustion of fossil fuels to the usage of renewable sources might help to achieve the dual goal of reducing green house gas emissions, hindering the consequent arising climatic problems and ensuring the cost-efficient delivery of clean energy. As to be seen in Figure 1.1 the highest contribution of harvestable energy is made by the sun. Making this energy usable would secure the worlds energy demand by far.

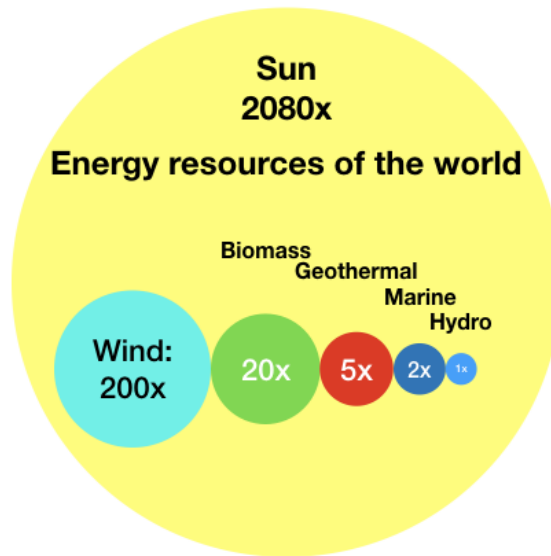
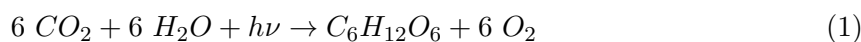


Figure 1.1: Energy provided by renewable resources have the potential of reaching the world energy’s demand by 3078 times. Figure after reference.^[4]

1.2 Natural photosynthesis

THE conversion of solar energy into chemical energy has its role model in nature. The process of photosynthesis takes place in the thylakoid membrane of chloroplasts, which can be found in plant and algae cells. Four major protein complexes in the membrane are involved: photosystem (PS) II, cytochrome b_6f complex, PS I and the ATP synthase. These four protein complexes are involved to ultimately produce ATP, the 'energy currency' of cells and the reduced form of nicotinamide adenine dinucleotide phosphate (NADP^+), NADPH, the hydrogen equivalent in cells.

As a side product, atmospheric oxygen is liberated, as well as carbon dioxide fixated according to equation 1.



On the right side of equation 1 carbohydrates (in this case glucose) as high energy molecules are synthesised and these high energy molecules are therefore again available for combustion of any kind. This biological cycle is depicted in Figure 1.2, where in the light reactions of photosynthesis oxygen is liberated and in the dark reactions carbon dioxide fixated. The light reaction has further two reaction centres, namely PS I and II. For the oxidation of H_2O a strong oxidant is needed (PS II) and for the reduction of NADP^+ to NADPH a strong reductant is needed (PS I) (see Figure 1.3). With the help of light harvesting complexes (LHCs) as antenna molecules it is possible to harvest a lot of photons of the required energy. This energy is transferred efficiently to the reaction centre of photosynthesis through energy transfer. In LHC II, which absorbs at 680 nm, the antenna molecules transfer the absorbed energy within <1 ps to the PSII. This generates a strong reducing singlet excited state PS680^* ($E^0(\text{P660}^+ / ^1\text{P680}^*) = -750$ mV vs NHE). PS680^* then reduces a pheophytin (Pheo)

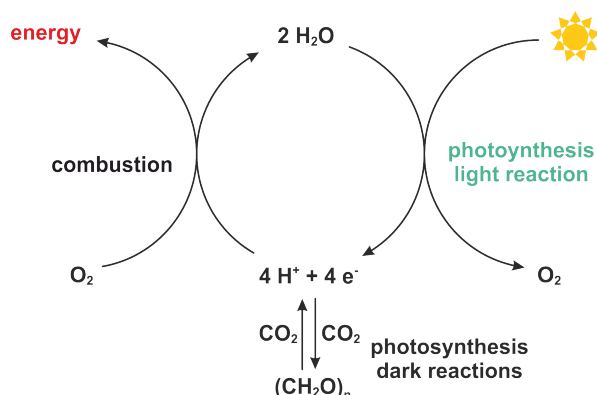


Figure 1.2: Depiction of the energy cycle in nature. In the light reactions atmospheric oxygen is produced and protons and electrons are provided for the reduction of carbon dioxide to higher energy molecules e.g. biomass, fossil fuels. Through combustion of these, oxygen is used and water and carbon dioxide are evolving.

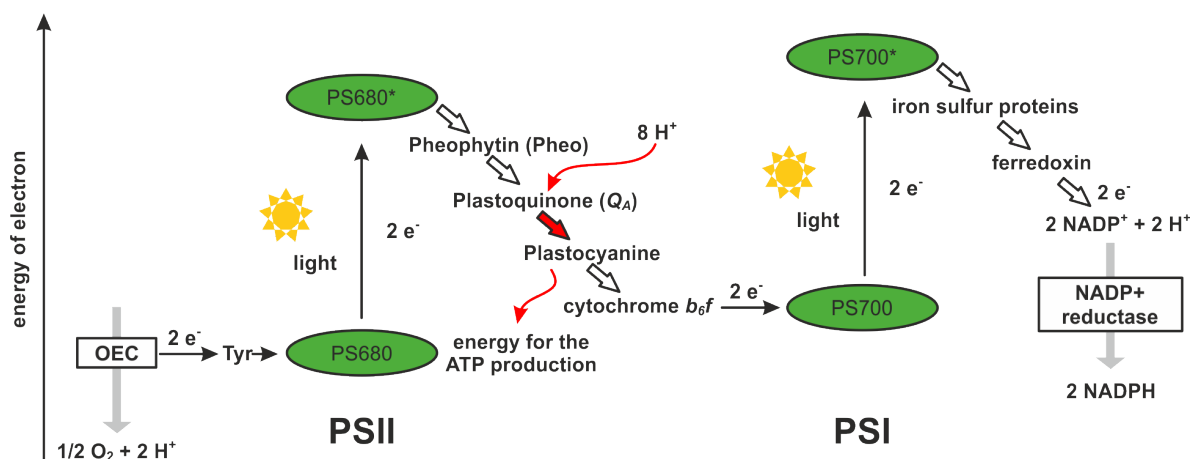


Figure 1.3: Z-Scheme for the light reactions occurring in algae, plants and cyanobacteria.^[5] To extract one electron, the energy of two photons is required. The first one is absorbed by PSII that requires a wavelength of 680 nm. Upon excitation the PS680* is generated which is a strong oxidising species that can drive the water splitting reaction. The other photon is absorbed by PSI that requires a wavelength of 700 nm and upon excitation form the very strong reducing species PS700*. This is able to generate NADPH, which in turn can deliver reducing equivalents to CO₂ to produce sugars and other organic molecules.^[5]

molecule ($E^0(\text{Pheo}/\text{Pheo}^-) = -600 \text{ mV vs NHE}$) whereupon a charge separated state is formed ($\text{PS680}^{+\cdot} - \text{Pheo}^-$, $\tau_{1/2} = 5 \text{ ps}$).^[5,6] The charge separation takes its course through electron transfer on a first plastoquinone within 250 ps, which is bound to the D2 protein (Q_A), that leads to the formation of $\text{PS680}^{+\cdot} - \text{Phe} - \text{Q}_A^-$ ($E^0(\text{Q}_A/\text{Q}_A^-) = -200 \text{ mV vs NHE}$).^[5,6] This formed charge separated state is stable for about 200 μs .^[7] Within this time frame, $\text{PS680}^{+\cdot}$ as very strong oxidising agent ($E^0(\text{P680}^+/\text{P680}) = +1200 \text{ mV vs NHE}$) is reduced by a tyrosine (Tyr) residue ($E^0(\text{Tyr}^+/\text{Tyr}) = +1100 \text{ mV vs NHE}$). This Tyr of the D1 polypeptide (Tyr_{YZ}) is in close proximity and re-reduces the P680⁺ back within 50 ns.^[6] The Tyr_{YZ}-radical is an oxidant strong enough to promote the abstraction of an electron from the oxygen evolving complex (OEC).



In the process of water splitting, which takes place in the OEC, 4 protons as well as 4 electrons are liberated and atmospheric oxygen is produced as a byproduct (see equation 2). The OEC has a unique structure which was investigated early with electron microscopy,^[8] where soon crystal structures with improving resolutions followed.^[9,10] In 2011 a crystal structure with a resolution of 1.9 Å was reported.^[10] In Figure 1.4 the unique structure of the oxygen evolving complex is shown. A cubane structure is formed with four manganese atoms with an additional calcium atom. Many attempts for mechanistic studies were made to understand the process, which is depicted in equation 2. The first proposal for a mechanism was made by

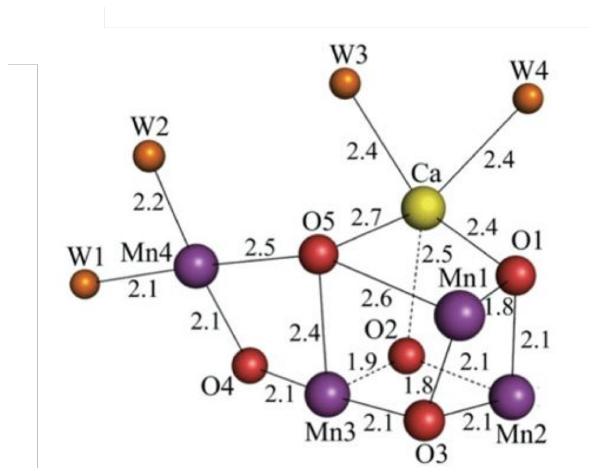


Figure 1.4: Structure of the Mn_4CaO_5 -cluster. The distances between the atoms are given in Å. Reprinted with permission from Nature Springer.^[10]

KOK.^[11] Though many further studies were performed to understand the mechanism of the OEC, the complete cycle remains somewhat turbid until today.^[12]

The initially reduced Q_A^- transfers its charge further to another plastoquinone (Q_B) with a time constant of approximately $\tau_{1/2} \sim 150 \mu\text{s}$ ($E^0(\text{Q}_B/\text{Q}_B^-) = -100 \text{ mV vs NHE}$).^[6] Q_B^- can be further reduced to Q_B^{2-} , that can undergo protonation to Q_BH_2 . These hydroquinones work as proton-shuttles to the cytochrome b_6f complex over the plastocyanines, where in the end the reducing equivalents are released at PSI. In Figure 1.5 the crystal structure of the co-factors involved in the electron transfer chain is shown. It is likely that PD1 in Figure 1.5 is PS680.^[13] This proton-shuttle leads to an electrochemical potential between the stroma and the lumen that can drive the ATP synthesis (Figure 1.3).

In PS I (PS700) a second cascade follows with the provided electrons from PSII and after

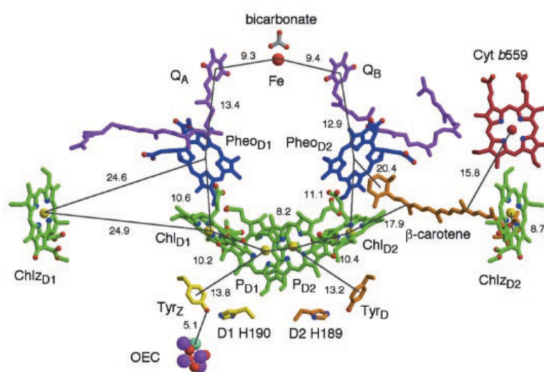


Figure 1.5: Crystal structure of the co-factors involved in the photosynthetic process. Reprinted with permission from AAAS.^[13]

absorption of another photon electrons are transferred via iron-sulfur clusters to ferredoxin, where under the aid of the enzyme ferredoxin NADP⁺ reductase NADPH is synthesised. The distance from the OEC to the plastoquinone moiety is about 50 Å. The interplay of photosensitisers, electron donors and acceptors with long range electron transfer with the creation of long living charge separated states is therefore of fundamental interest.

Due to that fact, researches strove to develop artificial systems to investigate long range electron transfer. Multiple systems were therein developed, with the goal to obtain long-living charge separated states. The basic principles of photosynthesis, which are desirable to be obtained in artificial systems are:

- Absorption of photons in the visible range of the spectrum
- Long range electron transfer
- Charge separated states with long living states
- Accumulation of charges

1.3 Artificial photosynthesis and theoretical background

DU^E to the importance of long-range electron transfer in photosynthesis, described in chapter 1.2, a lot of model systems, where photoinduced electron transfer takes place came under particular intense scrutiny. Due to the manifold of steps in natural photosynthesis, model systems are designed to explore an individual aspect. Studies were performed with systems that were designed to obtain long-lived charge separated states.^[14–16] A possible sys-

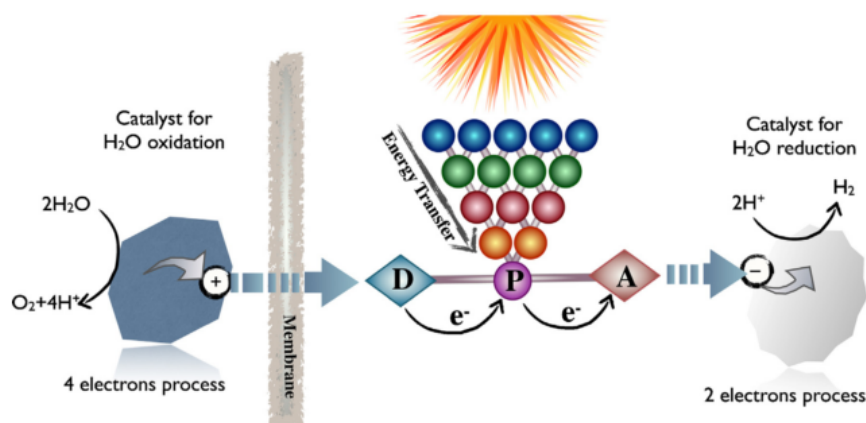


Figure 1.6: Possible systems for artificial photosynthesis. Long-range electron transfer is a key-mechanism in these systems and therefore of particular interest. Reprinted with permission from Elsevier.^[14]

tem for artificial photosynthesis as depicted in Figure 1.6 is comprised of a photosensitiser or antenna system (P) to harvest photons in the visible region of the electromagnetic spectrum and an electron donor (D) and acceptor (A). The electrons for re-reducing the oxidised donor come desirably from the water splitting reaction as in equation 2. Therefore a water oxidising catalyst is needed. The liberated electrons however could be used for the reduction of water, for hydrogen generation. The spatial separation of the two catalysts to inhibit charge recombination and to generate enough driving force is crucial, therefore a membrane may be applied.

1.4 Distance dependence of electron transfer

A key mechanism in this hypothetical system is long-range electron transfer. It is therefore desirable to gather a thorough understanding of this process. Model systems are usually comprised of an electron donor and an electron acceptor which are connected through a bridging unit. Several systems of Donor - bridge - Acceptor (D - b - A) compounds were reported.^[17]

Long-range electron transfer occurs primarily via two different mechanisms: either coherent superexchange (tunnelling) or incoherent hopping.^[18,19] An early finding was that concerning the dominant mechanism the bridging unit has a major influence on the electron transfer properties.^[20]

A prerequisite for hopping being the prevalent mechanism, is the matching of the redox-potential of the D - b - A assembly. This means, the energy levels of the bridge should be close enough to the levels of the electron donor. The bridge can thereby be intermediately reduced leading to nearly distance independent electron transfer. In the case of hole transfer, the oxidation potentials of the bridge need to be considered and intermediate oxidation takes place.^[21] Electron tunnelling however occurs, when the energy levels of the bridge are too high, but donor and acceptor are weakly electronically coupled via the bridging unit (Figure 1.7).^[22] MARCUS provided a theoretical background for the latter case, where donor and acceptor

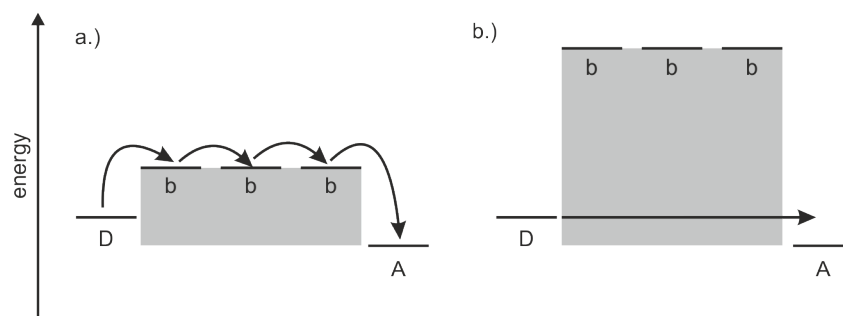


Figure 1.7: Phenomenological depiction of a.) hopping mechanism vs b.) tunneling mechanism.

are weakly coupled and a one-electron transfer reaction takes place.^[23] The semi-classical treatment of inner-sphere electron transfer leads to equation 3. The so called MARCUS-theory describes electron transfer between two weakly interacting redox centres being hold at fixed distances.

$$k_{ET} = \sqrt{\frac{4 \cdot \pi^3}{h^2 \cdot \lambda \cdot k_B \cdot T}} \cdot H_{DA}^2 \cdot \exp\left(-\frac{(\Delta G^0 + \lambda)^2}{4 \cdot k_B \cdot T}\right) \quad (3)$$

Here the electron transfer rate k_{ET} is dependent on the standard free energy (ΔG^0), the reorganisation energy (λ) and the electronic coupling between the redox centres (H_{DA}). In equation 3 h is further the Planck-constant and k_B the Boltzmann-constant.

λ can be described as the expenditure which has to be paid for the reorganisation of the reactant and the solvent molecules. Therefore λ can be further divided into:

$$\lambda = \lambda_{in} + \lambda_{out} \quad (4)$$

Here λ_{in} originates from the contribution from intramolecular modes in the course of an electron transfer event.^[24] The main contribution however is often accounted to the 'outer' reorganisation (λ_{out}), which is attributed to the reorganisation of the solvent shell. The electronic coupling H_{DA} can be described as the coupling between donor and acceptor, but this coupling is further dependent on the coupling strength between the redox sites and the bridge.^[25]

$$H_{DA} = \frac{h_{Db}}{\Delta\epsilon} \left(\frac{h_{bb}}{\Delta\epsilon}\right)^{n-1} \cdot h_{bA} \quad (5)$$

Equation 5, developed by MCCONNELL describes the electronic coupling between the two redox sites D and A as a function of the coupling from D with the bridge (h_{Db}), the individual bridging units b (h_{bb}) (when considering a bridge with n identical repeat units) and between b and redox partner A (h_{bA}).^[26] $\Delta\epsilon$ describes the so called tunnelling energy gap, which is related to the redox potentials of donor, bridge and acceptor in the transition state configuration. That makes this parameter somewhat difficult to be determined experimentally.^[19]

$$H_{DA}^2 = H_{DA}^0 \exp(-\beta_{el} \cdot r_{DA}) \quad (6)$$

The distance dependence of electron transfer rates is strongly dependent on the electronic coupling H_{DA} . H_{DA} however can be described as in equation 6. The electronic coupling is expected to decrease exponentially and the steepness of the decrease is described by the distance decay parameter β . Equation 6 can be rearranged in terms of electron transfer rates, leading to:

$$k_{ET} = k_{ET}^0 \cdot \exp(-\beta \cdot r_{DA}) \quad (7)$$

In equation 7 k_{ET} is the electron transfer rate at a certain donor - acceptor distance (r_{DA}). k_{ET}^0 is the transfer rate when donor and acceptor are in direct contact and β describes the steepness of the distance dependence.^[20] This leads to the conclusion that for a superexchange mechanism, the electron transfer rates are decreasing exponentially with the donor - acceptor distance r_{DA} , because $k_{ET} \propto H_{DA}$.

1.5 Electron transfer across *para*-connected phenylene bridges

WITH the theory developed by MARCUS at hand many studies with *para*-connected phenylene systems involving photoinduced long-range electron transfer were conducted. In the following section a few of these will come under particular intense scrutiny.

To obtain a bridge which could be understood as a molecular wire, it would be desirable to get to a regime, where the bridge is acting as an incoherent electron mediator.^[20] WASIELEWSKI *et al.* discovered that this regime is accessible with *para*-phenylene vinylenes as bridging units.^[20] With increasing length of the bridging unit, the charge separation (CS) rate constants are expected to decrease exponentially. However it was observed that the charge separation in these systems (Figure 1.8) occurs in two different regimes. The bridges (1 and 2) show a significant decrease in electron-transfer rate constants, which is expected. For the D - b - A assemblies incorporating bridges 3 to 5 (Figure 1.8), an increase in the rate constant is observable (see Table 1), and a shallower decrease when further lengthening the bridge. This can be explained with the energy gap ($\Delta\epsilon$), which was described in chapter 1.4. With the energy gap between donor and the bridging levels becoming smaller, due to the increase of

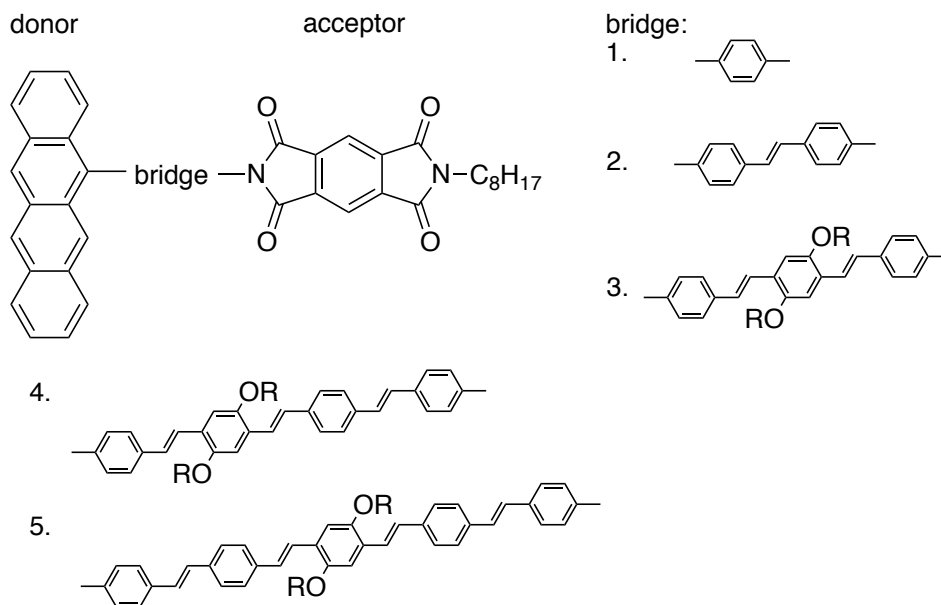


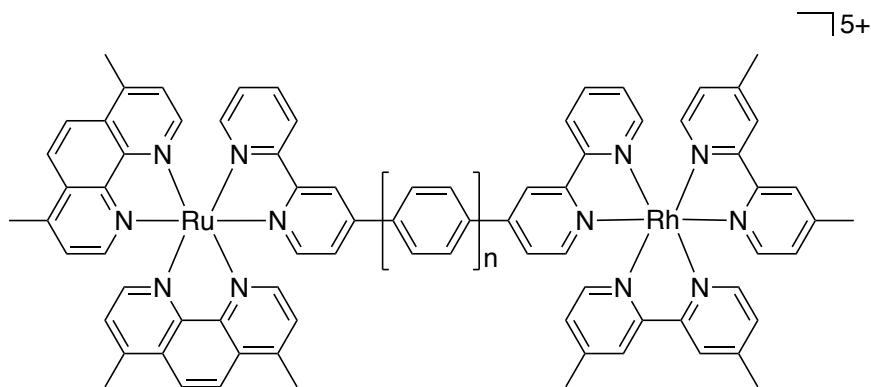
Figure 1.8: Structures of the D - b - A compounds investigated by WASIELEWSKI.^[20]

Table 1: Donor - acceptor distances of the 5 different dyads in Figure 1.8 and their corresponding time constants for the charge separation.^[20]

bridge	r_{DA} [Å]	k_{CS} [s ⁻¹]
1	11.1	$1.31 \cdot 10^{11}$
2	17.7	$2.27 \cdot 10^{10}$
3	24.3	$3.88 \cdot 10^{11}$
4	30.9	$2.63 \cdot 10^{11}$
5	38.0	$2.18 \cdot 10^{11}$

conjugation when incorporating more bridging units, the electron from the donor can reduce the bridge as an intermediate leading to $D^+ - b^- - A$. This leads to a minor dependence on length and leads to a β -value for bridges 3 - 5 of 0.04 \AA^{-1} . The same study illustrated the importance of the energy gap between donor and bridging units and showed that it is possible to lower the electron injection costs into the bridge so that the mechanism changes from purely superexchange to an accessible hopping mechanism.

In comparison to the *para*-phenylene vinylenes, *para*-phenylenes have the advantage of being rigid and exhibiting a good π -conjugation, without lowering the energy levels of the bridge too far. The superexchange mechanism is thereby usually still the dominant mechanism. This is attributed to the equilibrium angle between each phenylene unit, which is around 40° in the gas phase.^[27] With these features, *para*-phenylenes become attractive as molecular wires. INDELLI *et al.* investigated long range electron transfer in oligo-*para*-phenylene bridges in Ru(II) - Rh(III) dyads (Figure 1.9).^[28] The distances between donor and acceptor varied between 16 to 24 Å when lengthening the bridge. Measuring the electron transfer rate constants lead to a β value of 0.65 \AA^{-1} .^[28] Other *para*-phenylene bridges, however, usually reflect their charge transfer properties with β -values between 0.2 and 0.8 \AA^{-1} .^[18,29-31] The bridges in INDELLIS

**Figure 1.9:** The three dyads in which photoinduced electron transfer was investigated, $n = 1-3$.^[28]

setup are therefore at the lower end of the range.

Further studies on *para*-phenylene bridges and the influence of substituents were conducted in the group of WENGER. Systems which hinder the π -conjugation of the conducting bridge, for example via methyl-groups on the side were found to mediate electron transfer less efficiently compared to plain phenylenes. This was attributed to the greater torsional angle between two adjacent phenylene units.^[31] When the torsion angle increases, h_{bb} decreases due to a weaker orbital overlap in the bridge. Xylenes are therefore gratefully taken as electron mediators, when the possibility of a hopping mechanism should be excluded. The greater electronic coupling of bridges can also be observed in the UV-vis absorption spectra of the respective compounds. These are characterised by a greater red-shift of π - π^* -absorption bands of compounds with an increasing electronic coupling of the bridges.^[32]

The β -value for distance dependent electron transfer studies allows for an estimation of the beneficial features of an organic molecular wire. Due to the fact that *para*-connected bridges, including oligo-fluorenes,^[33–35] -phenylenes and -xylenes,^[14,30–32,36] and oligo-*para*-phenylene vinylenes and -ethynylenes were investigated thoroughly,^[37–39] but their *ortho*-connected counterparts were completely unexplored until today, we strove to investigate photoinduced electron transfer through *ortho*-phenylenes - a bridging unit that has never been applied in D – b – A constructs before.

1.6 *Ortho*-oligo-phenylenes

Unlike their rigid rod-like *para*-connected relatives, *ortho*-phenylenes exhibit numerous orientations along the backbone (see Figure 1.10).^[40] An interesting feature about this class of compounds is the possibility of folding into discrete helical structures.^[41] The initial inspiration of other researches was to better understand folding phenomena in different materials such as DNA, molecular wires and other π -stacked molecules.^[42] Progress was made towards the synthesis of mono-disperse oligomers by HARTLEY^[43] and discrete chain lengths became accessible, whereas before polymerisation reactions were state of the art.^[44,45] *Ortho*-phenylenes show an interesting conformational behaviour. The first conformational analyses were performed in 2010,^[46] where it was found that these molecules often disarray at the ends (so called frayed ends) and further that these feature unusual electronic properties. After initial studies

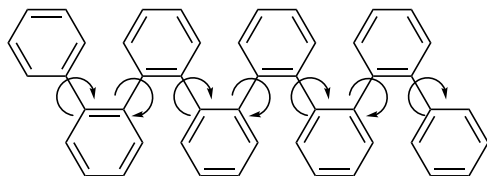


Figure 1.10: Depiction of an oligo-*ortho*-phenylene molecule. Arrows show the possible rotations around the C – C-bonds.

it was found that terminal end-groups have a major influence on the folding.^[47] Though it was assumed that the solvent has a major influence on the folding properties it was discovered in 2017 that this is not necessarily the case.^[48] Despite the interesting configurational properties, their charge-transfer behaviour would be of high interest.

1.7 Luminophores based on 3*d*-transition metals

An artificial system as depicted in Figure 1.6 would not function without chromophores. Usually noble metals from late transition metals with a d^6 , d^8 and d^{10} configuration are applied to obtain luminescent complexes.^[49] Only a few examples are reported so far for the 3*d* row, which underlines how the development of new luminophores from these metals proved to be rather challenging. Recent developments were made with isonitrile ligands to obtain luminescence for example from Cr(III)^[50] or Ni(0)-based complexes.^[51] Fe(II) as another d^6 metal would be a desirable candidate. However not much success has been reported in this regard, due to the very short lived ³-MLCT excited state which is deactivated by low-lying metal-centred states of Fe(II) complexes.^[52,53] A 'record lifetime' of a 100 ps could be obtained with N-heterocyclic carbene (NHC) based ligands.^[53] However, chromophores from more earth-abundant metals, despite their challenges are worth pursuing. Based on recent findings developments towards luminophores from earth-abundant metals can be made to increase the so far small library of promising examples.

2 Electron transfer across *ortho*-oligo-phenylenes

LONG-range electron transfer plays a pivotal role in many biological systems. As described in the introduction, photosynthesis would not be possible as it is without it. For a better understanding of this fundamental process model systems are still designed and their electron transfer properties investigated. As described in the introduction, electron transfer studies over long distances have been thoroughly explored in *para*-connected phenylene systems, but their *ortho*-connected counterparts are completely unexplored in this regard. Therefore we designed a set of molecular dyads comprised of a Ru(II)-chromophore and a triarylamine donor which are bridged via 2 to 6 *ortho*-connected phenylenes. In this chapter the photoinduced charge separation (CS) as well as the thermal back reaction (ET) will be described. Due to the flexibility of the bridging unit which results in interconverting conformers in solution, the forward reaction remains somewhat difficult to describe. However, the thermal reverse electron transfer allows for a similar analysis made for *para*-connected systems. The current work is already in a form of manuscript and will be the foundation for submission to a scientific journal.

2.1 Synthesis

TO investigate *ortho*-phenylenes as molecular wires and study their distance dependence for electron transfer it was crucial to obtain dyads with a discrete chain length. HARTLEY *et al.* reported on the synthesis of mono disperse *ortho*-oligo phenylenes.^[54] Their procedure allowed for the synthesis of three dyads with 2, 4 or 6 *ortho*-connected phenylene units (Figure 2.1). *Ortho*-phenylenes are reported to fold into helical structures, however it was not expected that this phenomena would be observed in these dyads due to the influence of the large end groups and the relative shortness of the bridges.^[55,56]

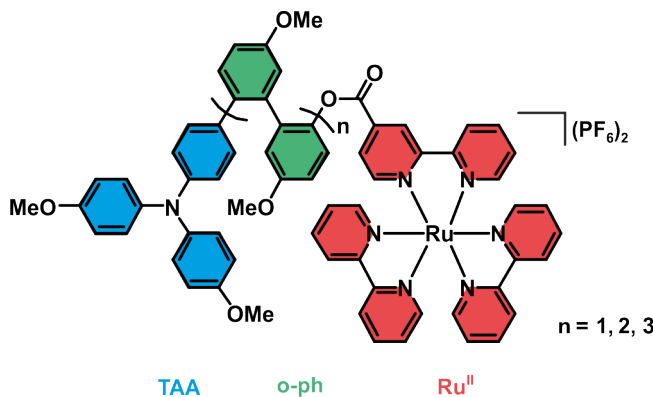


Figure 2.1: Synthesised dyads with $n = 1, 2, 3$ for the investigation of photoinduced charge-shift as well as thermal back electron transfer.

Further a reference complex was synthesised to allow for a thorough spectroscopic analysis of the obtained data. Detailed synthetic procedures can be found in chapter 7.

2.2 Electrochemistry and reaction free energies

FOR the determination of the reaction free energies cyclic voltammetry (CV) was performed with all three dyads. With the relevant oxidation and reduction potentials at hand, the reaction free energies can be estimated. All electrochemical measurements were conducted in acetonitrile (MeCN) containing 0.1 M tetra-*n*-butylammonium hexafluorophosphate (TBAPF₆) as electrolyte. The solutions were deaerated by bubbling argon through the solutions prior to each measurement. The redox potentials for (quasi)-reversible peaks were determined by taking the average between the oxidation and reduction peaks. For non-reversible oxidations the half-way potential of the occurring oxidation waves were taken or the maxima of the first derivation. In Figure 2.2 three reduction waves are observable for all three dyads. The first reduction wave belongs usually to a reversible process, whereas the two following reduction waves can be attributed to quasi-reversible waves. The observation of these three reduction waves is in line with a priorly reported Ru(bpy)₃²⁺ parent complex.^[57]

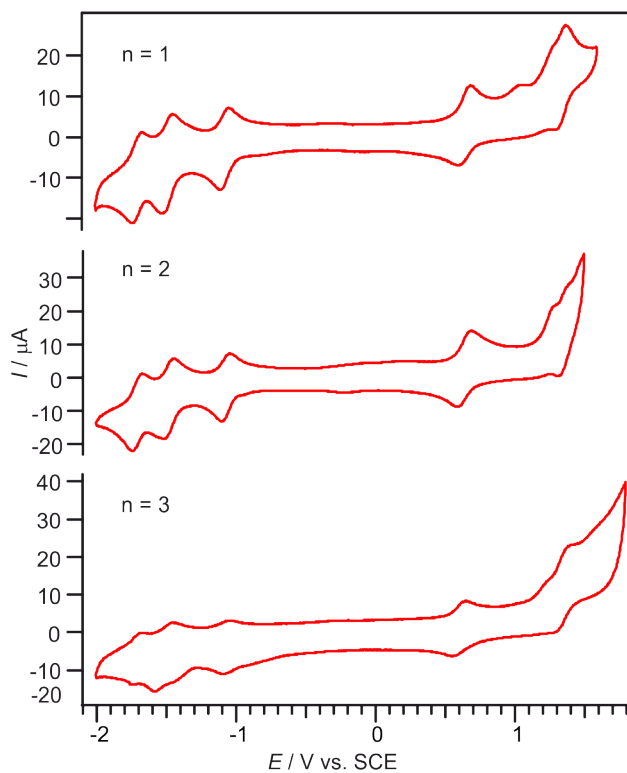


Figure 2.2: Cyclic voltammograms of the three donor-acceptor dyads, measured in deaerated MeCN at 22 °C with a potential sweep rate of 0.1 V s⁻¹ and 0.1 M TBAPF₆ as electrolyte.

Table 2: Reduction and oxidation potentials of the three molecular dyads measured in MeCN at 22 °C. $E_{p,a}-E_{p,c}$ is the difference between the anodic and cathodic peak currents of the waves.

redox couple	E_0 [V vs. SCE]			$E_{p,a}-E_{p,c}$ [mV]		
	n = 1	n = 2	n = 3	n = 1	n = 2	n = 3
TAA ^{+ / 0}	0.65	0.64	0.61	53	65	35
TAA ^{2+ / +}	0.98	1.23	1.25			
Ru(III/II)	1.36	1.35	1.35	44	53	58
bpy ^{0 / -}	-1.08	-1.04	-1.07	53	65	35
bpy ^{0 / -}	-1.48	-1.47	-1.51	71	54	123
bpy ^{0 / -}	-1.70	-1.71	-1.72	60	61	66
*Ru(bpy) ₃ ²⁺ /Ru(bpy) ₃ ⁺	1.02	1.06	1.03			

The quasi-reversible oxidation wave around 650 mV vs. SCE is observable for all three dyads and corresponds to the oxidation of the TAA donor moiety.^[58] At higher potentials around 1.35 V vs. SCE the reversible oxidation wave of Ru(II) to Ru(III) is observable, which is partly overlapped by the the irreversible oxidation of the TAA⁺ to the dication around 1.0 (n = 1) to 1.2 V vs. SCE (n = 2, 3). For all three dyads the oxidation as well as the reduction potentials are essentially invariant with increasing bridge length (Table 2). With these potentials at hand it is possible to calculate the driving forces for the photoinduced forward - and the thermal back-electron transfer reactions. The reaction free energy (ΔG^0) for an electron transfer event can be estimated with equation 8 established by WELLER.^[59]

$$\Delta G^0 = -e \cdot (E_{red} - E_{ox}) - E_{00} - \frac{e^2}{4 \cdot \pi \cdot \epsilon_0 \cdot \epsilon_s \cdot r_{DA}} \quad (8)$$

Here E_{red} and E_{ox} are the relevant ground state reduction and oxidation potentials, e is the elemental charge, ϵ_0 the vacuum permittivity, ϵ_s the dielectric constant of the used solvent (35.9 for MeCN)^[60] and r_{DA} the donor-acceptor distance (further information on the estimation of the donor - acceptor distance in section 2.7). With the relevant potentials taken from Table 2 in combination with the lowest excited state energy of Ru(bpy)₃²⁺ [$E_{00} = 2.12$ eV]^[61] the driving force for the forward charge-shift reaction can be estimated to roughly -0.4 eV.

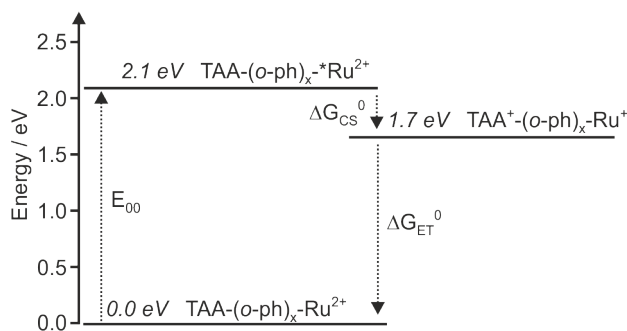


Figure 2.3: Energy-level scheme for the molecular dyads in MeCN. E_{00} corresponds to the $^3\text{MLCT}$ -energy of the Ruthenium-photosensitiser. ΔG_{CS}^0 is the reaction free energy for the forward charge shift reaction and ΔG_{ET}^0 the reaction free energy for the thermal back electron transfer.

For the thermal back reaction from the reduced $\text{Ru}(\text{bpy})_3^+$ to the TAA^+ cation the reaction free energy can be estimated in an analogous manner. Here E_{ox} corresponds to the $\text{TAA}^{+/0}$ couple, whereas the first potential of the $\text{bpy}^{0/-}$ has to be taken for E_{red} . This gives a reaction free energy of -1.7 eV for the thermal back reaction. A complete overview with all involved potentials is depicted in Figure 2.3. Therefore photoinduced electron transfer should be exergonic by 0.4 eV for all three dyads and in principle possible. In order to identify the photoproducts, electrochemical measurements combined with UV-vis spectroscopy were performed. The ground state absorption spectrum was taken as baseline, then a potential was applied to either oxidise the TAA or reduce a bipyridine ligand of the sensitiser. The measurements were performed for the shortest dyad in deaerated MeCN, with 0.1 M TBAPF_6 as supporting electrolyte. Figure 2.4 shows that upon selective oxidation of the TAA to the

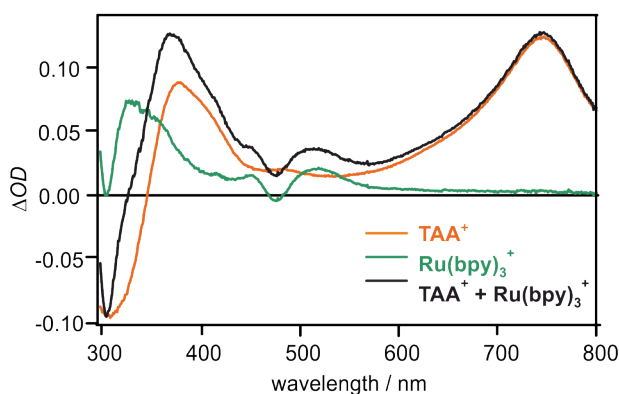


Figure 2.4: Spectro-electrochemical difference spectra of the shortest dyad ($n = 1$) in deaerated MeCN with 0.1 M TBAPF_6 as supporting electrolyte and 205 μM complex concentration. Selective oxidation of the TAA moiety (orange trace) occurs at a potential of +0.8 V vs. SCE. Selective reduction (green trace) of a bipyridine ligand of the $\text{Ru}(\text{II})$ -chromophore occurs at -1.2 V vs. SCE. The black trace is a linear combination of the oxidation and reduction spectra.

TAA⁺-cation, bands arise at 370 and 750 nm (orange trace). When applying a negative potential of -1.2 V vs. SCE a bipyridine ligand of the Ru(bpy)₃²⁺ is reduced and bands appear at 330 and 510 nm (green trace in Figure 2.4). The obtained photoproduct after an induced charge-shift reaction would show both features combined and therefore a linear combination of these two traces leads to the expected spectrum of the photoproducts (black trace in Figure 2.4).

2.3 Optical spectroscopy

THE ground state absorption spectra for all the three dyads were recorded as 20 μM solutions in MeCN and dichloromethane (DCM) at 22 °C (Figure 2.5). The band at 450 nm is caused by an MLCT-transition of the Ru(bpy)₃²⁺. At 290 nm a π* ← π transition of the bipyridine ligands is observable. All spectra, independent of the solvent, have nearly identical features. Elongation of the bridge has only minor effects on the absorption spectrum in the region of the UV in MeCN (Figure 2.5, a.)). Nevertheless there is a more intense absorption which is attributed to the increase in absorbing phenylene units. Before the solvent cut-off at 235 nm, a small red-shift of the absorption of the bridge can be detected in DCM (Figure 2.5, b.)). Notably upon elongation of the bridge, a red-shift is not observable in MeCN and barely in DCM what means that there is no significant increase of the π-conjugation of the bridge. Further it is confirmed that excitation in the visible region of the spectrum (~450 nm) will selectively excite the Ru(bpy)₃²⁺ photosensitiser.

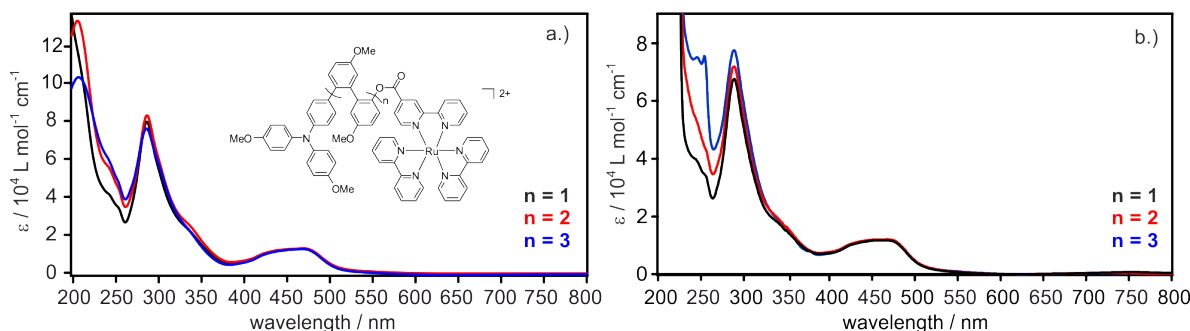


Figure 2.5: UV-Vis ground state absorption spectra of all three dyads measured in 20 μM solutions at 22 °C in a.) MeCN and b.) DCM.

2.4 Steady state luminescence

STEADY state luminescence spectra were recorded of all three dyads in MeCN and DCM. It was expected that in comparison to the ruthenium-reference complex the ³MLCT-emission would be quenched when efficient electron transfer occurs. On this behalf 20 μM solutions of all three dyads in deaerated MeCN or DCM were excited to their ³MLCT state at 450 nm and the emission was recorded. The same was performed with the reference compound

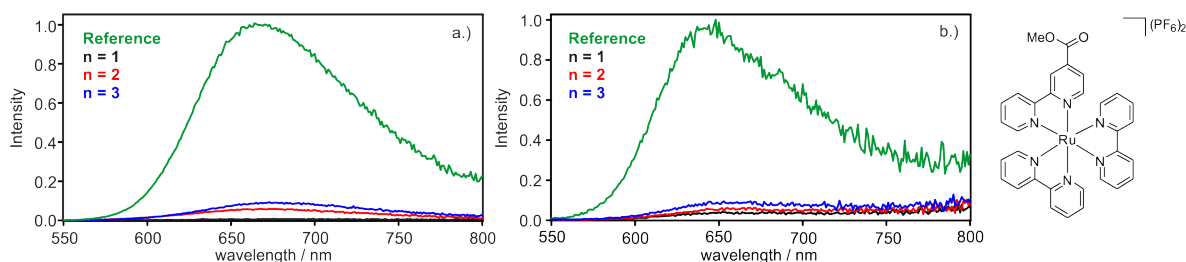


Figure 2.6: UV-Vis ground state absorption spectra off all three dyads measured in 20 μM solutions at 22 $^{\circ}\text{C}$ in a.) MeCN and b.) DCM. Right: Reference complex.

(Figure 2.6). The emission of the parent complex was set to 1 and the emission of the dyads referenced to it, taking the individual concentrations of the measured solutions into account. As expected the emission of the shortest dyad is completely quenched in MeCN (see Figure 2.6 a.)) and nearly completely quenched in DCM. It can be seen that the longer the dyad, the more residual emission from the $^3\text{MLCT}$ can be detected. The longer the dyad, the slower the electron transfer and that leads to the assumption that electron transfer becomes less efficient the longer the dyad. I attribute this effect further to the flexibility of the bridge where subsets of conformers coexist and electron transfer is not competitive in some of these. The $^3\text{MLCT}$ excited-state lifetime of the ruthenium reference complex was determined via transient absorption spectroscopy, monitoring the decay of the $^3\text{MLCT}$ luminescence intensity after excitation at 532 nm with laser pulses of ~ 10 ns duration (Figure 2.7). The luminescence lifetime was determined to be 1200 ns in deaerated MeCN. To further investigate the kinetics of the charge-shift reaction transient absorption (TA) spectroscopy was carried out.

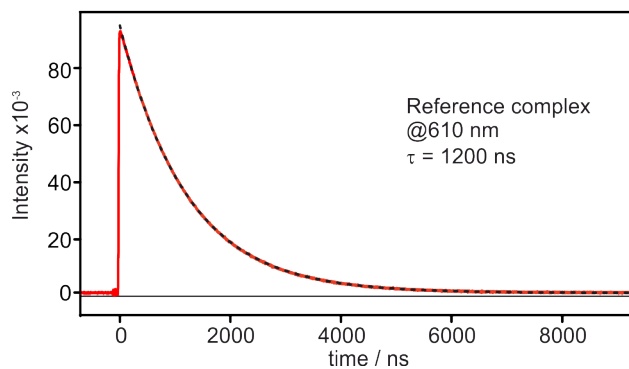


Figure 2.7: Decay of the $^3\text{MLCT}$ luminescence emitted by a 10 μM solution of the reference complex in deaerated MeCN at 610 nm following excitation at 532 nm with pulses of ~ 10 ns duration. The red trace shows the experimentally observable decay whilst the dashed black trace is a mono-exponential fit.

2.5 Transient absorption spectroscopy

After the spectro-electrochemical characterisation of the spectroscopic signatures of the photoproducts of the dyads (Figure 2.4, black trace), TA spectroscopy was performed with all three dyads. On this behalf, 20 μM solutions were prepared in either deaerated MeCN or DCM. These solutions were then excited with 532 nm laser pulses of ~ 10 ns duration. As a

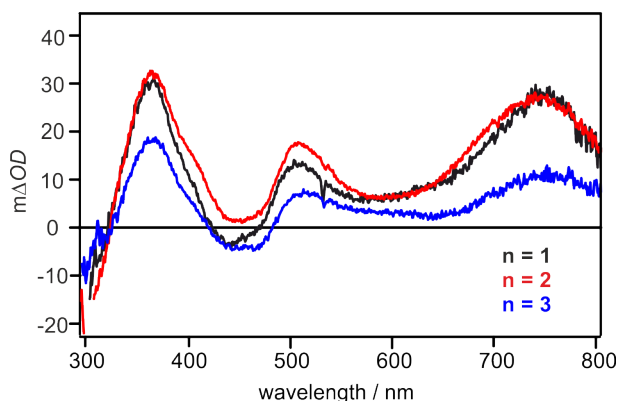


Figure 2.8: Transient absorption spectra of all three dyads recorded immediately after excitation at 532 nm with laser pulses of ~ 10 ns duration in deaerated MeCN. The spectra were time integrated over an interval of 200 ns.

result the expected charge separated state ($\text{TAA}^+ - o\text{-ph}_x\text{-Ru}(\text{bpy})_3^+$) could be observed in all three dyads (Figure 2.8). Transient bands arise at 370, 510 and 750 nm in all compounds. The obtained data is in excellent agreement with the superposition of the bands obtained from spectro-electrochemical measurements (black trace in Figure 2.4). The data recorded in DCM with the same method can be found in the Appendix Figure A.1 and shows the same spectroscopic features. Charge-separation is completed within the 10 ns laser pulse. The time constants for the photoinduced forward charge-shift reaction for all three dyads were determined via ps-transient absorption spectroscopy (chapter 2.5.1)

2.5.1 Photoinduced forward charge shift reaction

After the revelation that electron transfer takes place in the dyads which was confirmed via quenching of the $^3\text{MLCT}$ -emissive state and by TA, the initial photoinduced forward reaction was monitored via ps-laser spectroscopy. To monitor this reaction the formation of the transient band at 750 nm that belongs to the TAA^+ species (Figure 2.4) was followed. Therefore 20 μM solutions of the dyads in deaerated MeCN and DCM were selectively excited in the $^3\text{MLCT}$ band at 532 nm at 22 $^\circ\text{C}$ with laser pulses of ~ 30 ps duration. The obtained kinetic traces are shown in Figure 2.9. A bi-exponential behaviour is observed and tentatively attributed to the coexistence of conformers in solution where some allow for faster charge-shift than others. The time constants and relative intensities of the fits are summarised in Table 3.

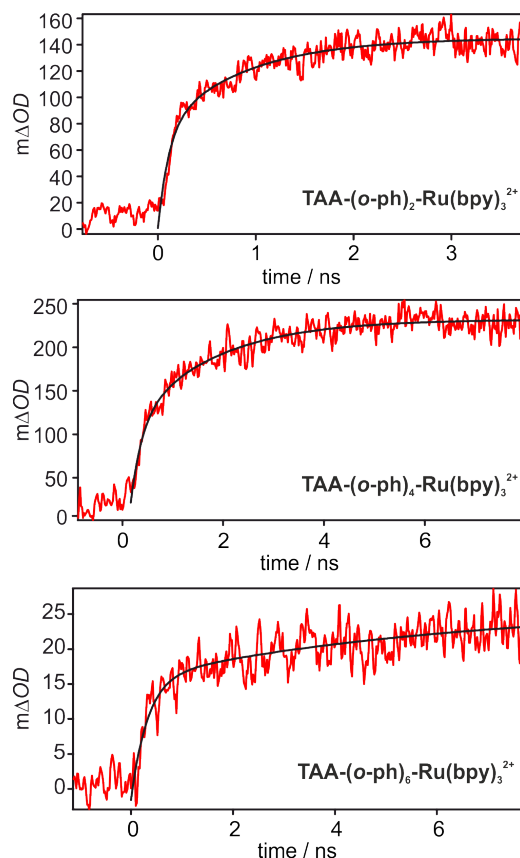


Figure 2.9: Temporal evolution of the transient signal at 750 nm after excitation at 532 nm with laser pulses of ~ 30 ps duration. The red traces belong to the obtained signal and the black curves depict the bi-exponential fit to it. The time constants are summarised in Table 3.

Unfortunately the obtained data in DCM is not of sufficient quality to allow for a reliable interpretation. Nevertheless the time resolved kinetics at 750 nm for TAA-*o*-ph₂-Ru(bpy)₃²⁺ and TAA-*o*-ph₄-Ru(bpy)₃²⁺ can be found in the Appendix Figure A.2. To explain the bi-exponential behaviour the conformation in solution was studied. This will be further explained in section 2.8.

2.5.2 Distance dependence of the forward charge shift reaction

THE distance dependence for the forward reaction was scrutinised for both, the long and the short component extracted from the data with a bi-exponential fit. The time constants used for the fit are given in Table 3. The distance of the dyads was determined as described in chapter 2.7. Both time constants show a very shallow dependency on the donor - acceptor distance and show β -values of 0.06 \AA^{-1} for the short component and 0.11 \AA^{-1} for the long component (Figure 2.10).

Table 3: Time constants for the intramolecular photoinduced charge-shift reaction from TAA to $^3\text{MLCT}$ -excited $\text{Ru}(\text{bpy})_3^{2+}$ measured in 20 μM solutions in deaerated MeCN after excitation at 532 nm with laser pulses of ~ 30 ps duration. In parentheses the percentage of the contribution of the respective lifetime is given.

complex	τ_{CS1} [ps]	τ_{CS2} [ps]
TAA- <i>o</i> -ph ₂ -Ru(bpy) ₃ ²⁺	110 (51%)	870 (49%)
TAA- <i>o</i> -ph ₄ -Ru(bpy) ₃ ²⁺	220 (43%)	1600 (57%)
TAA- <i>o</i> -ph ₆ -Ru(bpy) ₃ ²⁺	320 (62%)	6200 (38%)

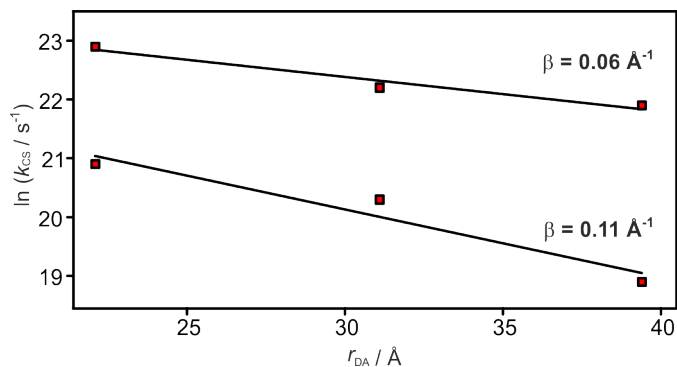


Figure 2.10: Logarithmic electron transfer rates for the photoinduced forward charge-shift reaction as a function of the donor - acceptor distance (r_{DA}). The two sets of data correspond to the short and long time constants extracted from bi-exponential fits to the data in Figure 2.9.

2.5.3 Thermal reverse electron transfer

THOUGH the forward charge-shift gives rise to a multi-exponential behaviour, the thermal back reaction allows for a similar treatment comparable to the *para*-phenylenes. The

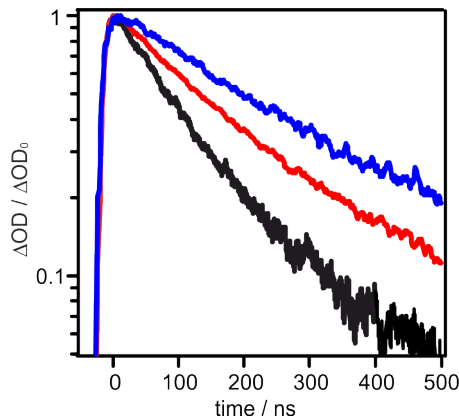


Figure 2.11: Decays of the transient absorption signals at 750 nm for all three dyads in MeCN. For analogous decays recorded at 370 and 510 nm see Appendix Figure A.3. Colour code is black: $n = 1$, red: $n = 2$, blue: $n = 3$.

measured kinetic traces (see Figure 2.11 for decays measured at 750 nm) show bi-exponential decays, which can be explained as the overlap of the signals from the thermal back reaction from $\text{Ru}(\text{bpy})_3^+$ to TAA^+ and of non-quenched excited state absorption of the photosensitiser. After the charge-shift reaction took place, a positive charge can be found on the oxidised TAA-moiety (TAA^+) as well as on the reduced chromophore ($[\text{Ru}(\text{bpy})_3]^+$). Due to Coulombic repulsion it is expected that the positive charges repel each other and therefore conformations with a maximum distance between donor and acceptor are favoured.

The thermal back reaction was followed at 370, 510 and 750 nm (see TA spectrum Figure 2.8 and data in DCM see Appendix Figure A.1). The temporal evolution of the signals was monitored in 20 μM , deaerated solutions of the dyads after excitation at 532 nm with laser

Table 4: Timeconstants of for the thermal back reaction in MeCN for the three dyads. Lifetimes were determined via fitting the data in Figure A.3. The data for the shortest dyad was fitted mono-exponentially ($n = 1$) whereas the data for the longer dyads ($n = 2, 3$) was fitted bi-exponentially. The second lifetime corresponds to the inherent $^3\text{MLCT}$ $\text{Ru}(\text{II})$ -photosensitizer. ($\tau_f = 1200$ ns, see Figure 2.7).

	n = 1	n = 2		n = 3	
λ [nm]	τ_{ET} [ns]	τ_{ET} [ns] (%)	τ_f [ns] (%)	τ_{ET} [ns] (%)	τ_f [ns] (%)
370	120	170 (93)	1200 (7)	230 (86)	1200 (14)
510	120	170 (99)	1200 (1)	210 (94)	1200 (6)
750	120	170 (94)	1200 (6)	220 (87)	1200 (13)

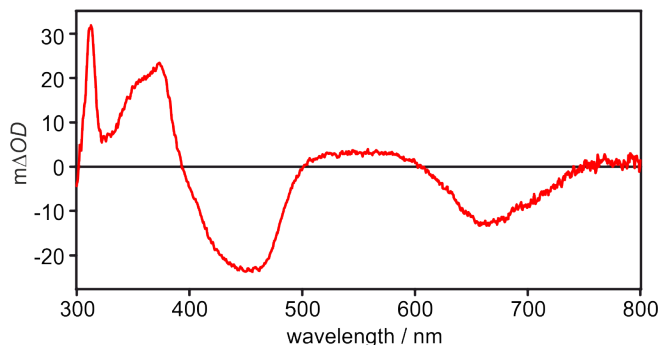


Figure 2.12: Transient absorption spectrum of the reference complex in deaerated MeCN (20 μM) at RT, time-integrated over an interval of 200 ns after excitation with 532 nm pulses of ~ 10 ns duration.

pulses of ~ 10 ns duration. The shortest dyad exhibits single-exponential transient absorption decays in MeCN at all measured wavelengths (Table 4). The longer dyads however show a bi-exponential decay. They are dominated by an initial decay of $\tau_{ET} = 170$ (n = 2) and 220 ns (n = 3), respectively, and a longer-lived component with smaller contribution (1-14%, values in parentheses in Table 4). The slower contribution is assigned to a small subset of conformers, not undergoing intramolecular photoinduced electron transfer, and therefore remaining as not-quenched $^3\text{MLCT}$ excited species. The possibility that the second component could have its origin from a product of decomposition is very unlikely, due to the stability of the complex during measurements, which is reflected in the reproducibility of the ratios from τ_{ET} to τ_f after long measurements. If the dyads would decompose, it is to be expected that the amount of $^3\text{MLCT}$ emission would increase. In the TA spectrum of the reference complex transient signals can be seen at 370, 510 and 750 nm (Figure 2.12), where the decay of the transient signals in the dyads was monitored. Further, no emission can be detected for the shortest dyad in MeCN and a mono-exponential decay can be observed here. Therefore we fitted the kinetic traces of the longer dyads with a fixed lifetime corresponding to the $^3\text{MLCT}$ lifetime of the reference complex ($\tau_f = 1200$ ns). The same measurements were performed in DCM, but the decays were only determined at 370 and 750 nm. The lifetimes are summarised in Table 5 and the determined time constants are slightly higher compared to the values in MeCN, which is expected for less polar solvents.^[62] Further it can be seen that the lifetimes for the longest

Table 5: Time constants for the thermal back reaction measured at 25 $^\circ\text{C}$ in deaerated DCM after excitation at 532 nm with laser pulses of ~ 10 ns duration.

λ [nm]	n = 1		n = 2		n = 3	
	τ_{ET} [ns]	τ_f	τ_{ET} [ns] (%)	τ_f [ns] (%)	τ_{ET} [ns] (%)	τ_f [ns] (%)
370	145 (99)	1790 (1)	160 (99)	1790 (1)	140 (96)	1790 (3)
750	145 (99)	1790 (1)	160 (99)	1790 (1)	145 (98)	1790 (2)

dyad become shorter compared to the second dyad in DCM. However this is a minor effect which is within the error range of the lifetimes and therefore not further considered.

2.6 Flash-quench experiments with the dyads

To further investigate the electron transfer properties of the dyads, flash-quench experiments were performed. Therefore a 20 μM solution of the dyad with ($n = 2$) in deaerated MeCN was prepared with additional 80 mM methyl viologen (MV) as oxidising agent to generate the highly oxidising $[\text{Ru}(\text{bpy})_3]^{3+}$ -species.^[63] The same was done for the reference complex. This leads to a further increase in the driving force for the electron transfer. First transient absorption spectra of the reference complex (Figure 2.13 a.) and TAA-(*o*-ph)₄-Ru(bpy)₃(PF₆)₂ (Figure 2.13 b.) with MV were recorded. The most prominent transient signals in both spectra in Figure 2.13 a.) and b.) are the signals of the MV⁺ radical cation - an intense and structured band at 395 nm and a less intense and broader band around 600 nm become visible. What can be further observed in spectrum a.) is a bleach of the signal at 450 nm, which can be attributed to the oxidised Ru-center (Ru(III)). In spectrum b.) of Figure 2.13 the spectroscopic signature of the MV⁺ radical is very prominent with the before mentioned structured band at 395 nm and the broad and less structured band at 600 nm. The transient signal in the red is further overlapped by the transient signal of the TAA⁺-moiety (see, Figure 2.4 for the spectroscopic signatures of TAA⁺) at 750 nm and no bleach at 450 nm (Ru(III)) anymore. Therefore it can be concluded that intramolecular electron transfer is accessible via the flash-quench technique. No time constants for the forward reaction were determined, due to the fact that the time constants were below the laser limit of 10 ns (see Appendix Figure A.4 for kinetic traces).

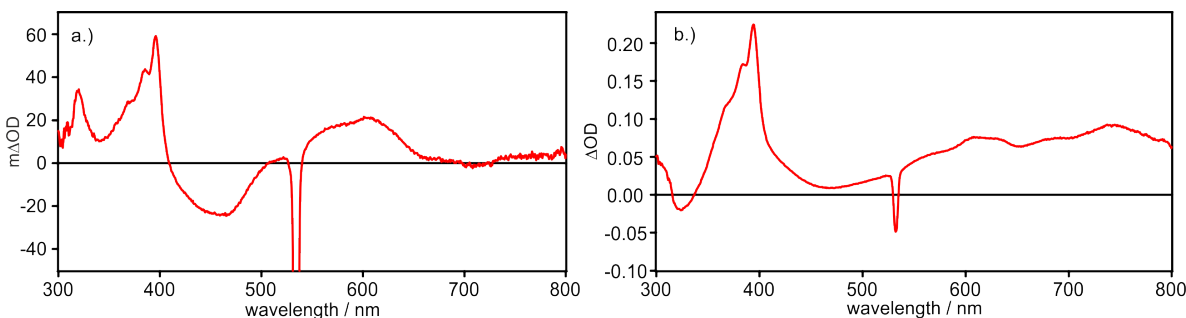


Figure 2.13: a.) Transient absorption spectrum of a 20 μM solution of the reference complex measured in deaerated MeCN containing 80 mM concentration of MV(PF₆)₂. b.) Transient absorption spectrum of a 20 μM solution of TAA-(*o*-ph)₄-Ru(bpy)₃(PF₆)₂ measured in deaerated MeCN containing 80 mM concentration of MV(PF₆)₂. Both spectra were recorded after excitation at 532 nm, with laser pulses of ~ 10 ns duration. The spectra were then integrated over a time of 200 ns.

2.7 Distance dependence for thermal back electron transfer and activation energies

THE values obtained from the transient absorption measurements are directly related to the electron transfer rates, in a manner that

$$\tau_{ET}^{-1} = k_{ET} \quad (9)$$

where τ_{ET} is the determined lifetime and k_{ET} is the electron transfer rate. From the determined time constants from the decays at 370, 510 and 750 nm (370 and 750 nm in DCM) the electron transfer rates can be calculated. As described in the introduction chapter 1.4 the transfer rates should exhibit an exponential dependence on the (through-bond) distance. This exponential decrease is a characteristic phenomenon which can be observed for example in tunnelling events in donor - bridge - acceptor systems with homologous bridges built from n -repeating units.^[30–32] The dependence of the distance is reflected in equation 7, where

$$k_{ET}(d) = k_{ET}^0 \cdot \exp(-\beta \cdot r_{DA}) \quad (7)$$

k_{ET} is the electron transfer rate, k_{ET}^0 is the electron transfer rate when donor and acceptor are in direct contact, r_{DA} the distance between donor and acceptor and β the distance decay parameter. The distance decay parameter β reflects the steepness of the exponential decrease of k_{ET} and is related to the tunnelling barrier height. Therefore β is a specific factor which takes into account the properties of the bridging medium. To determine β , the donor - acceptor distances in the dyads need to be determined at first.

On behalf of this, all three dyads were structure optimised with molecular mechanics energy minimisation calculations performed at the Molecular Mechanics Force Field (MMFF) level of theory using Spartan '08 Version 1.2.0. The distance was then measured from the nitrogen-atom of the TAA-donor to the Ru(II)-atom of the photosensitiser. Through the phenylene

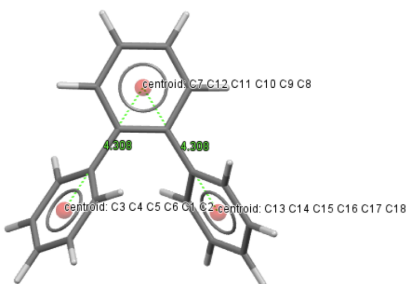


Figure 2.14: *Ortho*-terphenyl fragments to illustrate how the distance was measured in the phenylene bridge. Therefore the centroids of each ring were calculated before.

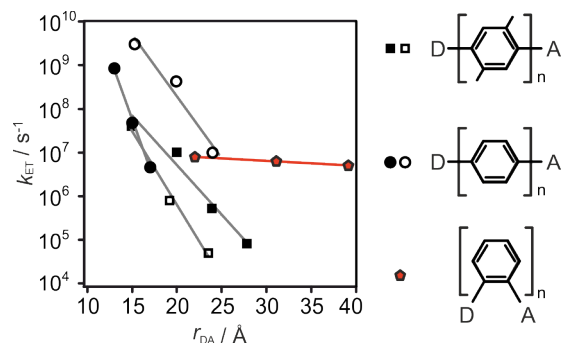


Figure 2.15: Electron transfer rates (k_{ET}) as function of the donor - acceptor distance (r_{DA}). Red pentagons belong to the *ortho*-phenylenes. Filled circles,^[18] empty circles,^[28] filled squares,^[30] empty squares.^[31]

bridges the distance was determined as follows; in each phenylene ring the centroid was calculated and the distance then measured from centroid to centroid (as depicted through the red dot in Figure 2.14). The measured distances are summarised in Table 6. When the logarithmic transfer rates are plotted as a function of the donor - acceptor distances these can be fitted linearly. The slope of the fit reflects in this case β . The shallower the slope, the more efficient is the transfer over longer distances. β is not only dependent on the bridge but further on the whole assembly of donor - bridge - acceptor. However a comparison between other systems with a *para*-connection is reasonable.^[19,36,64–67] Due to the fact that all considered systems make use of different donor - acceptor systems what leads to different driving forces for the electron transfer (for detailed structures see Appendix Figure A.5). This results in horizontal shifts between the different data sets (Figure 2.15). The determined β -value for the *ortho*-phenylene system is as low as 0.04 \AA^{-1} , a value that is one order of magnitude lower than for most prior reported *para*-phenylene based systems. In *para*-connected systems the values for β were found to be in a range of $0.4 - 0.8 \text{ \AA}^{-1}$ (see chapter 1.4). The value for the *ortho*-system is the so far lowest reported with 0.04 \AA^{-1} and is as low as it would be expected for a hopping mechanism.^[34,68,69] As mentioned in section 1.5 the only comparable well conducting bridges so far reported are fluorene bridges, OPVs and OPEs, where also a hopping mechanism is predominant. When a hopping mechanism is operative in a charge

Table 6: Donor - acceptor distances given in \AA measured through bonds or through counting the number of σ -bonds from the Nitrogen-atom of the donor to the Ru-atom of the photosensitiser.

compound	$r_{DA} [\text{\AA}]$	number of σ -bonds
TAA- <i>o</i> -ph ₂ -Ru(bpy) ₃ ²⁺	22.1	11
TAA- <i>o</i> -ph ₄ -Ru(bpy) ₃ ²⁺	31.1	15
TAA- <i>o</i> -ph ₆ -Ru(bpy) ₃ ²⁺	39.4	19

transfer process, an oxidation or reduction of the bridge is involved.^[25,67] To rule out this possibility, reference molecules were synthesised comprised of 2, 4 and 6 connected phenylene units and their oxidation potentials determined via CV (Figure 2.16). It can be seen, that the shortest bridge is oxidised at a potential of 1.7 and 2.0 V vs. SCE. The longer molecules are both oxidised around 1.25 V vs. SCE (all data is summarised in Table 7). For the longest molecule a second oxidation can also be seen at a potential of 1.46 V vs. SCE. Therefore hole transfer from TAA^+ to $\text{Ru}(\text{bpy})_3^+$ would be energetically uphill by 0.6 to 1.1 eV, due to the reduction potential of TAA^+ at 0.6 eV, making hole hopping very unlikely.

Similar to hole hopping, electron hopping could be another possible pathway. For that mechanism a reduction of the bridging medium would be necessary. Extending the potential range in the CV for the longest dyad shows that there is no reduction occurring until -2.0 V vs. SCE (Figure 2.17) and reduced $[\text{Ru}(\text{bpy})_3]^+$ is oxidised at -1.2 V vs. SCE. Therefore the possibility of electron hopping can be ruled out as well. The distance dependence for

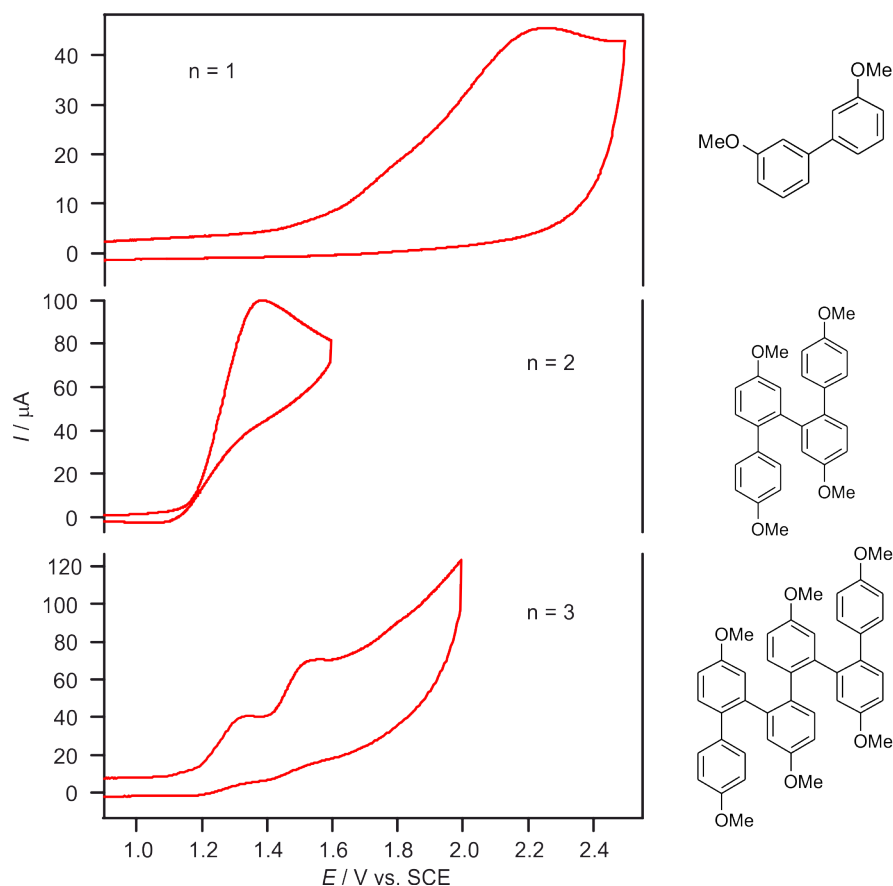
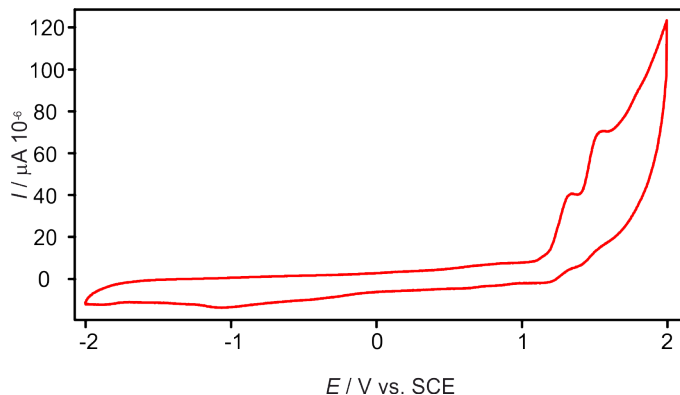


Figure 2.16: Cyclic voltammograms of the reference molecules for the bridges, measured in MeCN at RT with 0.1 M TBAPF_6 as electrolyte. The potential sweep rate was 0.1 V s^{-1} in all cases.

Table 7: Oxidation potentials of the reference compounds measured in deaerated MeCN at RT.

redox couple	E [V vs. SCE]		
	n = 1	n = 2	n = 2
$o\text{-ph}_{2n}^{+}/0$	1.72	1.23	1.25
$o\text{-ph}_{2n}^{2+}/+$	2.02		1.46

**Figure 2.17:** Cyclic voltammogram of the longest dyad ($n = 3$) in an extended potential range. No reductions are detectable in the potential range between 0.0 and -2.0 V vs. SCE.

the *ortho*-phenylenes shows a remarkable shallow distance dependence, with a β -value as low as 0.04 \AA^{-1} . To proof that there were no anomalies regarding the activation energy for this reaction, temperature dependent measurements were performed. The measurements were performed in either deaerated MeCN or DCM and the analysis was done in analogy to the described method in section 2.5.3. In MeCN the decays were measured at 370 and 750 nm from 5 °C to 65 °C in 10 °C intervals. The measurements in DCM were performed at the same detection wavelengths and from -5 to 25 °C in 10 °C intervals.

The obtained data set was then treated in the framework of the ARRHENIUS law (10).

$$k_{ET}(T) = A_0 \cdot \exp\left(\frac{-E_a}{k_B \cdot T}\right) \quad (10)$$

Here $k_{ET}(T)$ is the temperature dependent electron transfer rate, A_0 an exponential prefactor, E_a the activation energy, k_B the Boltzmann-constant and T the temperature in K. Based on the decays of the transient absorption signals at 370 and 750 nm (Table 8, Table 9), Arrhenius plots were made with the afterwards calculated logarithmic electron transfer rates. On this behalf this logarithmic electron transfer rates were plotted versus the inverse temperature (Figure 2.18). The slope of the linear regression fit then corresponds to $-E_a/k_B$. It can be seen that the values for the activation energy measured in DCM are higher compared to MeCN and especially that the change from $n = 2$ to $n = 3$ is very small in DCM.

Table 8: Time constants for the thermal back reaction of the intramolecular electron transfer from Ru(bpy)₃⁺ to TAA⁺ at different temperatures. The time constants were determined via transient absorption spectroscopy on 20 μM solutions in deaerated MeCN. The values are the averages of the decays at 370 and 750 nm. See Appendix Table 16 for all data points.

T [°C]	n = 1		n = 2		n = 3		Ref. τ _f [ns]
	τ _{ET} [ns]	ln (k _{ET} /s ⁻¹)	τ _{ET} [ns]	ln (k _{ET} /s ⁻¹)	τ _{ET} [ns]	ln (k _{ET} /s ⁻¹)	
5	125	15.89	220	15.33	315	14.97	1315
15	120	15.94	205	15.40	280	15.09	1250
25	112	16.00	182	15.52	240	15.21	1190
35	105	16.00	165	15.62	215	15.31	1130
45	102	16.10	150	15.71	190	15.48	1050
55	95	16.17	133	15.83	164	15.62	970
65	87	16.26	125	15.89	157	15.89	880

However, the values show that the longer the distance for the thermal back electron transfer, the higher the activation energy. The data in MeCN shows therefore no anomalies for the activation energy (E_a). The data set measured in DCM follows a similar trend, though the activation energies are overall higher. With the activation energies at hand it is possible to estimate with equation 11 the reorganisation energies of the dyads.

$$E_A = \frac{(\lambda + \Delta G_{ET}^0)^2}{4 \cdot \lambda} \quad (11)$$

In equation 11 E_A equals the activation energy, λ is the reorganisation energy and ΔG_{ET}^0 the driving force for the reaction. The reorganisation energy λ is as described in chapter 1.4 a sum of λ_{in} and λ_{out} and is mainly associated with the expenditure of the reorganisation of the solvent molecules (λ_{out}) and the reactant (λ_{in}) in the course of the electron transfer.

Table 9: Time constants for the thermal back reaction of the intramolecular electron transfer from Ru(bpy)₃⁺ to TAA⁺ at different temperatures. The time constants were determined via transient absorption spectroscopy on 20 μM solutions in deaerated DCM. The values are the averages of the decays at 370 and 750 nm. See Appendix Table 17 for all data points.

T [°C]	n = 1		n = 2		n = 3		Ref. τ _f [ns]
	τ _{ET} [ns]	ln (k _{ET} /s ⁻¹)	τ _{ET} [ns]	ln (k _{ET} /s ⁻¹)	τ _{ET} [ns]	ln (k _{ET} /s ⁻¹)	
-5	205	14.40	295	15.04	270	15.13	2120
5	185	15.50	240	15.24	215	15.35	2000
15	167	15.61	200	15.42	185	15.50	1920
25	147	15.73	160	15.65	143	15.76	1790

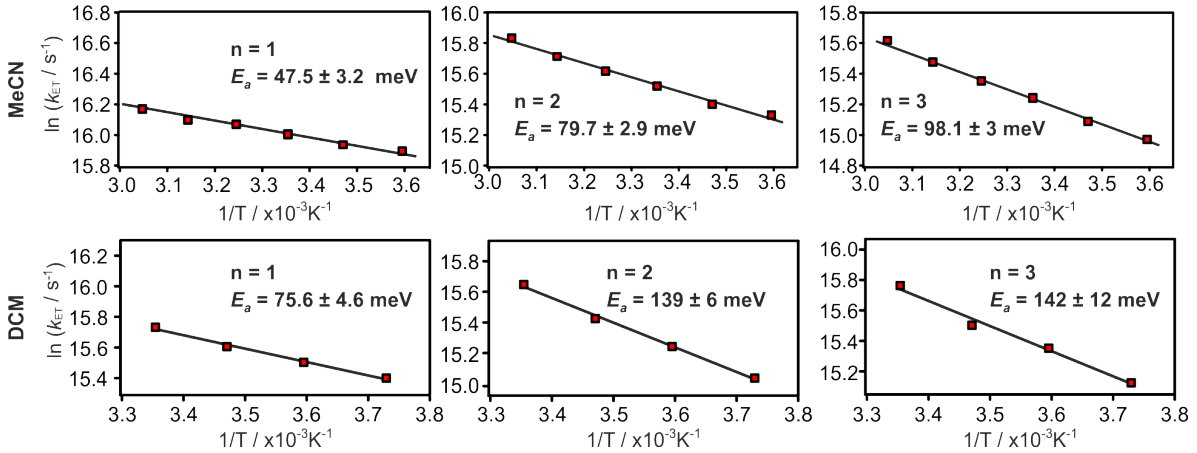


Figure 2.18: Arrhenius plots of all three dyads based on transient absorption spectroscopy measurements at 370 and 750 nm using 20 μ M solutions of the dyads in deaerated MeCN (top) or DCM (bottom). The determined activation energies (E_a) from the slopes are reported in the insets. The uncertainties of the calculated activation energies (E_a) correspond to the standard deviations resulting from the linear regression fits to the individual data sets.

Rearranging equation 11 on λ yields a quadratic equation in the form of:

$$\lambda_{1,2} = -\frac{(2 \cdot \Delta G_{ET}^0 - 4 \cdot E_A)}{2} \pm \sqrt{\left(\frac{2 \cdot \Delta G_{ET}^0 - 4 \cdot E_A}{2}\right)^2 - \Delta G_{ET}^0} \quad (12)$$

With all other values at hand this approach leads to two possible results for the reorganisation energy. The values obtained are essentially the same for all three dyads and equation 12 yielded 2.4 and 1.3 eV as possible values for the reorganisation energy. On behalf of priorly carried out studies, 2.4 eV seems to be the more realistic value. In molecular triads, where photoinduced electron transfer was investigated through rigid rod-like bridges, reorganisation energies were calculated with values up to 1.3 eV.^[70] Taking the flexibility of the *ortho*-phenylene system into account it can be assumed that the inner reorganisation energy has a much larger contribution compared to the before reported rigid systems where the inner contribution usually stays the same and the reorganisation energy itself increased upon elongation.^[70,71] This increase was contributed to the more isolated point charges with increasing r_{DA} .^[72] Consequently the higher value seems to be the more likely one for the flexible *ortho*-phenylene system. Due to the non-existent change of the reorganisation energy in any case it can be stated that the electron transfer in *ortho*-phenylenes is mainly dependent on the electronic coupling of donor and acceptor H_{DA} .

Prior studies of *para*-phenylenes as molecular wires have shown that the torsion angles of the phenylene units strongly affect the electronic coupling and therefore the distance dependence of k_{ET} . To put it in a nutshell: the flatter the better.^[31] For *ortho*-phenylene systems even greater dihedral angles compared to unsubstituted phenylenes are expected between the indi-

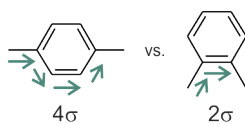


Figure 2.19: Illustration of the shortest σ -bond pathways in *para*-phenylenes (left) compared to *ortho*-phenylenes (right). Arrows count for one σ -bond.

vidual phenyl-rings and consequently a weaker electronic coupling would be expected due to the perturbation of the π -system (no red-shift in the UV-Vis absorption region of the bridge Figure 2.5). Nevertheless, when considering the shortest possible pathway along σ -bonds, *ortho*-phenylenes offer the advantage of introducing a new phenyl unit with only two σ bonds, whereas *para*-phenylenes need 4 σ bonds to introduce the next phenyl-unit (Figure 2.19). To compare the dependence of k_{ET} on the number of σ -bonds, the dimensionless parameter β_n was determined where the logarithmic rate constants are plotted vs. the number of σ -bonds via the shortest pathway between donor and acceptor. A linear fit to the data points as seen in Figure 2.20 reveals a β_n -value of 0.07, which reflects the decrease of k_{ET} per additional σ -bond and is not substantially more different than the β -value. The β_n values were also calculated for the *para*-connected systems, and were in a range between 0.57 and 0.83 (see Table 10). All detailed structures of the compounds can be found in the Appendix Figure A.5. Taking this into account and the fact that there are no anomalies in the activation energy in

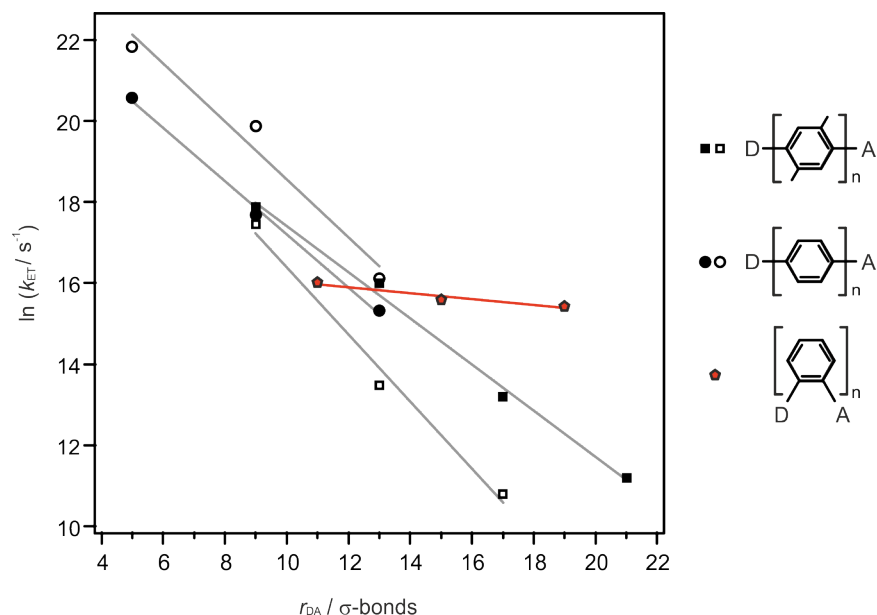


Figure 2.20: Logarithmic electron transfer rates vs. donor - acceptor distance measured in number of σ -bonds. Red pentagons belong to the *ortho*-phenylenes. Filled circles,^[18] empty circles,^[28] filled squares,^[30] empty squares.^[31]

Table 10: Distance decay constants for the herein presented system with an *ortho* connection in comparison with a variety of *para* connected systems. All detailed structures can be found in the Appendix Figure A.5.

symbol	β [Å]	β_n	ΔG_{ET}^0 [meV]	structure
◻	0.77	0.83	-450	I
○	0.65	0.71	-50	II
◼	0.52	0.57	-660	III
●	0.67	0.65	-10	IV
◈	0.04	0.07	-1700	TAA- <i>o</i> -ph _n -Ru(bpy) ₃ ²⁺

MeCN, it seems likely that the distance dependence of k_{ET} is dominated by a change in the donor - acceptor coupling H_{DA} .

2.8 Conformational analysis of the molecular dyads

FOR a better understanding of the kinetic studies of the photoinduced forward reaction, a conformational analysis of the dyads was performed. The ¹H-NMR spectra at RT appear very broad and an assignment to certain peaks is not possible (Figure 2.21). Therefore temperature dependent measurements were carried out and it was hoped that this would

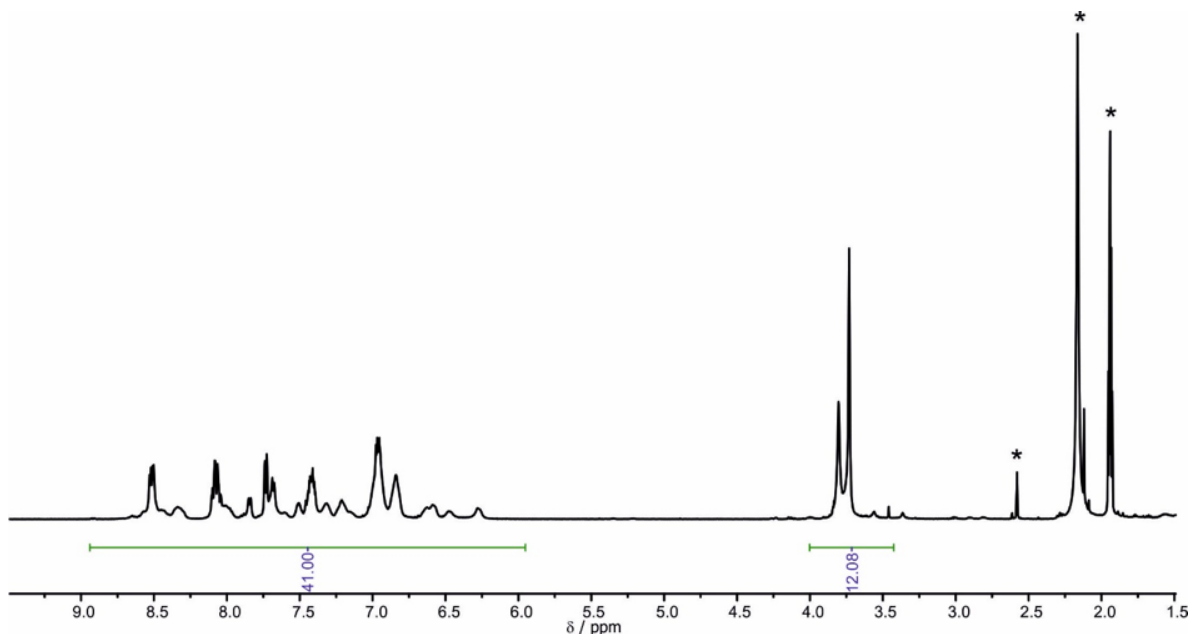


Figure 2.21: ¹H-NMR-spectrum of [TAA-(*o*-ph₂)-Ru(bpy)₃²⁺](PF₆)₂ in CD₃CN at room temperature. The residual solvent peak of CD₃CN, water from the deuterated solvent used and a peak which could not be assigned are marked with an asterisk (*). The other spectra can be seen in the Appendix A.

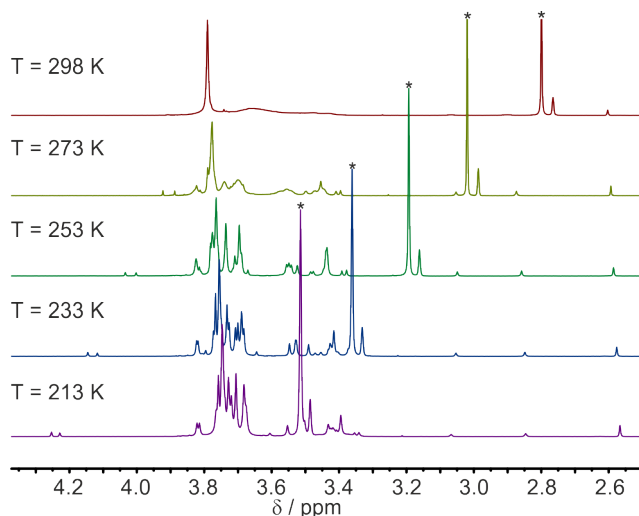


Figure 2.22: ^1H -NMR-spectra of $[\text{TAA}-(o\text{-ph}_2)\text{-Ru}(\text{bpy})_3]^{2+}(\text{PF}_6)_2$ in acetone- d_6 measured from 213 K to 273 K in 20 K intervals showing the region from 2.6 to 4.4 ppm. On top is the spectrum at RT. The residual H_2O peak is marked with an asterisk (*).

allow for an exact conformational analysis. The measurements were performed with $\text{TAA-}o\text{-ph}_4\text{-Ru}(\text{bpy})_3^{2+}$ in acetone- d_6 due to its low solubility in other solvents and with a similar accessible temperature range like acetone. ^1H -NMR spectra were recorded in a range from 213 K to 273 K in 20 K intervals. Even though the cooling was not sufficient to only obtain one conformer in solution which could then be analysed, it is clear that the resonance peaks become sharper and more distinct and especially in the region between 2.5 - 4.5 ppm a significant change of the spectrum is observable (Figure 2.22). The complete ^1H -NMR-spectra at different temperatures can be found in the Appendix Figure A.8. However, the spectra reveal that in solution there are subsets of conformers coexisting at RT. This finding further supports the aforementioned assumption for the multi-exponential forward charge-shift reaction, that was based on subsets of conformers in solution. (see chapter 2.5.1).

$$\Delta G^\ddagger = R \cdot T_c \cdot \ln \frac{R \cdot T_c \cdot \sqrt{2}}{\pi \cdot N_A \cdot h \cdot \Delta\delta} \quad (13)$$

Using equation 13 by EYRING allows for the calculation of the barrier for the conversion from one conformer into the other. In equation 13 R is the universal gas constant, T_c is the coalescence temperature of the respective process, N_A is the Avogadro-constant, h the Planck-constant and $\Delta\delta$ the difference of two adjacent methoxy-singlets at the respective temperature. The analysis revealed that in solution are subsets of conformers coexisting with two related coalescence temperatures. The energies and the values taken for the calculations are summarised in Table 11.

To get an idea what the main conformers could be in solution, molecular mechanics energy

Table 11: Parameters determined from the analysis of the variable-temperature NMR data: coalescence temperatures (T_c), difference in chemical shift ($\Delta\delta$) between two methoxy-singlets, and calculated energy barrier (ΔG^\ddagger) for the interconversion from one conformer into the other.

T_c [K]	$\Delta\delta$ [Hz]	ΔG^\ddagger [kJ/mol]
298	24	52
243	14.8	65

minimization calculations were performed at the MMFF level of theory using Spartan '08 version 1.2.0. It was possible to identify 2 main conformers, each with a local thermodynamic minimum (Figure 2.23). One conformer allows for the donor and acceptor to come to close proximity and is therefore called the 'closed' form (on the left in Figure 2.23). The other conformer is a more 'open' form, where donor and acceptor are not that close anymore (right in Figure 2.23).

Table 12: Distances measured through space from the N-atom of the TAA to the Ru-atom of the photosensitiser. The structures were priorly optimised and the distances measured with Mercury 3.9.

Form	n = 1 [Å]	n = 2 [Å]	n = 3 [Å]
open	11.8	12.6	16.4
closed	7.6	8.6	10.4

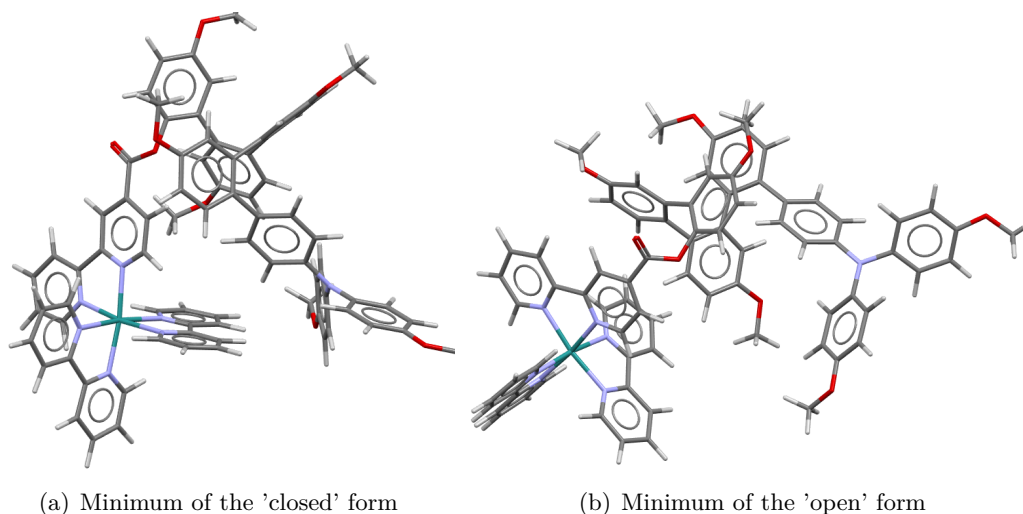


Figure 2.23: Calculated minima of $[\text{TAA}-(o\text{-ph}_4)\text{-Ru}(\text{bpy})_3]^{2+}$. Through space distances of donor and acceptor are given in Table 12.

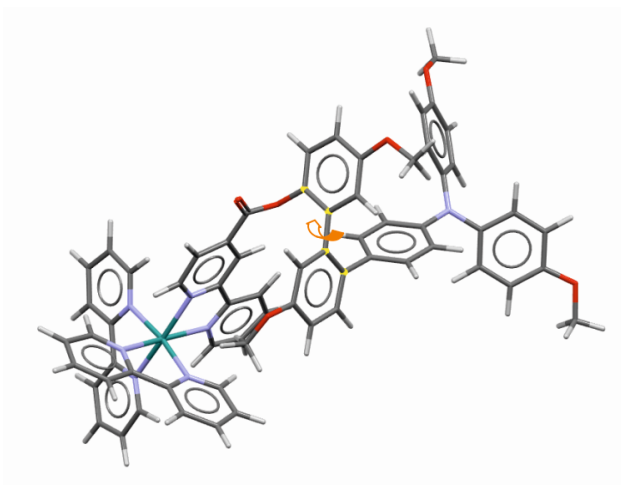


Figure 2.24: Molecular mechanical energy-minimised structure of [TAA-(*o*-ph₂)-Ru(bpy)₃](PF₆)₂ in the open form. Changing the torsional angle around the highlighted atoms (orange arrow) leads to a conversion from the 'open' to the 'closed form'.

The two conformers could be converted into one another through rotating around the C–C bond between the first phenylene rings after the ester bond (Figure 2.24, orange arrow). A successive turn of 15° around that bond with a subsequent energy minimisation leads to an energy diagram where two distinct minima could be identified and leads to the before mentioned 'open' and 'closed' form. The calculations revealed as shown in Figure 2.25 that for all three dyads two distinct minima can be observed. The lowest obtained value was always set to 0 and the energy is given in ΔE in respect to the minimum.

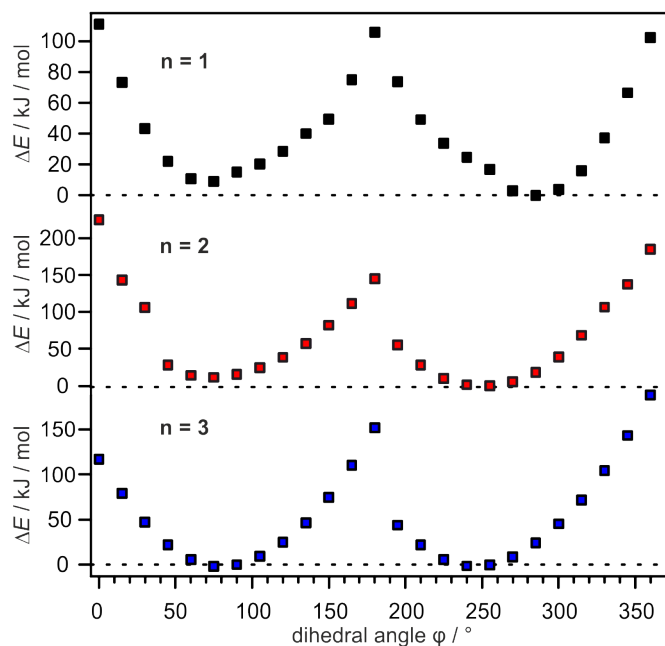


Figure 2.25: Energy of MMFF minimised structures with a set torsion angle which was rotated in 15° steps around the C – C-bond marked through orange arrow (Figure 2.24). Two distinct minima are observable for all structures.

2.9 Summary and Outlook

FOR the first time electron transfer mediated through oligo-*ortho*-phenylenes was reported. This bridge shows a remarkable shallow distance dependence for electron transfer, which leads to a β -value of 0.04 \AA^{-1} . This type of bridge mediates electron transfer even better than their oligo-*para*-phenylene relatives. The charge transfer properties are as good as for example for fluorene, OPV and OPE bridges, though in these systems hopping is the current mechanism which is basically length independent. The prevailing mechanism for hole transfer across *ortho*-phenylenes is tunnelling and it seems likely that the comparatively short σ -pathway compared to *para*-phenylenes has an important role within the mechanism. Therefore oligo-*ortho*-phenylenes can be accounted as a new promising class of molecular wires.

3 Electron transfer through oligo-*ortho*-naphthalenes

In collaboration with the group of SPARR, a system similar to the *ortho*-oligo-phenylenes was designed and investigated. Instead of oligo-*ortho*-phenylenes, the bridge should be

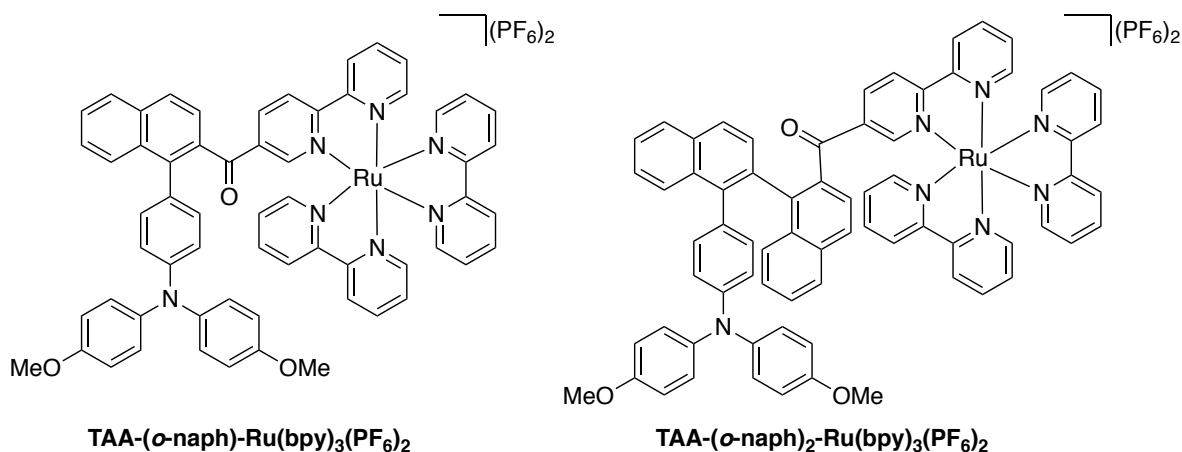


Figure 3.1: Dyads investigated in collaboration with the group of SPARR.

comprised of oligo-*ortho*-naphthylenes (Figure 3.1). After the exploration of configurationally stable oligo-1,2-naphthylenes,^[73] it was of interest to explore photoinduced electron transfer in atropisomeric bridges. Atropisomers are stereoisomers resulting from a restricted rotation around a single bond that allows to isolate these different stereoisomers.^[74] In Figure 3.2 the concept of atropisomers is explained. The rotation around the C – C bond of the phenylenes is restricted and therefore results in two enantiomers **A1** and **A2**. Usually in biphenyls the atropisomer stability is higher, the bigger the substituents. This concept is applied on the *ortho*-naphthylenes and the electron transfer in the different diastereomers should come under particular intense scrutiny. In the following chapters, the spectroscopic data obtained for the two dyads, shown in Figure 3.1, will be presented.

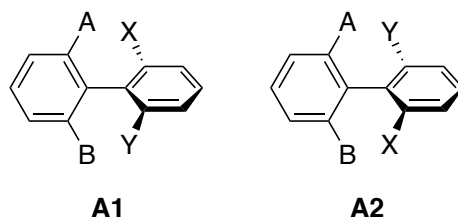


Figure 3.2: Example of atropisomers A1 and A2. Both are enantiomers due to their chirality axis with a defined sense of chirality.^[74]

3.1 Optical spectroscopy

DUe to the same applied donor and acceptor moieties in the dyads, similar oxidation potentials, as well as driving forces are expected. Further a similar transient spectrum should be obtained after electron transfer, due to the fact that the spectroscopic signatures of TAA^+ and $\text{Ru}(\text{bpy})_3^+$ will stay the same.

The ground state absorption spectra of the so far synthesised dyads were recorded in 20 μM MeCN-solutions. The band at 450 nm can analogously to the priorly reported dyads (chapter 2.3) be attributed to MLCT transitions of the $\text{Ru}(\text{bpy})_3^{2+}$ -sensitiser. At 290 nm $\pi^* \leftarrow \pi$ transitions localised on the bipyridine ligands of the photosensitiser are observable (Figure 3.3).

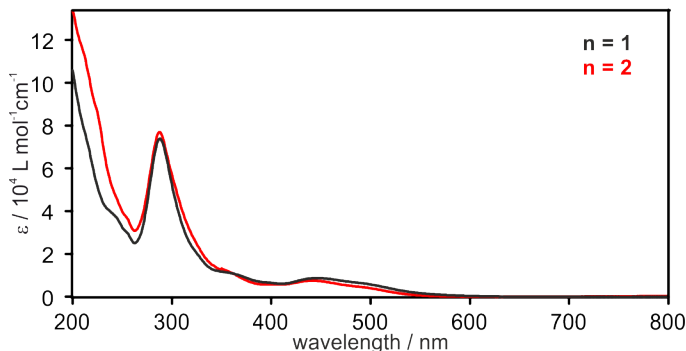


Figure 3.3: UV-Vis spectra of the two dyads synthesised by the group of SPARR. The spectra were recorded in MeCN at RT.

3.2 Steady state luminescence

STEADY state luminescence spectra were recorded for the two dyads in MeCN after excitation in the $^1\text{MLCT}$ state of the $\text{Ru}(\text{bpy})_3^{2+}$. For both dyads no emission could be recorded, therefore it is assumed that through electron transfer from the TAA to the photosensitiser efficient excited state quenching took place. An energy transfer from the excited Ru-photosensitiser to the naphthalene can be ruled out due to the higher triplet energy E_T of the naphthalene which is 2.63 eV and therefore roughly 0.5 eV higher, when compared to $E_{00}(\text{Ru}(\text{bpy})_3^{2+}) = 2.12 \text{ eV}$.^[75]

3.3 Transient absorption spectroscopy

SINCE there was no $^3\text{MLCT}$ -emission from the chromophore visible in the steady state emission spectrum, the dyads were subjected to transient absorption measurements. Therefore 20 μM solutions of the two dyads in MeCN were excited at 532 nm with laser pulses of ~ 10 ns duration. The evolution of transient signals was monitored and the spectra were time inte-

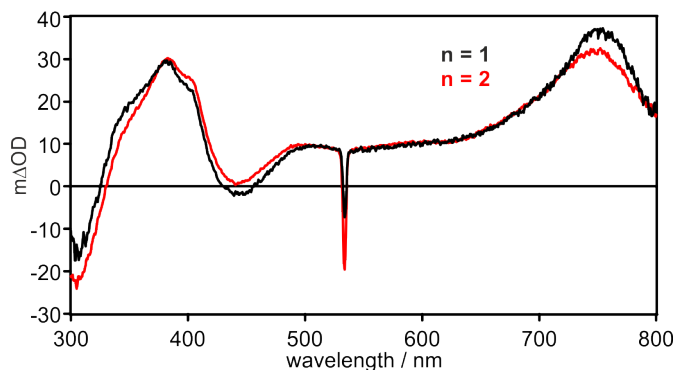


Figure 3.4: Transient absorption spectra of the two dyads. The spectra were recorded after excitation at 532 nm with laser pulses of ~ 10 ns duration. The spectra were then integrated over a time of 200 ns.

grated over 200 ns. Transient bands arise at 380, 500 and 750 nm and are in good agreement with the before shown spectro-electrochemical measurements for the *ortho*-phenylene bridged dyads (Figure 2.4), which should have the same spectroscopic features.

3.3.1 Photoinduced forward charge shift reaction

THE photoinduced forward reaction was monitored via ps-laser spectroscopy. The formation of the transient band at 750 nm (TAA^+) after excitation at 532 nm with laser pulses of ~ 30 ps duration was monitored. In Figure 3.5 the red traces are the recorded rises for the transient band at 750 nm. Black curve depicts the mono-exponential fit to the data. The time constants are summarised in Table 13.

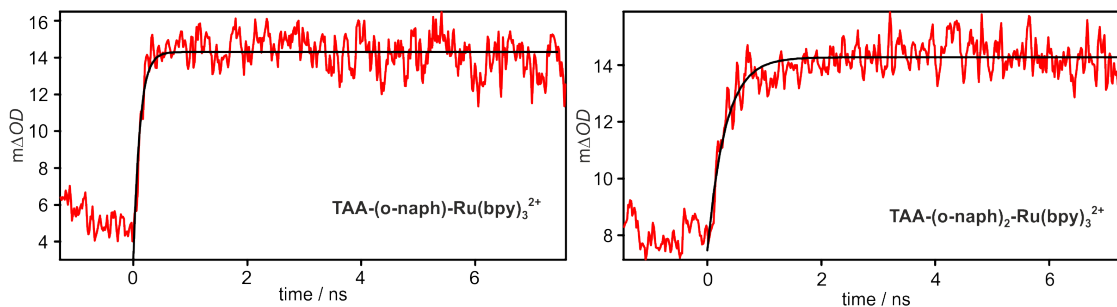


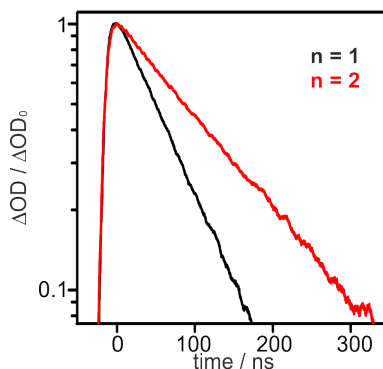
Figure 3.5: Temporal evolution of the transient signal at 750 nm after excitation at 532 nm with laser pulses of ~ 30 ps duration. The red traces belong to the obtained signal and the black curves depict the exponential fit to it. The time constants are summarised in Table 13.

Table 13: Time constants for the intramolecular photoinduced charge-shift reaction from TAA⁺ to excited Ru(bpy)₃²⁺ in MeCN.

compound	τ_{CS} [ps]
TAA-(<i>o</i> -naph)-Ru(bpy) ₃ ²⁺	110
TAA-(<i>o</i> -naph) ₂ -Ru(bpy) ₃ ²⁺	320

3.3.2 Thermal back electron transfer

AFTER the photoinduced forward charge-shift reaction has been investigated, the back reaction from the charge separated state came under particular intense scrutiny. The

**Figure 3.6:** Decays of the transient absorption signals at 750 nm for the two dyads in MeCN. For analogous decays recorded at 380 and 500 nm see Appendix Figure A.9. Colour code is black: $n = 1$, red: $n = 2$.

decay of the transient signals at 380, 500 and 750 nm was therefore monitored. In Figure 3.6 the decay of the signal at 750 nm for the two dyads can be seen. For both dyads this revealed mono-exponential decay curves (to see the complete decay curves see Appendix Figure A.9). The decay was measured in 20 μ M solutions of the dyads in deaerated MeCN, after excitation at 532 nm with laser pulses of ~ 10 ns at 22 °C.

Table 14: Timeconstants for the thermal back reaction of the two so far synthesised dyads in MeCN. Lifetimes were determined via fitting the kinetic traces in Figure A.9 mono-exponentially.

compound	τ_{ET} [ns]
TAA-(<i>o</i> -naph)-Ru(bpy) ₃ ²⁺	70
TAA-(<i>o</i> -naph) ₂ -Ru(bpy) ₃ ²⁺	120

3.4 Summary and outlook

FOR the first time, electron transfer through *ortho*-1,2-naphthalynes has been reported. The special feature about this bridging unit is the possibility of forming different atropoisomers. So far the herein reported dyads consist of enantiomers which exhibit the same physical properties, due to the number of naphthalene units. When incorporating another

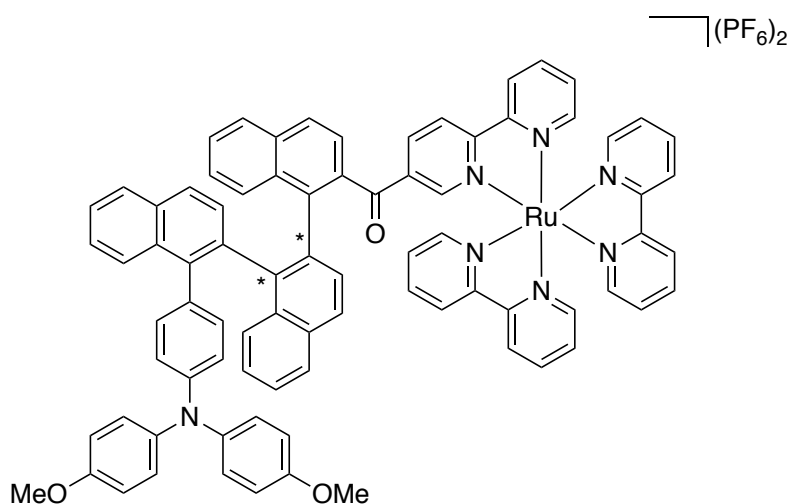


Figure 3.7: The future dyad of interest. Through the chirality centers (marked with an asterisk *) it should be possible to isolate two distinct isomers.

naphthalene unit, two stereogenic axes become available. This leads to four different configurations: R_aR_a , S_aS_a , R_aS_a and S_aR_a . In Figure 3.8 the different possible configurations are depicted. Only the ones connected with a green arrow exhibit different physical properties. These two atropisomers should then be accessible upon elongation and the electron transfer through these should be investigated.

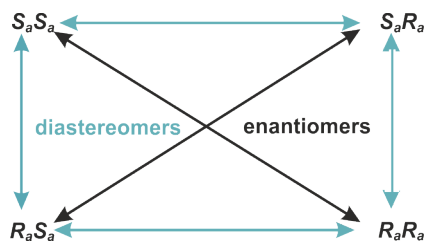


Figure 3.8: Through two stereogenic axes the four possible configurations exist: R_aR_a , S_aS_a , R_aS_a and S_aR_a . The connection through a black arrow shows the enantiomers who have the same physical properties. The green arrows mark the diastereomers, which exhibit different physical properties.

4 Luminescent Ni(0) complexes

THE following review summarises the scarce examples of emissive Ni(0) complexes at room temperature. Only a handful have been reported until today which show emission at RT and these will be presented in the review. The relevance of these complexes will be illustrated and a prospect of future ligand designs will be given to explore their potential. After the introductory review two examples of naphthalene based ligands which are envisaged in the outlook of the review and first preliminary results will be shown.

Author contribution

- S. M. did the literature research, contributed equally to the manuscript and analysis of the data presented.
- O. S. W. did the literature research, contributed equally to the manuscript and analysis of the data presented.



Contents lists available at ScienceDirect

Coordination Chemistry Reviews

journal homepage: www.elsevier.com/locate/ccr

Review

Luminescent Ni(0) complexes

Sabine Malzkuhn, Oliver S. Wenger*

Department of Chemistry, University of Basel, St. Johannis-Ring 19, 4056 Basel, Switzerland



ARTICLE INFO

Article history:

Received 30 October 2017

Received in revised form 26 December 2017

Accepted 1 January 2018

Available online 11 January 2018

Keywords:

Metal-to-ligand charge transfer

Isocyanide, phosphine

N-Heterocyclic carbene

 π -Acceptor

Earth-abundant metal element

ABSTRACT

With its $3d^{10}$ valence electron configuration Ni(0) is isoelectronic with Cu(I). While many Cu(I) complexes emitting from metal-to-ligand charge transfer (MLCT) excited states have been explored, the number of luminescent Ni(0) complexes known to date is very limited. Ni(0) is typically stabilized by carbonyls, phosphines or isocyanides due to the π -acceptor properties of these ligands, and photoluminescence has been reported in a few selected cases that are reviewed herein. Recent studies indicate that chelating isocyanide ligands are promising for obtaining Ni(0) complexes with long-lived 3 MLCT states, and this could be interesting for a similar range of applications as with photoactive Cu(I) complexes, including for example luminescent devices, solar cells, and organic photoredox reactions.

© 2018 Elsevier B.V. All rights reserved.

Contents

1. Introduction	52
2. From early structural studies to emissive complexes	52
3. Summary and conclusions	55
Acknowledgment	56
References	56

1. Introduction

The photophysics and the photochemistry of Cu(I) complexes with long-lived 3 MLCT excited states have received significant attention over the past few decades [1–4]. Cu(I) is an attractive earth-abundant alternative to traditional d^6 3 MLCT emitters made from precious metals such as Ru(II), Re(I), Os(II), and Ir(III) [5]. While many initial studies of emissive Cu(I) complexes focused on basic photophysical aspects such as the distortion in the MLCT excited states [6–9], more recent studies tend to put a stronger emphasis on possible applications. This includes for example the use of Cu(I) complexes as luminophores in light emitting devices

[10,11], as dyes in solar cells [12], and as sensitizers for organic photoredox conversions [4,13,14]. At the same time, isoelectronic Ni(0) complexes have received very little attention, despite the fact that similarly favorable excited-state properties could be anticipated. Herein we provide a survey over the currently known luminescent Ni(0) complexes and discuss their properties in the context of other MLCT emitters made from earth-abundant metals.

2. From early structural studies to emissive complexes

The low oxidation state of Ni(0) asks for stabilization by π -acceptor ligands such as carbonyl, isocyanides, phosphines, or phosphites. Ni(CO)₄ can be considered the prototype of a tetrahedral Ni(0) complex and some analogous isocyanide complexes have long been known [15–17]. Early infrared spectroscopic studies demonstrated that isocyanides can indeed simultaneously act as good σ -donors and π -acceptors to Ni(0). These initial IR studies also indicated that the actual point symmetry of the Ni(CNC)₄

Abbreviations: dbiy, 1,3-di-*t*-butylimidazol-2-ylidene; dpp, 2,9-diphenyl-1,10-phenanthroline; dppe, 1,2-bis(diphenylphosphino)ethane; MLCT, metal-to-ligand charge transfer; NHC, N-heterocyclic carbene; PPh₃, triphenylphosphine; P(OPh)₃, triphenylphosphite; P(O-*o*-cresyl)₃, tri(*o*-xylyl)phosphite.

* Corresponding author.

E-mail address: oliver.wenger@unibas.ch (O.S. Wenger).<https://doi.org/10.1016/j.ccr.2018.01.003>

0010-8545/© 2018 Elsevier B.V. All rights reserved.

groupings in homoleptic complexes with monodentate isocyanide ligands is lower than T_a , compatible with the view that the M—C—N—C entities are nonlinear as a result of the metal–carbon π -bonding [18]. Initial studies focused on tetrakis(arylisocyanide) complexes of Ni(0), whereas tetrakis(alkylisocyanide) complexes became accessible in analytically pure form somewhat later [19,20]. Crystallographic studies of different tetrakis(arylisocyanide)nickel(0) complexes provided direct evidence for the anticipated slightly distorted structures [21,22], and in one rather special case a macrocyclic tetra-arylisocyanide complex of Ni(0) was reported [23]. More recent studies of Ni(0) isocyanide complexes have focused on coordinatively unsaturated Ni(CNR)₃ complexes as isolable analogues of unsaturated metal carbonyls, such as for example Ni(CO)₃ or Fe(CO)₄ [24–27]. However, the potential luminescence properties of Ni(0) isocyanide complexes did not seem to receive any attention until very recently [28].

By contrast, luminescent Ni(0) phosphine complexes were already reported by Dori and co-workers nearly 50 years ago [29]. The respective early study explored more than 50 different d^{10} metal complexes with phosphine and arsine ligands. In addition to Ni(0), complexes with several other d^{10} metals were investigated, including Pd(0), Pt(0), Cu(I), Ag(I), Au(I), Zn(II), Cd(II), and Hg(II). The study reported that, in the solid state at 77 K, all of these complexes exhibited luminescence after irradiation with a mercury-vapor lamp, although quenching was observed for Ag(I), Au(I), Cd(II), and Hg(II) at higher temperatures [29]. The general structure of the Ni(0) complexes was as represented in Scheme 1a with R^1 = phenyl or substituted phenyl and R^2 = aryl, alkyl, cycloalkyl and alkoxy. Unfortunately, actual luminescence spectra of Ni(0) complexes were not shown in this short communication. However, it was noted that the emission is likely due to $d \rightarrow \pi^*$ charge-transfer type excitations [29].

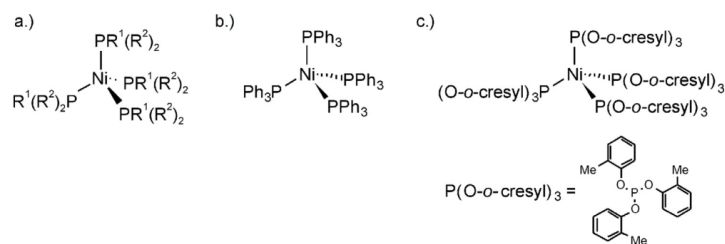
The first report of Ni(0) phosphine and phosphite complexes which possess long-lived emissive excited states in fluid solution at room temperature appeared in 1985 [30]. THF solutions of Ni(PPh₃)₄ and Ni(P(O-*o*-cresyl)₃)₄ (Scheme 1b, c) were reported by Caspar to show luminescence with band maxima at 740 and 645 nm, respectively. For the latter, an excited-state lifetime of 5.13 μ s and a luminescence quantum yield of 0.293% in N₂-saturated THF solution at 25 °C was reported [30]. However, several lines of evidence indicated that in the investigated class of NiL₄, PdL₄, and PtL₄ complexes the luminescence originates from species that are three-coordinate in both the ground and excited states. This interpretation made sense, since it was known that in solution the respective ML₄ complexes exist in equilibrium with ML₃ and ML₂ species. Luminescence quantum efficiencies were found to decrease upon addition of excess ligand, compatible with the view that coordinatively unsaturated species are the emitters. Organic triplet acceptors did quench the luminescence with rates depending systematically on the triplet energies of the organic acceptors, indicating that the emission originates from triplet states. The

relative insensitivity of the observed emission spectra to the nature of the phosphine, phosphite, and arsine ligand for a given metal (either Ni(0), Pd(0), or Pt(0)) suggested that the excited state is largely metal-localized in character. Based on extended Hückel calculations it was hypothesized that the lowest excited state for planar ML₃ d^{10} complexes involves the promotion of an (n) d -electron to a vacant metal-localized ($n + 1$) p -orbital [30]. In light of studies on Cu(I) complexes it seems possible that THF solvent molecules can weakly coordinate to these ML₃ complexes [9].

The next report on luminescent Ni(0) complexes appeared 12 years later in a comparative study of Ni(dppe)₂, Ni(CO)₂(SbPh₃)₂, and NiL₄ with L = AsPh₃, SbPh₃, P(OPh)₃ by Frem and coworkers [31]. These complexes were synthesized from a Ni(II) source using NaBH₄ as a reducing agent. Ni(AsPh₃)₄ could be stored in stoppered vials for 3 years, Ni(OPh)₃ was found to decompose over the period of a few days, and Ni(SbPh₃)₄ decomposed instantly when exposed to air. All complexes exhibited orange luminescence in the solid state and in fluid solution at room temperature. From the solid-state excitation and emission spectra in Fig. 1 it is seen that there are fairly large Stokes shifts of ca. 11,000 cm⁻¹, and this was interpreted in terms of luminescence from a spin-forbidden transition. Given the π -accepting characters of the ligands, the emissive excited state was assigned to ³MLCT. Luminescence lifetimes could not be determined due to instrumental limitations.

The structurally related Ni(CO)₂(PPh₃)₂ complex was investigated in the year 2000 by Kunkely and Vogler [32]. Compared to Ni(CO)₄ which exhibits efficient photodissociation, the heteroleptic Ni(CO)₂(PPh₃)₂ complex was found to be relatively stable. Following excitation at 356 nm, the complex showed red emission with a band maximum at 650 nm (dotted line in Fig. 2) both at room temperature in fluid acetonitrile and at 77 K. At such low temperature, the luminescence quantum yield was 10⁻³. The excitation spectrum roughly matched the absorption spectrum (solid line in Fig. 2). Similar to the complexes discussed above, there is a large shift between the emission band maximum and the maximum of the energetically lowest detectable absorption band. It was noted that in principle the lowest energy transitions could be either MLCT or intraligand (IL) transitions on the arylphosphine ligands (as observed previously in some Cu(I) arylphosphine complexes), but the assignment to ³MLCT states was favored. From the very large shift between absorption and emission (Fig. 2) it was inferred that excitation to the emissive state is associated with a considerable structural change, in analogy to what is commonly observed for Cu(I) polypyridyl complexes upon MLCT excitation.

In 2003 the same investigators reported on an interesting conceptual advance from phosphine to *N*-heterocyclic carbene (NHC) ligands (Scheme 2), leading them from the previously investigated Ni(CO)₂(PPh₃)₂ to the new Ni(CO)₂(dbiy)₂ complex (dbiy = 1,3-di-*t*-butylimidazol-2-ylidene) [33]. NHC ligands are comparatively weak π -acceptor ligands and hence MLCT transitions are expected to occur at higher energies than with phosphines. Indeed, the



Scheme 1. Molecular structures of some Ni(0) complexes investigated in the context of luminescence in the early literature [29,30].

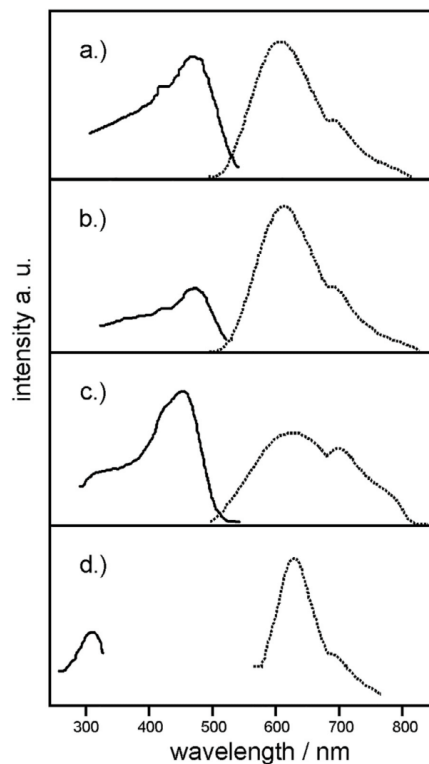


Fig. 1. Excitation (solid lines) and luminescence (dotted lines) spectra of (a) Ni(dppe)₂; (b) Ni(CO)₂(AsPh₃)₂; (c) Ni(CO)₂(SbPh₃)₂; (d) Ni(CO)₂(P(OPh)₃)₂ at room temperature in the solid state [31].

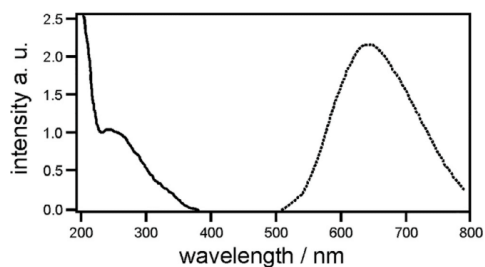
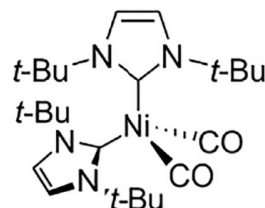


Fig. 2. Absorption (solid line) and luminescence (dotted line) spectra of Ni(CO)₂(PPh₃)₂. Absorption was recorded in CH₃CN at room temperature, emission in the solid state at 77 K [32].

emission band maximum for Ni(CO)₂(dbyi)₂ in CH₃CN was at 510 nm at room temperature (Fig. 3) [33], compared to 650 nm for Ni(CO)₂(PPh₃)₂ under identical conditions (Fig. 2) [32]. Due to lack of significant overlap between the lowest-energetic MLCT absorption and the MLCT luminescence band, the emissive state was assigned to a triplet, and it was noted that this is somewhat



Scheme 2. Molecular structure of a Ni(0) complex with N-heterocyclic carbene ligands [33].

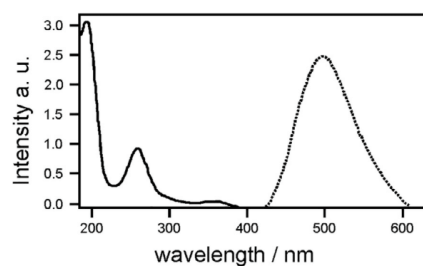
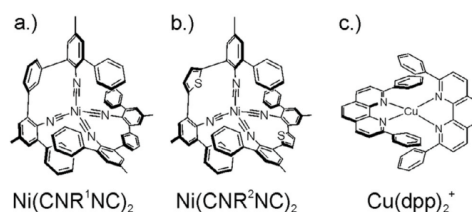


Fig. 3. Absorption (solid line) and luminescence (dotted line) spectra of Ni(CO)₂(dbyi)₂ in CH₃CN under Ar at room temperature [33].



Scheme 3. Molecular structures of two Ni(0) complexes with bidentate isocyanide ligands (a, CNR¹NC; b, CNR²NC) and (c) the Cu(dpp)₂ parent complex (dpp = 2,9-diphenyl-1,10-phenanthroline) [28].

intriguing because Ni(0) should not exert a strong heavy atom effect. On the other hand, it was also noted that this behavior is in line with isoelectronic Cu(I) complexes.

The next publication on luminescent Ni(0) complexes appeared in 2017 after a break of 14 years, when we reported on two homoleptic complexes with bidentate isocyanide ligands (Scheme 3a and b) [28]. We had previously discovered that such chelating isocyanides provide access to relatively robust d⁶ metal complexes made from Cr(0) and Mo(0) that are luminescent analogues of well-known Ru(II) polypyridyl and cyclometalated Ir(III) complexes [34–38]. The molecular design of the Ni(0) complexes in Scheme 3a and b was inspired by the structure of the Cu(dpp)₂ parent complex (dpp = 2,9-diphenyl-1,10-phenanthroline), in which the phenyl-substituents in α -position to the ligating N-atoms are used to impede planarization in the MLCT state, thereby enhancing the luminescence properties [1,5]. ³MLCT luminescence is indeed observed, albeit only in frozen solvent matrices at 77 K, but not at room temperature (dotted lines in Fig. 4) [28]. The cyclic voltammogram recorded in THF for one of the two complexes resembles some of the voltammograms typically reported

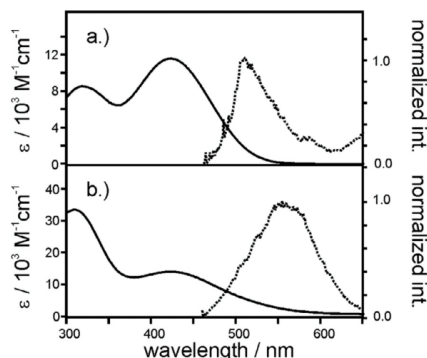


Fig. 4. Absorption (solid lines) and luminescence (dotted lines) spectra of the two Ni(0) complexes from Scheme 3 (a, Ni(CNR¹NC)₂; b, Ni(CNR²NC)₂). Absorption was recorded in THF at room temperature, emission in toluene at 77 K [28].

for Cu(I) bis(diimine) complexes. These undergo a (reversible) change in coordination number upon oxidation to Cu(II), as exploited in molecular machines [39]. This observation and the lack of MLCT luminescence at room temperature suggest that the ligand design is sub-optimal, in that planarization in the MLCT state is not sufficiently suppressed. Alternatively, it is conceivable that hemi-lability of the diisocyanide ligands represents an important pathway for nonradiative excited-state relaxation.

3. Summary and conclusions

While luminescent Cu(I) complexes have received enormous attention resulting in hundreds of publications, there seem to be only 6 papers reporting luminescence of isoelectronic Ni(0) complexes. The first study appeared in 1970 [29], and then there were scattered reports by different researchers in 1985 [30], 1997 [31]; 2000 [32], 2003 [33], and 2017 [28]. Ligand classes that have been used so far comprise phosphines [29–32], phosphites [30,31], arsines [31], antimonines [31], *N*-heterocyclic carbenes [33], and isocyanides [28]. In most cases, monodentate ligands were employed [29–33], but some bidentate chelators were also used [28,31]. Emission in the solid state (at 77 K or at 298 K) was observable in all cases, but luminescence in fluid solution at room temperature is rare. The luminescence originates from an MLCT

excited state in most cases [28,31–33], but it was noted that several of the used ligands could have π – π^* transitions that are energetically close [32]. In one early study, the luminescence was attributed to coordinatively un-saturated NiL₃ species exhibiting an emissive d → p transition [30]. The long luminescence lifetimes detected in most cases are compatible with spin-forbidden transitions from triplet excited states. Table 1 summarizes luminescence data for all Ni(0) complexes for which a minimum level of detail is known; this excludes some of the very early compounds [29]. Assignment of the luminescence transitions proved somewhat challenging in many of the Ni(0) cases studied so far. For several examples it was not clear whether MLCT, intraligand, or some other type of transition is responsible for the emission, and future studies will have to address this issue both from an experimental and computational perspective.

The small number of known luminescent Ni(0) complexes compared to isoelectronic Cu(I) species most likely reflects the fact that Ni(0) complexes are substantially more readily oxidizable, making their synthesis and characterization more tricky and perhaps limiting their (immediately evident) application potential relative to Cu(I) complexes. Nevertheless it seems worthwhile to explore the possibility of obtaining Ni(0) complexes with improved luminescence properties. Currently, Ni(0) ³MLCT emission is restricted to the solid state or to cryogenic temperatures in most cases, and large Stokes shifts indicate sizeable excited-state distortions. The strategies applied so successfully in Cu(I) bis(diimine) complexes to suppress excited-state distortions should in principle be applicable to Ni(0) complexes as well [1,5]. The step from monodentate to chelating bidentate ligands is a first advance in that direction [28,31], and future avenues could include rigidification of such chelators, introduction of sterically more demanding groups, and the synthesis of heteroleptic complexes made from two different types of chelating ligands.

Some of the many known Cu(I) complexes have remarkably good luminescence properties, and one may of course question whether Ni(0) complexes will ever perform equally well. However, one aspect in which Ni(0) complexes with sufficiently long-lived excited states are likely to be highly competitive with Cu(I) species is their reducing power in the emissive ³MLCT state [28], and this could be of interest for photoredox applications.

Currently, there is yet significant room for improvement regarding the luminescence properties of Ni(0) complexes, but the same is true for many other emitters made from non-precious metals. In addition to the abovementioned Cr(0) [35], Mo(0) [34], and W(0) isocyanide complexes [36,40,41], recent promising discoveries include for example Fe(II) [42], Fe(III) [43], Cr(III) [37,44,45], Zr(IV) [46], and Ce(III) complexes [47,48].

Table 1

Luminescence properties of Ni(0) complexes (λ_{max} = emission band maximum; τ = luminescence lifetime; ϕ = luminescence quantum yield).

Compound	$\lambda_{\text{max}}/\text{nm}$	Stokes shift/ cm^{-1}	$\tau/\mu\text{s}$	ϕ (%)	Assignment
Ni(PPh ₃) ₄	740 ^a				NiL ₃ , d → p
Ni(P(O- <i>o</i> -cresyl) ₃) ₃	645 ^a		5.13 ^a	0.293 ^a	NiL ₃ , d → p
Ni(P(OPh) ₃) ₄	634 ^b		32.4 ^b		MLCT
Ni(AsPh ₃) ₄	620 ^b	~11,000 cm^{-1}	20.2 ^b		MLCT
Ni(SbPh ₃) ₄	634 ^b	~11,000 cm^{-1}	9.7 ^b		MLCT
Ni(dppe) ₂	613 ^b	~11,000 cm^{-1}	7.6 ^b		MLCT
Ni(CO) ₂ (PPh ₃) ₂	650 ^c			0.1 ^c	MLCT
Ni(CO) ₂ (SbPh ₃) ₂	639 ^b				MLCT
Ni(CO) ₂ (dbiv) ₂	510 ^d				MLCT
Ni(CNR ¹ NC) ₂	520 ^e		0.20–1.10 ^e		MLCT
Ni(CNR ² NC) ₂	560 ^e		0.23–1.20 ^e		MLCT

^a In N₂-saturated THF at 25 °C, from Ref. [30].

^b In the solid state at room temperature, from Ref. [31].

^c In the solid state at 77 K, from Ref. [33].

^d In CH₃CN under Ar at room temperature, from Ref. [33].

^e In frozen toluene at 77 K, from Ref. [28].

Acknowledgment

Financial support by the Swiss National Science Foundation through grant number 200021_156063/1 is gratefully acknowledged.

References

- [1] N. Armaroli, G. Accorsi, F. Cardinalli, A. Listorti, *Top. Curr. Chem.* 280 (2007) 69–115.
- [2] M. Ruthkosky, C.A. Kelly, F.N. Castellano, G.J. Meyer, *Coord. Chem. Rev.* 171 (1998) 309–322.
- [3] A. Lavie-Cambot, M. Cantuel, Y. Leydet, G. Jonusauskas, D.M. Bassani, N.D. McClenaghan, *Coord. Chem. Rev.* 252 (2008) 2572–2584.
- [4] O. Reiser, *Acc. Chem. Res.* 49 (2016) 1990–1996.
- [5] N. Armaroli, *Chem. Soc. Rev.* 30 (2001) 113–124.
- [6] M.T. Buckner, D.R. McMillin, *J. Chem. Soc., Chem. Commun.* (1978) 759–761.
- [7] C.O. Dietrich-Buchecker, P.A. Marnot, J.P. Sauvage, J.R. Kirchoff, D.R. McMillin, *J. Chem. Soc., Chem. Commun.* (1983) 513–515.
- [8] D.G. Cottrell, S.M. Kuang, P.E. Fanwick, D.R. McMillin, R.A. Walton, *J. Am. Chem. Soc.* 124 (2002) 6–7.
- [9] L.X. Chen, G.B. Shaw, I. Novozhilova, T. Liu, G. Jennings, K. Attenkofer, G.J. Meyer, P. Coppens, *J. Am. Chem. Soc.* 125 (2003) 7022–7034.
- [10] R.D. Costa, E. Orti, H.J. Bolink, F. Monti, G. Accorsi, N. Armaroli, *Angew. Chem. Int. Ed.* 51 (2012) 8178–8211.
- [11] M. Hashimoto, S. Igawa, M. Yashima, I. Kawata, M. Hoshino, M. Osawa, *J. Am. Chem. Soc.* 133 (2011) 10348–10351.
- [12] C.E. Housecroft, E.C. Constable, *Chem. Soc. Rev.* 44 (2015) 8386–8398.
- [13] A.C. Hernandez-Perez, S.K. Collins, *Acc. Chem. Res.* 49 (2016) 1557–1565.
- [14] C.B. Larsen, O.S. Wenger, *Chem. Eur. J.* (2017), <https://doi.org/10.1002/chem.201703602>.
- [15] W. Hieber, *Z. Naturforsch. B* 5 (1950) 129–130.
- [16] F. Klages, K. Mönkemeyer, *Ber.* 83 (1950) 501–508.
- [17] H. Behrens, K. Meyer, *Z. Naturforsch. B* 21 (1966) 489–490.
- [18] F.A. Cotton, F. Zingales, *J. Am. Chem. Soc.* 83 (1961) 351–355.
- [19] S. Otsuka, A. Nakamura, Y. Tatsuno, *J. Am. Chem. Soc.* 91 (1969) 6994–6999.
- [20] R. Nast, H. Schulz, H.D. Moerler, *Ber.* 103 (1970) 777–784.
- [21] F.E. Hahn, M. Münder, R. Fröhlich, *Z. Naturforsch. B* 59 (2004) 850–854.
- [22] C.L. Perrine, M. Zeller, J. Woolcock, T.M. Styraneac, A.D. Hunter, *J. Chem. Crystallogr.* 40 (2010) 289–295.
- [23] Y. Ito, K. Kobayashi, T. Saegusa, *J. Organomet. Chem.* 303 (1986) 301–308.
- [24] B.J. Fox, M.D. Millard, A.G. DiPasquale, A.L. Rheingold, J.S. Figueroa, *Angew. Chem. Int. Ed.* 48 (2009) 3473–3477.
- [25] B.M. Emerich, C.E. Moore, B.J. Fox, A.L. Rheingold, J.S. Figueroa, *Organometallics* 30 (2011) 2598–2608.
- [26] B.R. Barnett, J.S. Figueroa, *Chem. Commun.* 52 (2016) 13829–13839.
- [27] S. Otsuka, T. Yoshida, Y. Tatsuno, *J. Am. Chem. Soc.* 93 (1971) 6462–6469.
- [28] L.A. Büldt, C.B. Larsen, O.S. Wenger, *Chem. Eur. J.* 23 (2017) 8577–8580.
- [29] R.F. Ziolo, S. Lipton, Z. Dori, *J. Chem. Soc., Chem. Commun.* (1970) 1124–1125.
- [30] J.V. Caspar, *J. Am. Chem. Soc.* 107 (1985) 6718–6719.
- [31] R.C.G. Frem, A.C. Massabni, A.M.G. Massabni, A.E. Mauro, *Inorg. Chim. Acta* 255 (1997) 53–58.
- [32] H. Kunkely, A. Vogler, *Inorg. Chem. Commun.* 3 (2000) 143–144.
- [33] H. Kunkely, A. Vogler, *J. Organomet. Chem.* 684 (2003) 113–116.
- [34] L.A. Büldt, X. Guo, A. Prescimone, O.S. Wenger, *Angew. Chem. Int. Ed.* 55 (2016) 11247–11250.
- [35] L.A. Büldt, X. Guo, R. Vogel, A. Prescimone, O.S. Wenger, *J. Am. Chem. Soc.* 139 (2017) 985–992.
- [36] L.A. Büldt, O.S. Wenger, *Angew. Chem. Int. Ed.* 129 (2017) 5770–5776.
- [37] L.A. Büldt, O.S. Wenger, *Chem. Sci.* 8 (2017) 7359–7367.
- [38] L.A. Büldt, O.S. Wenger, *Dalton Trans.* 46 (2017) 15175–15177.
- [39] F. Durolo, J.P. Sauvage, O.S. Wenger, *Coord. Chem. Rev.* 254 (2010) 1748–1759.
- [40] W. Sattler, L.M. Henling, J.R. Winkler, H.B. Gray, *J. Am. Chem. Soc.* 137 (2015) 1198–1205.
- [41] W. Sattler, M.E. Ener, J.D. Blakemore, A.A. Rachford, P.J. LaBeaume, J.W. Thackeray, J.F. Cameron, J.R. Winkler, H.B. Gray, *J. Am. Chem. Soc.* 135 (2013) 10614–10617.
- [42] Y.Z. Liu, P. Persson, V. Sundström, K. Wärnmark, *Acc. Chem. Res.* 49 (2016) 1477–1485.
- [43] P. Chabera, Y. Liu, O. Prakash, E. Thyryhaug, A. El Nahhas, A. Honarfar, S. Essén, L. A. Fredin, T.C.B. Harlang, K.S. Kjaer, K. Handrup, F. Ericsson, Y. Tatsuno, K. Morgan, J. Schmidt, L. Häggström, T. Ericsson, A. Sobkowiak, S. Lidin, P. Huang, S. Styring, J. Uhlig, J. Bendix, R. Lomoth, V. Sundström, P. Persson, K. Wärnmark, *Nature* 543 (2017) 695–699.
- [44] S. Otto, N. Scholz, T. Behnke, U. Resch-Genger, K. Heinze, *Chem. Eur. J.* 23 (2017) 12131–12135.
- [45] S. Otto, M. Gräbelle, C. Förster, C. Kreitner, U. Resch-Genger, K. Heinze, *Angew. Chem. Int. Ed.* 54 (2015) 11572–11576.
- [46] Y. Zhang, J.L. Petersen, C. Milsmann, *J. Am. Chem. Soc.* 138 (2016) 13115–13118.
- [47] H.L. Yin, P.J. Carroll, B.C. Manor, J.M. Anna, E.J. Schelter, *J. Am. Chem. Soc.* 138 (2016) 5984–5993.
- [48] H.L. Yin, Y. Jin, J.E. Hertzog, K.C. Mullane, P.J. Carroll, B.C. Manor, J.M. Anna, E.J. Schelter, *J. Am. Chem. Soc.* 138 (2016) 16266–16273.

4.1 Ligand design

DU^E to its before mentioned $3d^{10}$ configuration, a ligand with a free π^* -orbital to allow for a metal to ligand charge transfer (MLCT) would be desirable. The π^* -orbitals of the ligands should be of such energy that the transition would occur in the visible region of the absorption spectrum. Due to a formal Ni(I) centre after the MLCT, this will result in a $3d^9$ configuration. Ni(0) favours a tetrahedral geometry, and it is to be expected that Ni(I) would prefer a higher coordination number where it could be possible that solvent molecules coordinate to the centre and further leading to radiationless deactivation of the excited state.^[76] In order to prevent excited state distortion, the ligand should provide enough steric bulk. Based on a previously published study on nickel-complexes with isonitrile ligands,^[51] it seemed promising to further develop the therein made discoveries. Namely to stabilise the Ni(0) center, π -accepting ligands should be applied. Here phosphines as a ligand motif were chosen. Further a ligand design with at least two equal coordination sites was desired, to further increase the complex stability through chelating ligands. This could further protect the complex against substitution reactions. The backbone of the ligand needed to be designed to enable a low-lying MLCT transition state and as mentioned before, the ligand should possess a certain bulkiness. These features were then combined and the ligand as shown in Figure 4.1 was designed. It was hoped that the π^* -orbitals of the naphthalene backbone would be of the right energy to allow for a low-lying MLCT excited state. The diphenylphosphines in 2 and 3 position should have a sufficient biting angle to coordinate a Ni-atom and the phenyls should be capable of increasing the steric demand to an extent enough to suppress significant excited state distortion and solvent molecule coordination.

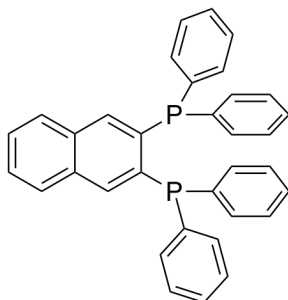


Figure 4.1: The designed phosphine ligand for possible emissive Ni(0)-complexes.

4.1.1 DFT calculations

D^FT calculations were performed to assess the success of the ligand design. Initially the structures were energy minimised at the MMFF level of theory using Spartan '08 version 1.2.0. These preoptimised structures were then calculated with Gaussian. Optimisation

of the ground-state geometry in different solvents was of interest as well as a calculation of the ground-state absorption spectrum. This was of special interest due to the desired MLCT absorption in the visible range of the spectrum. Different functionals were applied, namely the B3LYP and CAM-B3LYP.^[77,78] B3LYP is known to underestimate the energy of MLCT-transitions in comparison to CAM-B3LYP, whereas the latter models charge-transfer transitions better.^[79] The 6-31G(d,p) basis set was chosen for C, H, P and O atoms due to its good balance between calculational accuracy and computational costs.^[80] For the nickel atom LANL2DZ as an effective core potential was chosen.^[81,82]

First of all it was of interest whether the biting angle is large enough for a coordination to Ni(0). Additionally the steric demand of the phenyl-rings was a concern which might prevent coordination by steric repulsion. The optimisation and frequency calculations were followed with time-dependent DFT calculations to obtain the UV-Vis spectra. At first the calculations were done *in vacuo* and to get a hint of the solvent influence subsequently performed for MeCN, DCM, hexane, tetrahydrofuran (THF) and toluene. The results of the structure optimisation predict a homoleptic Ni(0) complex (Figure 4.2), therefore the attempt with the designed ligand seemed promising. The following calculations should reveal whether an absorption band in the visible is to be expected. The calculated UV-Vis absorption spectra (Figure 4.3) show that for all used functionals and solvents an absorption band in the visible can be expected. In all cases the CAM-B3LYP functional describes a spectrum shifted more

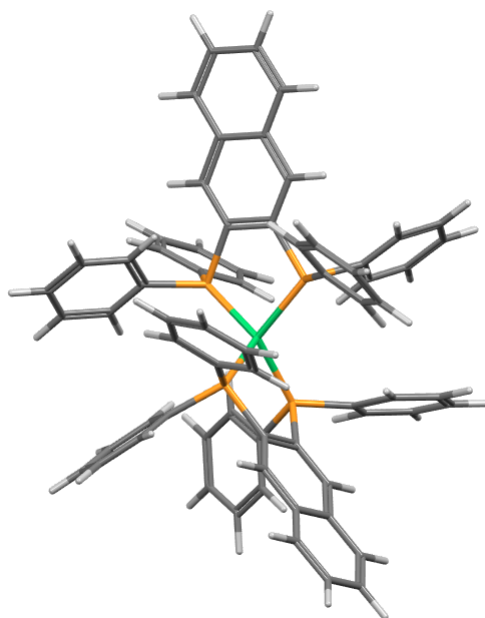


Figure 4.2: Calculated structure in toluene with with the B3LYP functional. Colour code is: Green the nickel-, orange the phosphorous-, black the carbon- and white the hydrogen-atoms.

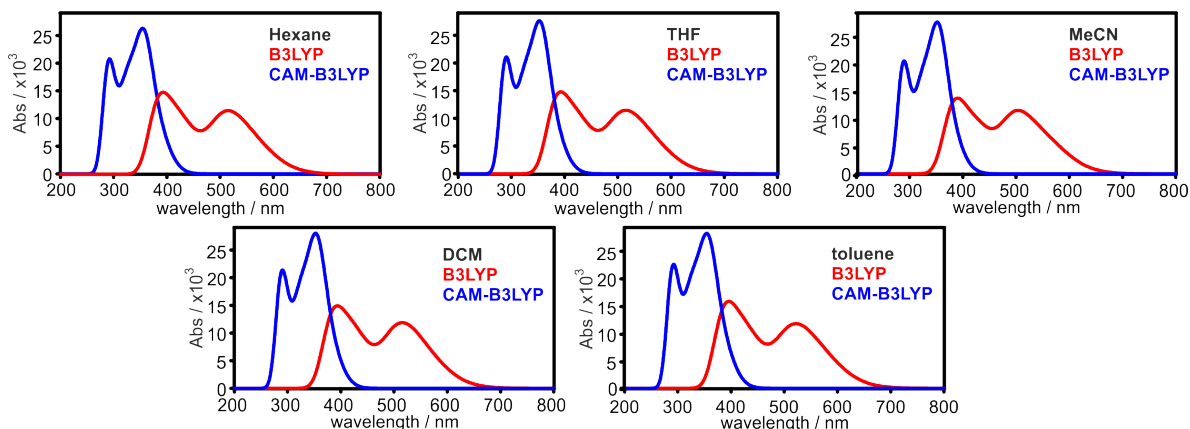


Figure 4.3: Calculated UV-Vis absorption spectra with the different functionals in different solvents.

to the red, whereas the B3LYP functionals predict an absorption spectrum more shifted to the blue. Anyhow an absorption in between these predictions can be expected. Both spectra show two distinct transition bands, independent of the used functional. From the calculations the main contribution is a transition from a nickel centred highest occupied molecular orbital (HOMO) to a naphthalene centred lowest unoccupied molecular orbital (LUMO). Due to the promising calculations, synthetic routes needed to be developed.

4.2 Synthesis

THE synthesis should start from easy available and cost efficient starting materials. Therefore 1,2,4,5-*tetra*-bromobenzene was chosen (Figure 4.4).

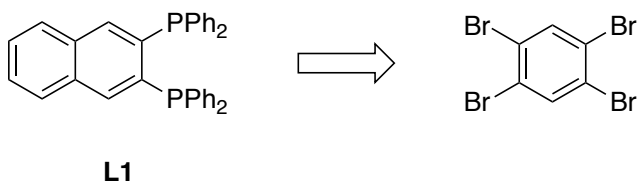


Figure 4.4: Retrosynthesis of the desired ligand **L1**.

Based on the work of the group of SPARR the 1,2,4,5-*tetra*-bromobenzene could be functionalised through a first treatment with *n*-butyl-lithium (BuLi) followed by a cycloaddition reaction with furan and a subsequent reduction to the 2,3-dibromonaphthalene (Figure 4.5).^[83–85] Both reaction steps worked with excellent yields (see chapter 7).

Different approaches for the transformation of the halides to the diphenyl phosphines were tried. First a double lithiation followed by an electrophilic attack with ClPPh₂ was attempted and did not lead to the desired product. Attempts were made to do the func-

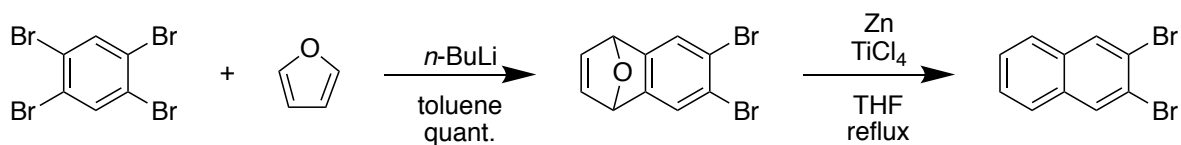


Figure 4.5: Synthesis of the precursor for the desired naphthalene based phosphine ligand **L1**.

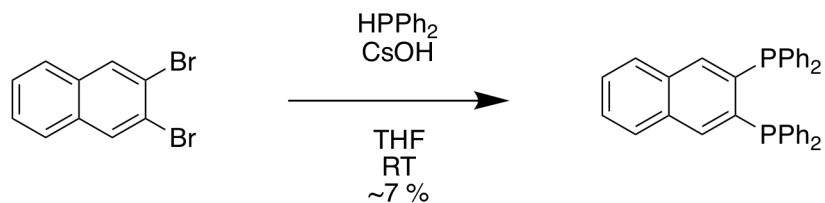


Figure 4.6: Synthesis after SALVATORE for the functionalisation to the diphenylphosphines.

tionalisation stepwise, but still no product could be obtained. Therefore the route by SALVATORE was applied which was reported for the functionalisation of 1,2-dibromobenzene to 1,2-bis(diphenylphosphino)benzene.^[86] The synthesis gave the desired ligand **L1**, though in low yields and the characterisation remained difficult (Figure 4.6). Though the $^1\text{H-NMR}$ spectrum shows the right integral of protons, there are several signals visible in the $^{31}\text{P-NMR}$ spectrum. However, a Matrix-assisted Laser Desorption/Ionization (MALDI) spectrum of the ligand could be obtained where no other species were visible (Figure 4.7). Therefore two equivalents of the tentative ligand were reacted with $\text{Ni}(\text{COD})_2$ in THF at RT. After removal

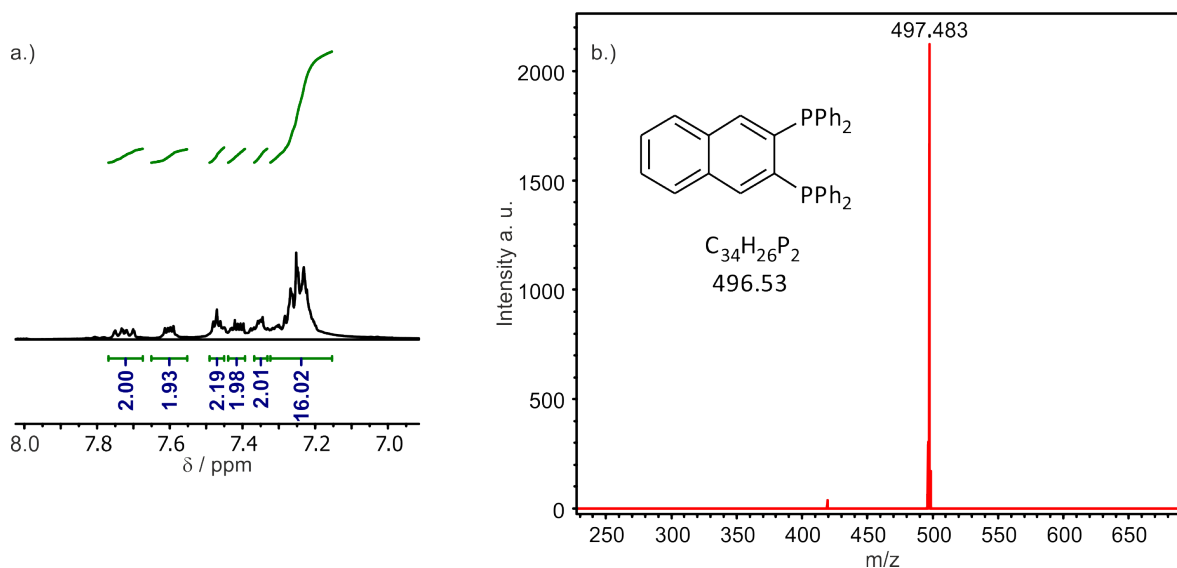


Figure 4.7: a.) Cut-out from the $^1\text{H-NMR}$ spectrum of the aromatic region of the tentative ligand **L1**. b.) MALDI spectrum of **L1**.

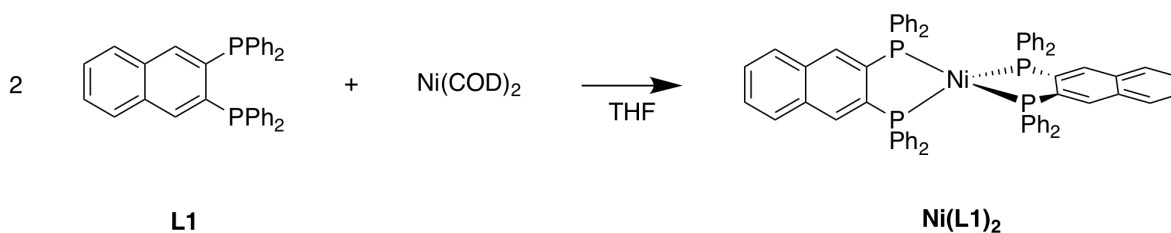


Figure 4.8: Synthesis of the complex after CUMMINS.

of the solvent a dark red crystalline solid was obtained (Figure 4.8).^[87] Solely a MALDI spectrum was obtained that only showed the desired mass peak, but only in very low intensity (Figure 4.9). A satisfying $^1\text{H-NMR}$ spectrum could not be obtained, due to the pronounced air- and water sensitivity of the compound. The compound proved to be significantly more robust in the solid state compared to solution. The decomposition in solution could be followed by the bleaching of the colour of the solution.

4.3 UV-Vis and steady-state luminescence spectroscopy

ALTHOUGH only a MALDI-spectrum gave indication of the successful synthesis, spectroscopic investigations were performed, to evaluate the potency of the complex as new luminophore. To determine the energy of the MLCT transition, a UV-Vis spectrum in dry and deaerated toluene under an Ar-atmosphere was recorded (Figure 4.10). The spectrum consists of a very broad and unstructured absorption band with a long tail in the red. The maximum is around 500 nm and around 380 nm slight maxima can be seen which could be

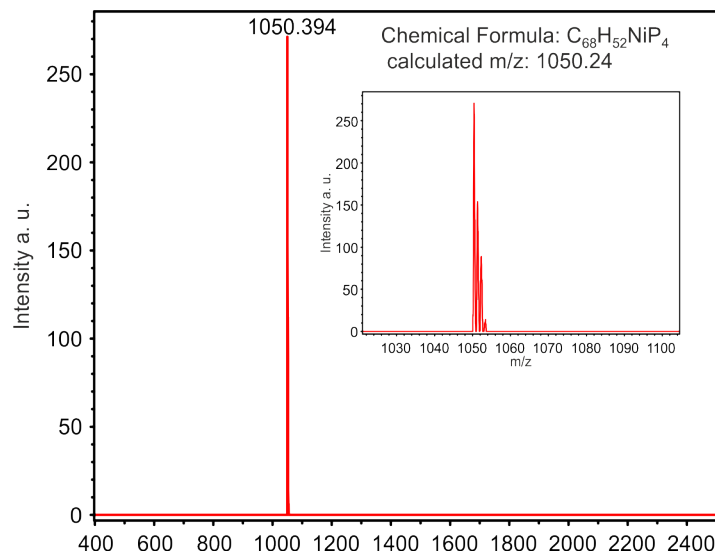


Figure 4.9: MALDI spectrum of the Ni(L1)_2 complex.

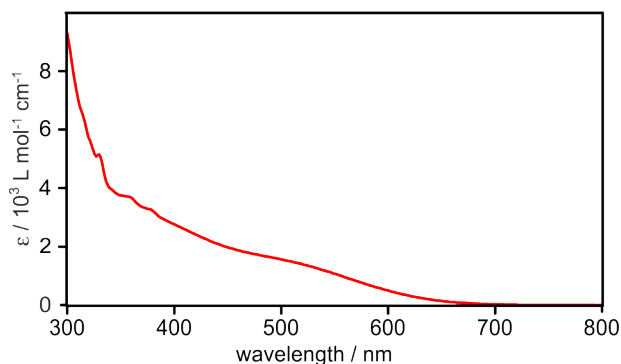


Figure 4.10: UV-Vis spectrum of the tentative $\text{Ni}(\mathbf{L1})_2$ complex was recorded in dry and deaerated toluene.

tentatively attributed to the vibronic fine structure for the naphthalene absorption, where this pattern is characteristic.^[88] It was assumed that the broad absorption feature which tails nearly to 640 nm can only be a result of an MLCT, therefore the emission of the complex was tested after excitation at 530 nm. After excitation of an 300 μM solution of the $\text{Ni}(\mathbf{L1})_2$ -complex in deaerated and dry toluene at 530 nm, emission bands with a maximum at 600 nm were visible (Figure 4.11). The emission spectrum shows the same structured pattern that was also slightly seen in the absorption spectrum. The maxima are at 565, 580, 595 and 610 nm. The structured emission leads to the assumption that the emission is ligand centred. Further a broad band around 750 nm is detectable and a sharp band at 790 nm. Most likely these are artifacts, due to the insufficient sensitivity of the detector in this region. To proof that at 530 nm it is not the ligand that was excited and the emission is solely originating from the complex $\text{Ni}(\mathbf{L1})_2$, an emission spectrum of the free ligand **L1** was recorded under the same conditions. After excitation at 530 nm, the free ligand **L1** shows no emission. In Figure 4.12 it can be seen that the ligand shows only emission after excitation at 350 nm, and the emission occurs shifted to the blue compared to the emission spectrum of the complex,

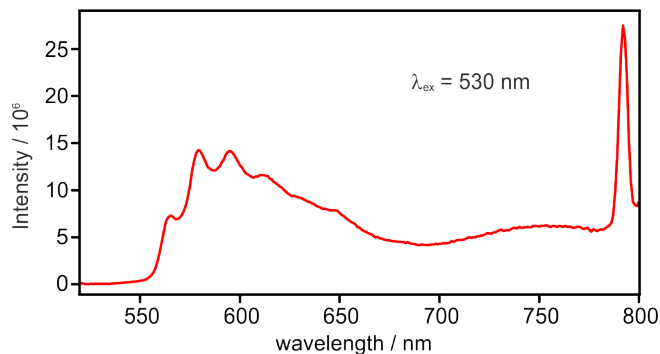


Figure 4.11: Photoluminescence spectrum of $\text{Ni}(\mathbf{L1})_2$ in 300 μM solution in deaerated and dry toluene after excitation at 530 nm.

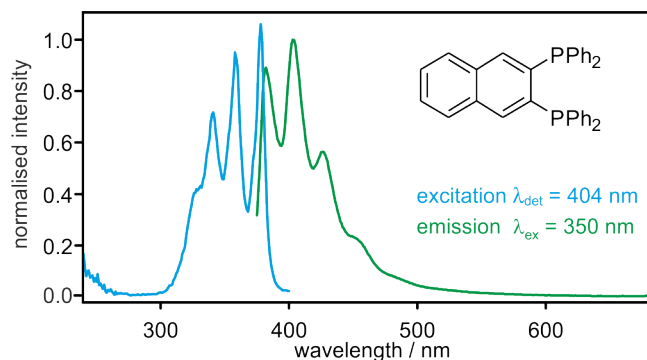


Figure 4.12: Green: Emission spectrum of the ligand **L1** after excitation at 350 nm. Blue: Excitation spectrum of the ligand with a detection wavelength $\lambda_{det} = 404$ nm.

which is expected due to the change in the electronic structure after complexation to the nickel-centre. Further an excitation spectrum of **L1** was recorded and the detection wavelength was $\lambda_{det} = 404$ nm. The structure is similar to the less prone visible structure in the UV-Vis spectrum (Figure 4.10).

4.4 Transient emission spectroscopy

THE steady-state emission spectrum showed a band with a maximum around 600 nm and a structured shape (Figure 4.11). To determine the time constant of the emission, the complex was subjected to transient emission spectroscopy. The emission can indeed be seen in the transient setup (Figure 4.13). Though the fine structure is not resolved, the maximum fits to the steady-state emission spectrum (Figure 4.11). The very sharp peak seen at 532 nm in Figure 4.13 can be attributed to stray light from the laser used as excitation source. The lifetime of the emission was too short to be measured with the transient setup (pulse length ~ 10 ns), therefore the sample was subjected to time correlated single photon counting (TCSPC) to determine the lifetime of the emissive state. The TCSPC-spectrometer

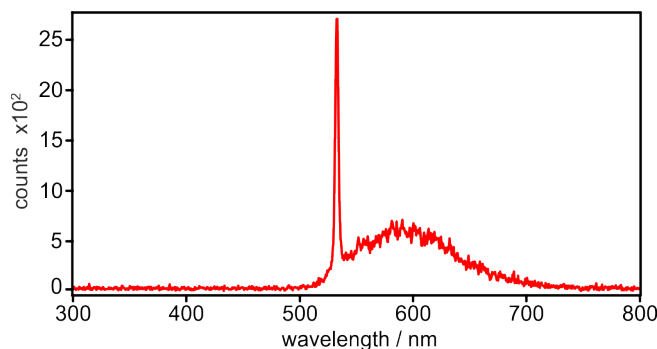


Figure 4.13: Transient emission spectrum recorded after excitation of a 300 μ M solution of $\text{Ni}(\mathbf{L1})_2$ in dry and deaerated toluene at 532 nm with laser pulses of ~ 10 ns duration.

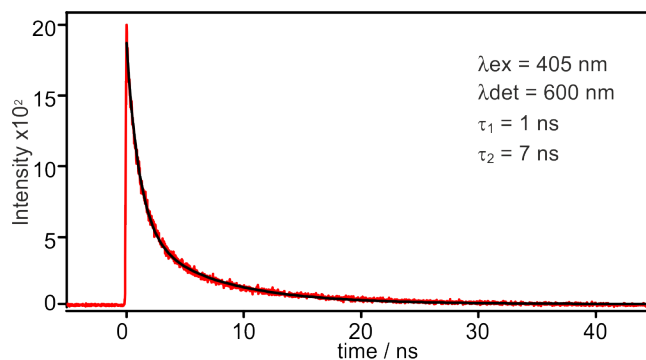


Figure 4.14: Decay of the emission measured at 600 nm after excitation at 405 nm of a 300 μM solution of $\text{Ni}(\mathbf{L1})_2$ in deaerated and dry toluene. The time constants as well as the excitation (λ_{ex}) and detection (λ_{det}) wavelengths are given in the inset.

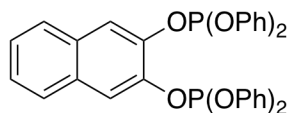
could only excite at 405 nm. The decay-curve shows an bi-exponential behaviour leading to two time constants with a short component $\tau_1 = 1$ ns (72%) and a longer component $\tau_2 = 7$ ns (28%) (Insets in Figure 4.14).

Due to the fact that 405 nm is close to the ligand absorption itself (Figure 4.12), it is not sure whether the emission observed originates solely from the complex or shows additional contributions from the free ligand. Anyhow, the emission from the complex appears at approximately 600 nm whereas the ligand emission maximum is at 404 nm. Therefore ligand centred emission as the origin of the second decay component is unlikely.

4.5 Summary and Outlook

IN this chapter a promising new Ni(0) based luminophore was presented. The synthesis of the phosphine-naphthalene ligand **L1** was presented as well as the complexation with $\text{Ni}(\text{COD})_2$. Problems remained in the characterisation of the complex, due to its high air- and moisture sensitivity. Anyhow, the preliminary results show that this complex could, after improvement of the synthesis, be a new photosensitiser with potential application in emitting devices, as dyes in solar cell or as sensitiser for organic photoredox catalysis.

To further improve the luminescent nickel-complexes, a promising approach could be the use of phosphites instead of phosphines, due to their higher π -accepting properties and therefore better stabilisation of the electron-rich nickel(0)-centre (Figure 4.15).^[89]



L2

Figure 4.15: Potential phosphite ligand.

4.5.1 Phosphite ligand

THE presented ligand in chapter 4.5 seemed to be worth exploring. Therefore synthetic approaches towards a phosphite naphthalene ligand **L2** were made. The clean synthe-

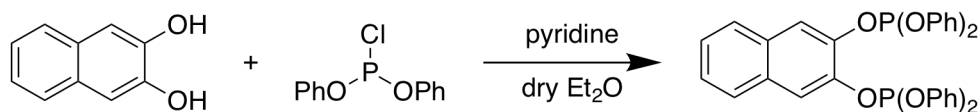


Figure 4.16: Synthetic approach towards the desired phosphite ligand **L2**

sis of the diphenyl phosphorochloridite turned out to be rather challenging. The diphenyl phosphorochloridite should be available through a direct coupling of phenol with phosphorus trichloride.^[90] The purification was reported via distillation.^[90] Unfortunately it was not possible to separate the diphenyl phosphorochloridite from the triphenylphosphite (Figure 4.17).^[91] Despite the failed purification of the diphenyl phosphorochloridite, the mixture was subjected to the procedure depicted in Figure 4.16 because it was expected that the triphenylphosphite will not undergo the coupling with the 2,3-dibromo-naphthalene and the purification might become easier after the reaction. Unfortunately this did not lead to the desired product and no product was obtained.

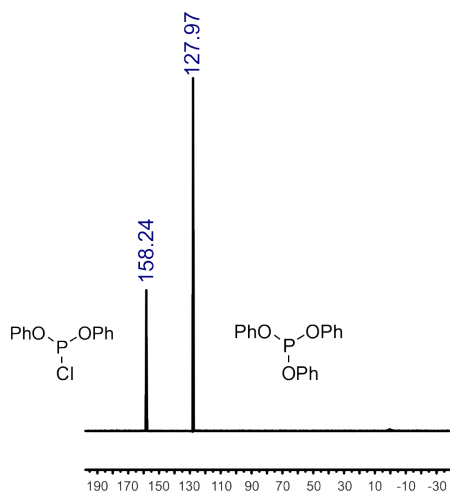


Figure 4.17: Excerpt from the ^{31}P -NMR spectrum after distillation. The diphenyl phosphorochloridite was not separable from the triphenylphosphite.

5 New luminescent Titanium-complexes

RUTHENIUM tris(bipyridine) is the benchmark for a class of photosensitisers exhibiting a long living $^3\text{MLCT}$ excited state. To this class many other complexes based on noble metals can be counted, such as Os(II),^[92] Re(I),^[93,94] and Ir(III).^[95–98] The use of more earth abundant metals as luminophores, combined with the same photo-physical properties as their noble role models, could be a promising alternative.

Titanium is the ninth most earth-abundant metal in the earth's crust (Figure 5.1).^[99] Its abundance makes it a desirable element for photoluminescent devices. A possible approach for photoluminescent devices is the utilisation of electron rich metals and π -accepting ligands (as discussed in chapter 4) to allow for a low-lying MLCT transition. Due to the heavy metal effect of the complex centre, these can often undergo Intersystem Crossing (ISC) that leads to a long living triplet excited state.^[101,102] Another possible strategy is the design of metal complexes with electron deficient metals and electron rich ligands in order to access low energy ligand to metal charge transfer (LMCT) states. Therefore titanium in its oxidation state +4 and other d^0 elements, seem to be a plausible choice for a photoactive transition metal compound. Only a few relying on these d^0 -metals have been reported until today. For example MILSMANN *et al.* reported on a luminescent Zr(IV)-complex with electron rich pyrrolide ligands.^[103] The titanium analogue was also synthesised and characterised via X-ray diffraction spectroscopy. For the synthesis of the complexes 2,6-bis(5-methyl-3-phenyl-1H-pyrrol-2-yl)-pyridine ($\text{H}_2^{\text{Me}}\text{PDP}$) served as a ligand. The $\text{Ti}(\text{MePDP})_2$ -complex shows two absorption bands with maxima at 777 nm ($\epsilon = 9669 \text{ M}^{-1} \text{ cm}^{-1}$) and 459 nm ($\epsilon = 22012 \text{ M}^{-1} \text{ cm}^{-1}$). Excitation in these tentatively assigned charge-transfer bands did not lead to any detectable emission. $\text{Zr}(\text{MePDP})_2$ shows a similar absorption spectrum, but shifted to the blue, with a maximum in the visible at 528 nm ($\epsilon = 27001 \text{ M}^{-1} \text{ cm}^{-1}$). Further absorption

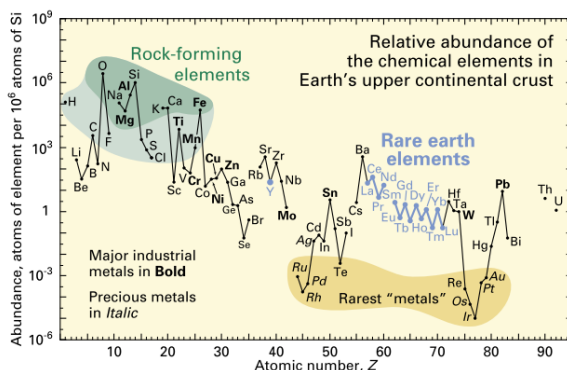


Figure 5.1: Earth abundance of the elements in the upper crust of the earth. The elements are grouped in Rock-forming elements (most common elements), Rare earth elements and rarest 'metals'. Illustration taken from USGS.^[100]

bands can be found at 346 nm ($\epsilon = 40028 \text{ M}^{-1} \text{ cm}^{-1}$) and 300 nm ($\epsilon = 61582 \text{ M}^{-1} \text{ cm}^{-1}$). Excitation in any of the bands lead to an emission at RT with a maximum at 594 nm.^[103] These results show, that luminescence can be achieved from d^0 transition metals with electron rich ligands, though the right ligand design to obtain RT emission is rather challenging.

5.1 Pyrrol-based ligands

5.1.1 Ligand design

THE results of MILSMANN set the foundation for LMCT based luminescence from d^0 transition metals. Following their path, a ligand should have strong donating characteristics to stabilise the electron deficient metal centre. Two approaches towards luminescent Ti-complexes were developed.

The idea was to synthesise a tridentate ligand that has a higher stability through the chelating effect compared to monodentate ligands, with pyrroles as binding motifs. A route towards a possible structure was developed based on priorly published protocols (Figure 5.2).^[104–107] It was hoped that two ligands would complex the titanium-centre in an octahedral fashion.

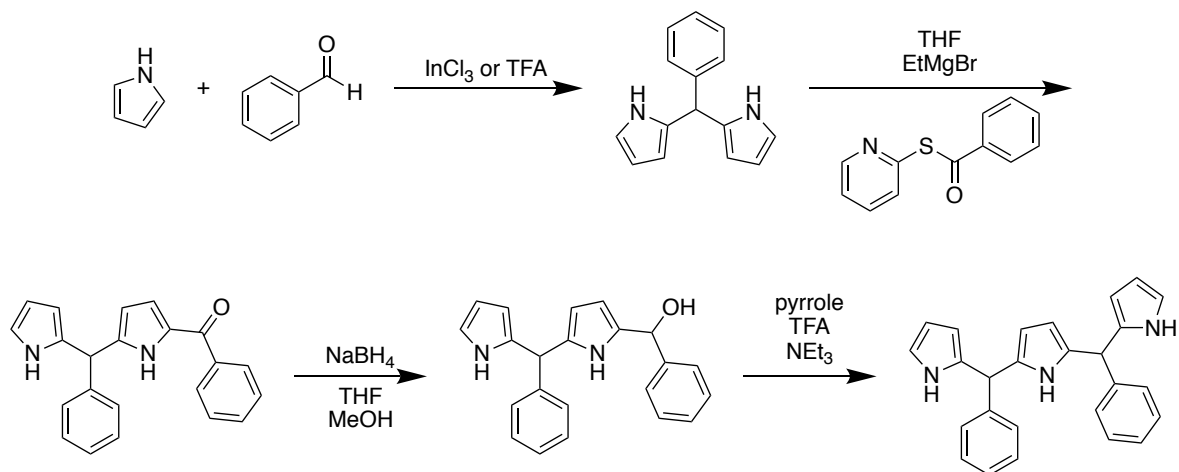


Figure 5.2: Developed synthesis of a pyrrol-based tridentate chelate ligand. Prior to complexation a reduction would be desired to extend the π -system of the ligand.

5.1.2 Synthesis

THE synthetic route presented in Figure 5.2 was tested. Freshly distilled pyrrole was supposed to be reacted with benzaldehyde to form the phenyl dipyrromethane. An indium chloride and trifluoro acetic acid catalysed method was tried. The indium chloride catalysed method followed a former published protocol which was slightly changed.^[108] The product could be obtained, but the purification from the N-confused byproduct was not possible.

Therefore the trifluoro acetic acid catalysed method was tried.^[109] Here the product could not be purified from any of the byproducts. The synthesis of the Mukaiyama coupling reagent S-2-Pyridyl benzothioate however worked in excellent yields (93%).^[106] The product mixture of the indium-catalysed reaction was therefore subjected to the coupling with EtMgBr and the Mukaiyama reagent, but this did not lead to any formation of the desired product. Due to the major synthetic issues, another approach for titanium complexes was developed (see chapter 5.2).

5.2 Scorpionate ligands

5.2.1 Ligand design

SCORPIONATE ligands were chosen as another promising class as ligands for a complexation with Ti(IV). Tris(pyrazolyl)borates are a very successful class of ligands which lead to the development of new strongly donating ligands.^[110] This class has been known since the 1960's,

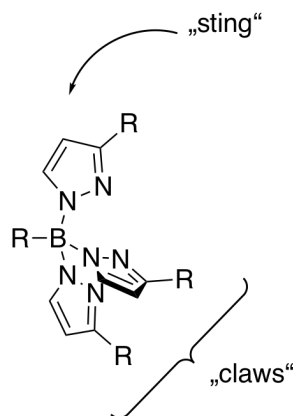


Figure 5.3: The so called 'scorpionate'-ligand was named after a scorpion holding its prey. Two ligands resemble the claws and the third one the sting.

discovered by TROFIMENKO, where he replaced the H-atoms from the borohydride anion with pyrazolyl rings.^[111,112] The name was developed due to the resemblance of the ligand to a scorpion holding its prey (Figure 5.3). Based on the aforementioned design, the pyrazolyl rings were exchanged to NHC rings, in order to obtain an even stronger σ -donating ligand.

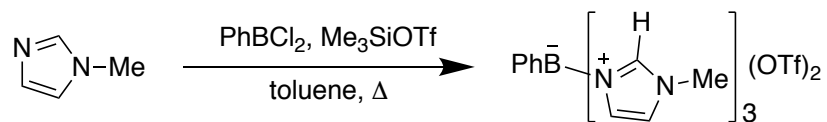


Figure 5.4: Developed synthesis for the NHC-based scorpionate ligand. The synthesis has been reported priorly with a mesityl or *tert*-butyl substitution instead of a methyl-group.^[113]

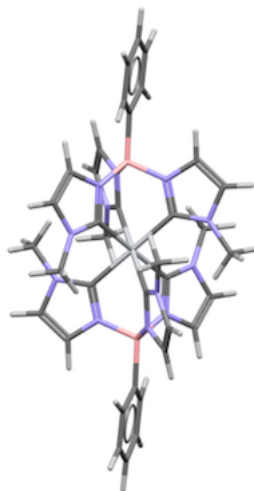


Figure 5.5: Molecular mechanics energy minimisation calculation of the $[\text{Ti}(\text{PhB-MeIm})_2]^{2+}$ complex.

The ligand was synthesised after a priorly reported protocol by SMITH *et al.* where instead of mesityl or *tert*-butyl substituents on the nitrogen-atom of the NHC, a methyl-group (MeIm) was chosen (Figure 5.4). This was due to the fact that SMITH only reported on iron and cobalt complexes with one ligand attached, whereas with the titanium a homoleptic complex with two ligands was desired. Therefore the steric bulk needed to be reduced, in order to allow for coordination of two ligands. To see whether the reduction of the steric bulk with a methyl-group would be sufficient, molecular mechanics energy minimisation calculations performed at the MMFF level of theory using Spartan '08 Version 1.2.0 were carried out. The outcome of the calculations can be seen in Figure 5.5 and reveals that a methyl-substitution should allow for a complexation to the titanium-centre.

5.2.2 Synthesis

THE synthetic route of the scorpionate ligand depicted in Figure 5.4 afforded the ligand in excellent yields (see chapter 7 for synthetic details). The obtained ligand was then deprotonated with lithium diisopropylamide (LDA) and further complexated with TiCl_4 . This procedure yielded a red, orange crystalline solid. This crystalline structure was then analysed via NMR (Figure 5.6). Chemical shifts of the ligands proton signals are shifted to the lower field. This would be expected due to the deshielding of the protons through the electron deficient Ti(IV) centre. Unfortunately the complex could not be measured via ESI-MS which was surprising, due to its charged character. It is assumed that the complex due to its quite compact structure decomposes during the ionisation process.

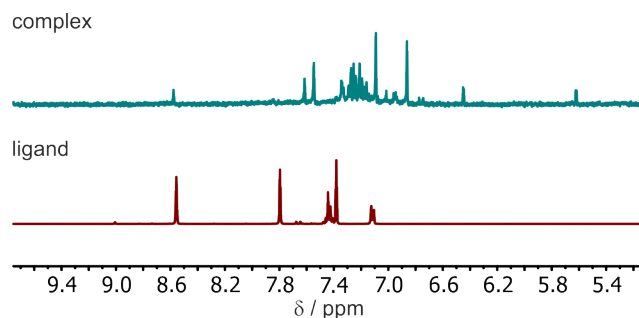


Figure 5.6: NMRs of the ligand (top) and the tentatively obtained $[\text{Ti}(\text{MeIm}_3)_2]\text{OTf}_2$ (bottom). It can be seen that the proton signals shift.

5.2.3 Spectroscopy

ALTHOUGH the characterisation of the obtained compound remained speculative, further spectroscopical investigations were performed, to see whether a further characterisation would be of interest. In the UV-Vis spectrum, an absorption band, which can be tentatively attributed to an LMCT, has a long tail into the visible region of the absorption spectrum up to 500 nm (see Figure 5.7 a.)). Further transitions can be seen in the UV with a maximum around 320 nm. This can most probably be attributed to a ligand centered $\pi^* \leftarrow \pi$ transition. Compared to the free ligand this absorption is shifted to the red. Due to its colour and the absorption around 430 nm, an emission spectrum was recorded. In the steady-state luminescence spectrum an emission band with a maximum at 490 nm can be detected (Figure 5.8). Due to the excitation further in the red compared to the ligand-absorption (see Figure 5.7 b.)), the detected emission seems likely to originate from an LMCT-transition.

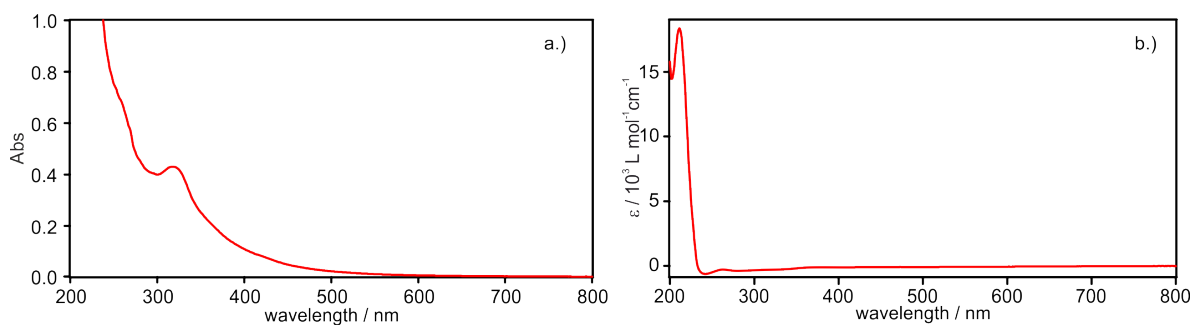


Figure 5.7: a.) UV-Vis spectrum of the tentatively obtained $[\text{Ti}(\text{MeIm}_3)_2]\text{OTf}_2$ complex measured in dry and deaerated MeCN. b.) UV-Vis spectrum of the free scorpionate ligand measured in MeCN. Both spectra were recorded at RT.

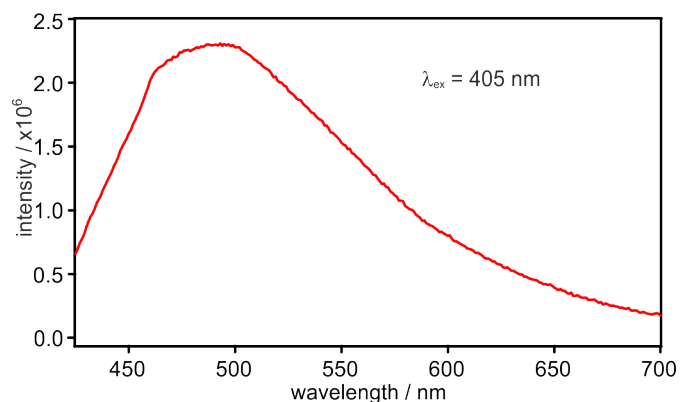


Figure 5.8: Steady-state luminescence spectrum of a solution of the tentatively obtained $[\text{Ti}(\text{MeIm}_3)_2](\text{OTf})_2$ complex in deaerated and dry toluene after excitation at 405 nm.

5.2.4 Summary and Outlook

The preliminary results obtained from the spectroscopic data of $[\text{Ti}(\text{MeIm}_3)_2](\text{OTf})_2$ definitely show that a further investigation is necessary. A complete characterisation will be of interest. Additionally, investigation of the corresponding Zr(IV) complex should be promising. The larger Zr(IV)-atom might have a better fit into the binding pocket of the scorpionate ligand and allows for a less dense structure, compared to the smaller Ti(IV) centre.

6 Experimental

6.1 General

All experiments that are air- or hydrolysis sensitive, were carried out in oven dried glass apparatuses under a nitrogen or argon atmosphere. All syringes and cannula were flushed with nitrogen / argon three times prior to usage.

Dry solvents were used as received from the producer and if necessary were degassed via the freeze, pump, thaw method or ultrasonification under N₂ flow, alternating with evacuation. Dry diethyl ether, THF and DCM were obtained from a solvent purification system of INNOVATIVE TECHNOLOGY.

6.2 Reagents

All purchased chemicals were used without further purification, if otherwise it is stated.

6.3 Chromatography

The purification via column chromatography was carried out with silica gel from SILICYCLE (silica flash, 40 - 63 μm , (230 - 400 mesh ASTM) for flash column chromatography). For thin layer chromatography (TLC) pre-coated aluminium sheets were used with silica 60 from MERCK with a fluorescence indicator F254 and a thickness of 0.25 mm. The detection was done with UV light with wavelengths of 254 nm and 365 nm.

6.4 Nuclear Magnetic Resonance Spectroscopy

All Nuclear Magnetic Resonance (NMR) spectra were recorded on the following machines:

- an Avance III 400 BRUKER (400 MHz)
- an Avance III 500 BRUKER (500 MHz).

All temperature dependent NMR experiments were performed on a Bruker Avance III NMR spectrometer operating at 600 MHz proton frequency. The instrument was equipped with an inverse 5-mm BBI probe. The experiments were performed at the indicated temperature which was calibrated using a methanol standard showing accuracy within ± 0.2 K.

The chemical shifts are given in δ values in ppm referred to the residual proton content of the nonperdeuterated solvents or its carbon atoms, respectively.^[114]

	¹ H-NMR	¹³ C-NMR
CDCl ₃	7.26 ppm	77.0 ppm
DMSO- <i>d</i> ₆	2.50 ppm	39.5 ppm
acetone- <i>d</i> ₆	2.84 ppm	29.8, 206.3 ppm
CD ₃ CN	1.94 ppm	1.32, 118.3 ppm

The deuterated solvents for NMR-spectroscopy were purchased from CAMBRIDGE ISOTOPE LABORATORIES.

To describe the signals and their coupling patterns the following abbreviations are used: s (singlet), d (doublet), dd (doublets of doublet), ddd (doublets of doublet of doublet), dt (doublets of triplet), t (triplet), q (quartet), sept (septet), m (multiplet). All coupling constants J are stated in Hertz (Hz).

6.5 Mass Spectrometry

Electrospray Ionization (ESI)-measurements were carried out on a BRUKER Esquire 3000plus Ion-Trap ESI-MS (positive and negative mode). The quotients of mass to charge (m/z) are given and the relative intensities related to the basis peak ($I=100$) are given in brackets.

MALDI-measurements were performed using a MALDI plate MSP 96 target ground steel on a BRUKER Microflex with *trans*-2-[3-(4-*tert*-Butylphenyl)-2-methyl-2-propenylidene]malononitrile (DCTB) as a matrix.

6.6 Elemental Analysis

Elemental Analysis was performed by Ms. Sylvie Mittelheisser (University of Basel, Department of Chemistry), with a Vario Micro Cube instrument from ELEMENTAR.

6.7 UVvis spectroscopy

All optical absorption measurements were performed with a Cary5000 UVvis-NIR spectrophotometer.

6.8 Cyclic Voltammetry

Cyclic Voltammograms were recorded with a Versastat3-200 potentiostat from PRINCETON APPLIED RESEARCH. The measurements were performed in dry, deaerated acetonitrile with TBAPF₆ as electrolyte (0.1 M). The potential sweep rate was 0.1 V/s. As working electrode, a glassy carbon disc electrode was used. As a counter electrode a silver wire was used and a saturated calomel electrode (SCE) electrode served as reference. The Versastat3-200 potentiostat was also used for spectro-electrochemical measurements, where a quartz cuvette equipped with a platinum grid as working electrode, a silver wire as a counter electrode and an SCE as reference were employed.

6.9 Transient UVvis absorption measurements

A LP920-KS spectrometer from EDINBURGH INSTRUMENTS, equipped with a R928 photomultiplier and an iCCD camera from ANDOR, was used for transient absorption measurements

on the nanosecond (ns)-timescale. As an excitation source a frequency doubled Quantel brilliant b Laser was used with an approximate pulse length of 10 ns. All measurements were performed in quartz cuvettes from STARNA. When working under inert conditions, Schlenk-cuvettes were used and the solutions were deaerated with three freeze-pump-thaw cycles. For measurements on the picosecond (ps)-timescale a TRASS instrument from HAMAMATSU and a mode locked Nd:YVO₄/YAG-laser (model PL2251B-20-SH/TH/FH with PRETRIG option from EKSPLA) as excitation source ($\lambda = 532$ nm) were used.

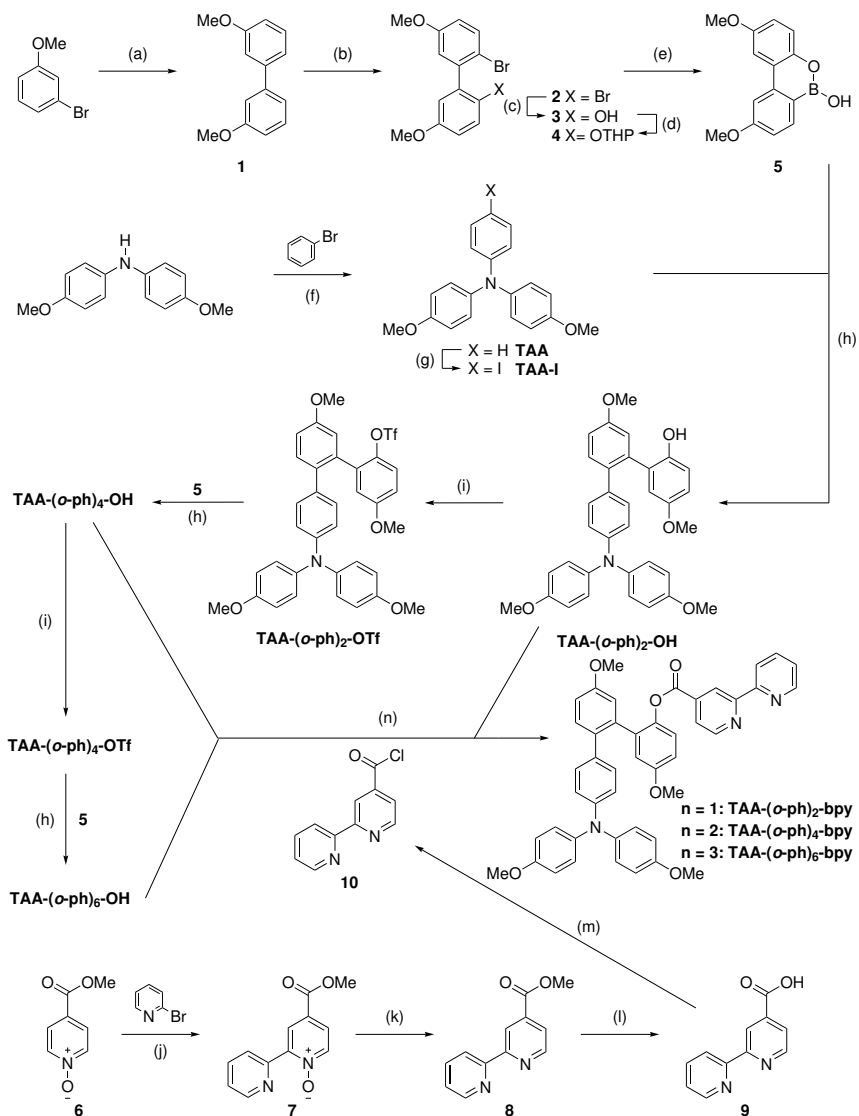
6.10 Luminescence Spectroscopy

Steady-state luminescence measurements were performed on a Fluorolog-322 from HORIBA JOBIN-YVON.

7 Syntheses

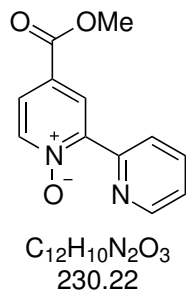
7.1 Synthesis of the oligo-*ortho*-phenylene dyads

The dyads were synthesised according to Scheme 1.



Scheme 1: (a) Mg, THF, FeCl₃, 1,2-dichloroethane (b) Br₂, AcOH (c) *n*-BuLi, B(*O*-*i*-Pr)₃, THF, NaOH, H₂O₂ (d) DCM, PPTS, DHP (e) *n*-BuLi, B(*O**i*Pr)₃, THF, HCl (f) CH₃CONa, Pd(*dba*)₂, HP^{*t*}Bu₃BF₄, toluene (g) [Bis(trifluoro)acetoxyiodo]benzene, I₂, DCM (h) Pd(OAc)₂, SPhos, K₃PO₄·H₂O, THF / H₂O (4:1) (i) Tf₂O, PPTS, DCM (j) Pd(OAc)₂, K₂CO₃, HP^{*t*}Bu₃BF₄, toluene (k) Pd / C, H₂, EtOH, (l) NaOH, MeOH (m) SOCl₂ (n) NaOH, N^{*t*}Bu₄Cl, DCM

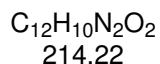
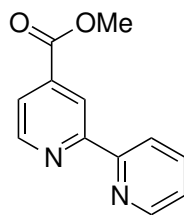
Synthesis of 4-(methoxycarbonyl)-[2,2'-bipyridine] 1-oxide (7)



Methylisonicotinate-*N*-oxide (**6**) (1.00 g, 6.52 mmol, 2.00 eq.), tri-*tert*-butylphosphonium tetrafluoroborate (114 mg, 0.39 mmol, 0.06 eq.), K_2CO_3 (900 mg, 6.52 mmol, 2.00 eq.), $Pd(OAc)_2$ (72 mg, 0.326 mmol, 0.05 eq.) and 2-bromopyridine (0.32 mL, 3.26 mmol, 1.00 eq.) were suspended in dry toluene under a nitrogen atmosphere. The solution was deaerated via bubbling N_2 through for 15 minutes (min). Afterwards, the solution was stirred at room temperature (RT) for 15 min, then sealed and heated to 120 °C for 22 h. The solution was allowed to RT and then directly purified via flash column chromatography (acetone) on silica. The desired product was obtained as a beige solid (562 mg, 2.44 mmol, 75% [Lit.^[115]: 60% (for ethoxy-derivative)]).

1H -NMR (400 MHz, $CDCl_3$): δ (ppm) = 8.83 - 8.76 (m, 3H), 8.32 (dd, J = 6.8, 0.7 Hz, 1H), 7.89 - 7.83 (m, 2 H), 7.41 - 7.37 (m, 1H), 3.96 (s, 3 H).

MS (ESI) m/z (relative intensities): $[2M+Na^+]^+$ 482.93 (50); calcd. 483.13, $[M+Na^+]^+$ 252.88 (50); calcd. 253.06, $[M+H^+]^+$ 230.92 (17); calcd. 231.08.

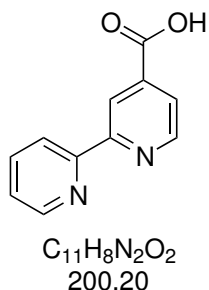
Synthesis of [2,2'-bipyridine]-4-carboxylic acid, methyl ester (8)

Compound **7** (246 mg, 1.09 mmol, 1.00 eq.) was dissolved in dry ethanol (EtOH) and the solution degassed via ultrasonification under N₂ flow, alternating with evacuation. Pd/C (10 mg) was added to the solution and a balloon filled with H₂ was attached via tap to the flask. The mixture was vigorously stirred overnight and then further Pd/C catalyst was added (20 mg), and the reaction further stirred for 3 h. The completion of the reaction was determined via TLC. The reaction mixture was filtered over celite, washed with EtOH and the solvent removed under reduced pressure. The desired product was obtained as a brownish solid (214 mg, 1.07 mmol, 98% [Lit.^[115]: 96% (for ethoxy-derivative)]).

¹H-NMR (400 MHz, CDCl₃): δ(ppm) = 8.93 (s, 1H), 8.82 - 8.89 (m, 1H), 8.72 - 8.69 (m, 1H), 8.42 - 8.40 (m, 1H), 7.87 - 7.78 (m, 2H), 7.36 - 7.28 (m, 1H), 3.97 (s, 3H).

¹³C-NMR (101 MHz, CDCl₃): δ(ppm) = 165.7 (C_q), 157.3 (C_q), 155.3 (C_q), 149.9 (CH), 149.4 (CH), 138.5 (C_q), 137.0 (CH), 124.1 (CH), 122.8 (CH), 121.2 (CH), 120.4 (CH), 52.6 (CH₃).

MS (ESI) *m/z* (relative intensities): [M+K⁺]⁺ 252.86 (40); calcd. 253.04, [M+Na⁺]⁺ 236.9 (100); calcd. 237.06, [M+H⁺]⁺ 214.94 (48); calcd. 215.08.

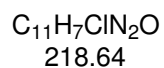
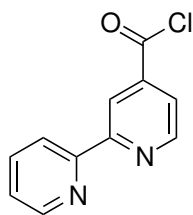
Synthesis of 2,2'-bipyridine-4-carboxylic acid (9)

Compound **8** (214 mg, 1.00 mmol, 1.00 eq.) was dissolved in hot methanol (MeOH) (1.0 mL). A solution of aqueous (aq.) sodium hydroxide (NaOH) solution (1 N, 1.00 mL, 1.00 mmol, 1.00 eq.) was added and then stirred at RT overnight. The solvent was removed under reduced pressure and then the aq. solution acidified to pH 3.5 - 4 with aq. 0.5 N hydrochloric acid (HCl) solution. Upon cooling a precipitate formed, which was filtered and washed with water. The product was obtained as an off-white solid (168 mg, 840 μ mol, 84% [Lit.^[61]: 89%]).

¹H-NMR (400 MHz, CDCl₃): δ (ppm) = 9.35 (s, 1H), 9.01 (d, J = 4.1 Hz, 1H), 8.89 (d, J = 4.6 Hz, 1H), 8.58 (d, J = 7.9 Hz, 1H), 8.01 - 7.96 (m, 1H), 7.72 - 7.63 (m, 1H), 7.58 - 7.43 (m, 2H).

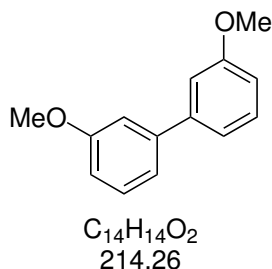
MS (ESI) m/z (relative intensities): [M+H⁺]⁺ 200.94 (100); calcd. 201.07.

Synthesis of 2,2'-bipyridine-4-carbonyl chloride (10)



The reaction followed a former published protocol.^[116]

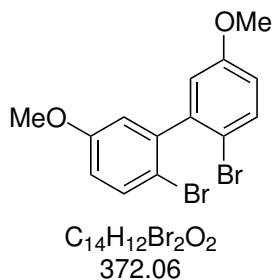
Compound **9** was refluxed in thionyl chloride for ~18 h. The excess thionyl chloride was removed under reduced pressure and the yellowish residue dried on high vacuum for at least 4 h. The reaction was assumed to furnish the desired product in quantitative yields and was used directly in the next step.

Synthesis of 3,3'-dimethoxy-1,1'-biphenyl (1)

The reaction followed a previously published protocol.^[117] Magnesium turnings (6.70 g, 275 mmol, 1.10 eq.) were covered with dry THF under a nitrogen atmosphere and subsequently dry THF (500 mL) and 2-bromoanisole (46.8 g, 250 mmol, 1.00 eq.) were added while the Grignard reaction was running. After the addition of 2-bromoanisole was complete, the black reaction mixture was refluxed for 1 h and meanwhile a solution of $FeCl_3$ (1.22 g, 7.5 mmol, 0.03 eq.) and 1,2-dichloroethane (11.85 mL, 250 mmol, 1.00 eq.) in dry THF (250 mL) was prepared. After allowing the Grignard reaction mixture to reach RT, it was transferred via cannula to the solution containing $FeCl_3$. The resulting mixture was then stirred for 10 min at RT and then aq. HCl-solution (250 mL, 1 M) was added. The aq. phase was extracted three times with DCM and the combined organic phases were dried over Na_2SO_4 . The desired product was obtained after a short filter column (DCM) as a colourless oil (25.96 g, 121 mmol, 97% [Lit.^[117]: 91%]).

1H -NMR (400 MHz, $CDCl_3$): δ (ppm) = 7.38 - 7.33 (m, 2H), 7.20 - 7.17 (m, 2H), 7.14 - 7.13 (m, 2H), 6.94 - 6.89 (m, 2H), 3.87 (s, 6H).

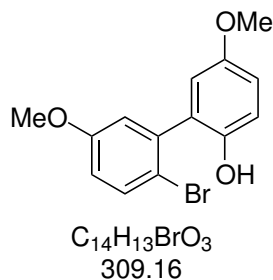
^{13}C -NMR (101 MHz, $CDCl_3$): δ (ppm) = 160.0 (C_q), 142.8 (C_q), 129.9 (CH), 119.8 (CH), 113.1 (CH), 113.0 (CH), 55.5 (CH_3).

Synthesis of 2,2'-dibromo-5,5'-dimethoxybiphenyl (2)

Compound **1** (12.0 g, 56.0 mmol, 1.00 eq.) was dissolved in glacial acetic acid (100 mL). Bromine (6.4 mL, 124 mmol, 2.22 eq.) was added dropwise over a time of 20 min. The reaction mixture was stirred at RT for 80 min and then quenched with saturated (sat.), aq. $Na_2S_2O_5$ solution and further stirred for 30 min. The crude product was extracted four times with DCM, dried over Na_2SO_4 and the solvent removed under reduced pressure. Upon addition of an excess of EtOH the organic residue solidified. The obtained solid was then washed several times with EtOH and the desired product was obtained as a white powder (13.75 g, 37.0 mmol, 66% [Lit.^[117]: 67%]).

1H -NMR (400 MHz, $CDCl_3$): δ (ppm) = 7.53 (d, J = 8.8 Hz, 2H), 6.84 - 6.79 (m, 4H), 3.81 (s, 6H).

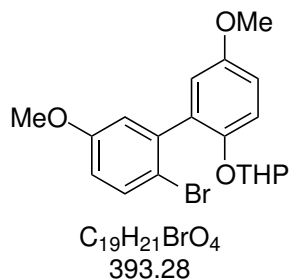
^{13}C -NMR (101 MHz, $CDCl_3$): δ (ppm) = 158.6 (C_q), 142.7 (C_q), 133.2 (CH), 116.3 (CH), 115.4 (CH), 113.8 (C_q), 55.6 (CH_3).

Synthesis of 2-bromo-2'-hydroxy-5,5'-dimethoxybiphenyl (3)

Compound **2** (1.22 g, 3.30 mmol, 1.00 eq.) was dissolved in dry THF (25 mL) under a nitrogen atmosphere. The solution was cooled to $-78\text{ }^{\circ}\text{C}$ and *n*-BuLi solution in hexane (1.6 M, 2.1 mL, 3.63 mmol, 1.10 eq.) was added dropwise whereupon the reaction mixture changed from colourless to red. After stirring for 30 min at that temperature, triisopropyl borate (1.52 mL, 6.60 mmol, 2.00 eq.) was added in one portion and the reaction mixture was allowed to reach RT overnight. A solution of NaOH (4.6 g) in H_2O_2 (46 mL, 35%) was prepared and added to the reaction mixture. The solution was stirred further for 5 h and afterwards the organic phase separated. The aq. phase was extracted twice with diethyl ether and the combined organic phases were washed with water and brine. After drying over Na_2SO_4 , the solvent was removed under reduced pressure. After purification via flash column chromatography on silica (pentane / EtOAc, 3:1) the product was obtained as an off-white solid (770.7 mg, 2.5 mmol, 76% [Lit.^[54]: 79%]).

$^1\text{H-NMR}$ (400 MHz, CDCl_3): $\delta(\text{ppm}) = 7.48$ (d, $J = 8.8$ Hz, 1H), 6.94 - 6.83 (m, 4H), 6.70 (d, $J = 3.0$ Hz, 1H), 4.48 (s, very broad, 1H), 3.81 (s, 3H), 3.79 (s, 3H).

$^{13}\text{C-NMR}$ (101 MHz, CDCl_3): $\delta(\text{ppm}) = 159.3$ (C_q), 153.4 (C_q), 146.3 (C_q), 138.7 (C_q), 134.1 (CH), 128.4 (C_q), 117.1 (CH), 116.9 (CH), 116.3 (CH), 115.5 (CH), 115.4 (CH), 114.4 (C_q), 55.9 (CH_3), 55.7 (CH_3).

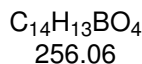
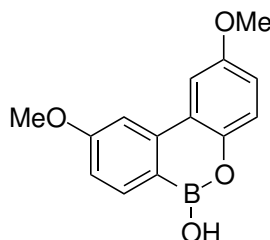
Synthesis of 2-bromo-5,5'-dimethoxy-2'-tetrahydropyranyloxybiphenyl (**4**)

Compound **3** (11.6 g, 37.5 mmol, 1.00 eq.) was dissolved in DCM, 3,4-dihydro-2H-pyran (DHP) (6.4 g, 82.5 mmol, 2.20 eq.) and pyridinium *p*-toluenesulfonate (955 mg, 3.8 mmol, 10mol%) were added and the reaction stirred at RT overnight. To the reaction mixture sat. aq. $NaHCO_3$ solution was added and the organic phase separated. The aq. phase was extracted three times with DCM, the combined organic phases were dried over Na_2SO_4 and the solvent removed under reduced pressure. Purification via flash column chromatography on silica (pentane / EtOAc, 17:3) yielded the desired product as a colourless oil (14.59 g, 37.1 mmol, 99% [Lit.^[54]:89%]).

1H -NMR (400 MHz, $CDCl_3$): δ (ppm) = 7.50 (d, J = 8.8 Hz, 1H), 7.17 (d, J = 8.8 Hz, 1H), 6.90 - 6.86 (m, 2H), 6.79 - 6.75 (m, 2H), 5.22 (s, 1H), 3.79 (s, 6H), 1.69 - 1.43 (m, 6H).

^{13}C -NMR (101 MHz, $CDCl_3$): δ (ppm) = 158.5, 154.1, 148.5, 140.7, 133.0, 132.5, 117.4, 117.0, 116.2, 115.4, 114.4, 98.6, 97.5, 95.8, 60.5, 55.84, 55.7, 30.9, 30.6, 21.2, 19.9, 14.4.

The spectrum contains additional signals and a direct assignment can not be made, probably due to the formation of atropisomeric diastereomers.^[54]

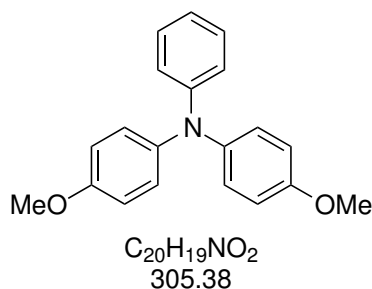
Synthesis of 2,9-dimethoxydibenzo[*c,e*]oxaborinin-6-ol (5)

The reaction followed a previously published protocol.^[54] Compound **4** (6.92 g, 17.6 mmol, 1.00 eq.) was dissolved in dry THF (100 mL) under a nitrogen atmosphere. The solution was cooled to -78°C and *n*-BuLi (1.6 M in hexane, 12.1 mL, 19.4 mmol, 1.10 eq.) was added dropwise. The solution was stirred for 30 min at that temperature and afterwards triisopropyl borate (6.62 g, 35.3 mmol, 2.00 eq.) was added in one portion. The reaction mixture was allowed to reach RT overnight. An aq. solution of hydrochloric acid (1 M, 100 mL) was added and the solution stirred for further 1.5 h. The organic phase was then separated and the aq. phase extracted three times with diethyl ether. The combined organic layers were washed with water and dried over Na_2SO_4 and the solvent was removed under reduced pressure. After purification by flash column chromatography on silica (pentane / EtOAc, 7:3) the desired product was obtained as beige solid (3.26 g, 12.7 mmol, 72% [Lit.^[54]: 87%]).

$^1\text{H-NMR}$ (400 MHz, CDCl_3): $\delta(\text{ppm}) = 7.99$ (d, $J = 8.3$ Hz, 1H), 7.54 - 7.51 (m, 2H), 7.18 (d, $J = 8.8$ Hz, 1H), 7.04 (dd, $J = 8.2, 6.1$, 1H), 6.95 (dd, $J = 8.8, 6.0$, 1H), 3.88 (s, 3H), 3.83 (s, 3H).

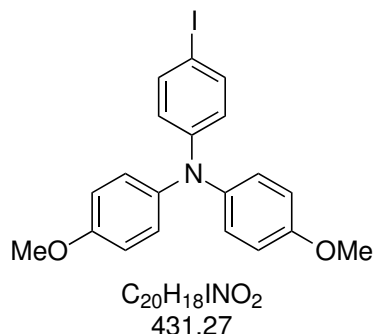
$^{13}\text{C-NMR}$ (101 MHz, CDCl_3): $\delta(\text{ppm}) = 163.0, 154.7, 146.0, 142.1, 135.3, 123.3, 120.2, 115.2, 114.0, 107.9, 106.0, 55.8, 55.2$.

As described before, a completely clean NMR-spectrum could not be obtained, presumably due to the fact that anhydrides form in solution.^[54] The compound was generally used in excess in the following Suzuki-Miyaura coupling reactions and any impurities seemed to not have a detrimental effect.

Synthesis of *N,N*-bis-(4-methoxyphenyl)aniline (TAA)

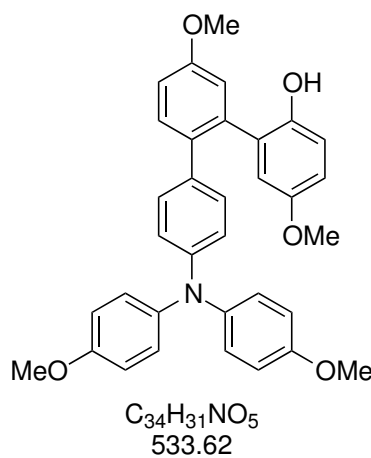
This compound was synthesised by adapting a known literature procedure.^[118] 4,4'-bis(methoxy)phenylaniline (3.6 g, 16.0 mmol, 1.00 eq.), bromobenzene (2.02 mL, 19.2 mmol, 1.20 eq.), sodium *tert*-butoxide (30.61 g, 319 mmol, 19.9 eq.), Pd(dba)₂ (460 mg, 0.8 mmol, 5mol%) and tri-*tert*-butylphosphonium tetrafluoroborate (232 mg, 0.8 mmol, 5mol%) were dissolved in dry toluene and degassed via ultrasonification under N₂ flow, alternating with evacuation. The reaction mixture was sealed and heated to reflux overnight. The reaction was allowed to RT, diluted with water and extracted three times with DCM. The combined organic phases were dried over Na₂SO₄ and the solvent removed under reduced pressure. Purification via flash column chromatography (100% DCM → pentane / DCM, 5:1 → pentane / DCM, 1:1) yielded the desired compound as a beige solid (4.54 g, 14.9 mmol, 93% [Lit.^[119]: 92%]).

¹H-NMR (400 MHz, acetone-*d*₆): δ (ppm) = 7.12 - 7.15 (m, 2H), 7.03 - 6.99 (m, 4H), 6.91 - 6.82 (m, 7H), 3.78 (s, 6H).

Synthesis of 4-Iodo-*N,N*-bis(4-methoxyphenyl)aniline (TAA-I)

Following a literature procedure that was slightly adapted.^[120] [Bis(trifluoro)acetoxy]iodo]benzene (1.87 g, 4.36 mmol, 1.00 eq.) and iodine (1.13 g, 4.45 mmol, 1.02 eq.) were stirred in dry DCM (15 mL) at RT under an inert atmosphere for 1 h. **TAA** (1.33 g, 4.36 mmol, 1.00 eq.) was added in one portion and the mixture heated to reflux for 1 h. Meanwhile a second solution of [bis(trifluoro)acetoxy]iodo]benzene (0.56 g, 1.30 mmol, 0.3 eq.) and iodine (550 mg, 2.18 mmol, 0.5 eq.) in dry DCM (10 mL) was prepared and stirred for 40 min at RT. This second solution was then added to the refluxing one. The latter was refluxed for an additional hour and then cooled to RT with an ice-bath. Sat. aq. Na_2SO_3 -solution was added, the organic phase separated and dried over Na_2SO_4 . After filtration, the solvent was removed under reduced pressure. The oily green residue was purified via flash column chromatography (100 % pentane \rightarrow pentane / DCM, 1:1) and this procedure yielded the desired compound as a beige solid (1.42 g, 3.3 mmol, 76% [Lit.^[119]: 80%]).

1H -NMR (400 MHz, acetone- d_6): δ (ppm) = 7.47 - 7.43 (m, 2H), 7.08 - 7.03 (m, 4H), 6.93 - 6.89 (m, 4H), 6.65 - 6.60 (m, 2H), 3.79 (s, 6H).

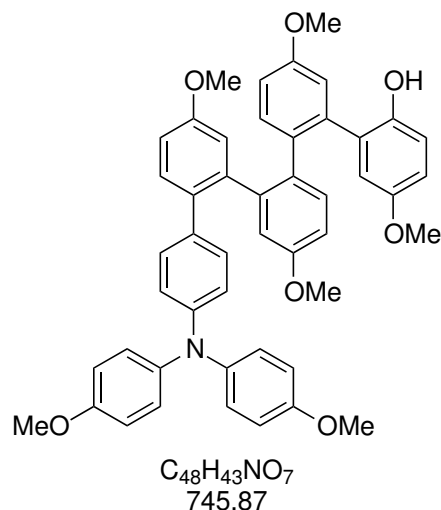
Synthesis of TAA-(*o*-ph)₂-OH

General procedure for the elongation of the chain to form TAA-(*o*-ph)_x-OH.^[54] TAA-I (2.0953 g, 4.86 mmol, 1.00 eq.), 2,9-dimethoxydibenzo[*c,e*]oxaborinin-6-ol (2.24 g, 8.75 mmol, 1.80 eq.), SPhos (240 mg, 580 μ mol, 12mol%) were dissolved in THF (10 mL) in a Schlenktube under an inert atmosphere. $K_3PO_4 \cdot H_2O$ (3.36 g, 14.58 mmol, 3.00 eq.) was dissolved in water (2.5 mL) and added to the mixture. The reaction mixture was degassed via ultrasonification under N_2 flow, alternating with evacuation and, after $Pd(OAc)_2$ (109 mg, 486 μ mol, 10mol%) was added, the mixture was degassed again. The reaction mixture was sealed and heated to 90 °C for 24 h. The mixture was allowed to reach RT, diethyl ether was added and the mixture washed with water and brine. The organic phase was dried over Na_2SO_4 and the solvent removed under reduced pressure. The crude product was purified via flash column chromatography (dry loaded on silica, pentane / EtOAc, 9:1 \rightarrow pentane / EtOAc, 5:1 \rightarrow toluene / EtOAc, 9:1) and obtained as a brownish foam (2.40 g, 4.49 mmol, 93%).

¹H-NMR (400 MHz, acetone-*d*₆): δ (ppm) = 7.33 (d, J = 8.3 Hz, 1H), 7.00 - 6.93 (m, 8H), 6.89 - 6.82 (m, 3H), 6.75 (d, J = 8.8 Hz, 1H), 6.70 - 6.64 (m, 4H), 6.47 (d, J = 3.0 Hz, 1H), 5.62 (s, weak OH), 3.84 (s, 3H), 3.77 (s, 6H), 3.61 (s, 3H).

¹³C-NMR (101 MHz, acetone-*d*₆): δ (ppm) = 159.3, 156.9, 147.9, 141.9, 139.0, 134.8, 134.7, 135.6, 130.7, 129.8, 129.0, 127.1, 126.1, 120.8, 117.5, 117.3, 117.1, 115.5, 114.9, 113.9, 55.9, 55.7, 55.6.

MS (ESI) m/z (relative intensities): $[M+H]^+$ 534.2 (100); calcd. 534.23.

Synthesis of TAA-(*o*-ph)₄-OH

Following the general procedure for TAA-(*o*-ph)_x-OH, TAA-(*o*-ph)₂-OTf (1.65 g, 2.48 mmol, 1.00 eq.) reacted with compound **5** (1.11 g, 4.33 mmol, 1.75 mmol) under the aid of the transition metal catalysed reaction conditions with Pd(OAc)₂ (56 mg, 248 μmol, 10mol%), SPhos (122 mg, 298 μmol, 12mol%), and K₃PO₄·H₂O (1.71 g, 7.44 mmol, 3.00 eq.) in a mixture of THF (10 mL) and water (2.5 mL). The product was obtained after purification via High Performance Liquid Chromatography (HPLC) (Gradient see Table 15) on a reverse phase column as a brownish solid (1.04 g, 1.40 mmol, 56%).

¹H-NMR (400 MHz, acetone-*d*₆): δ(ppm) = 7.16 - 7.06 (m, broad, 2H), 7.01 (d, *J* = 8.5 Hz, 3H), 6.93 - 6.84 (m, 3H), 6.76 (ddd, *J* = 12.9, 8.5, 2.7 Hz, 1H), 6.70 - 6.40 (m, 13H), 6.35 (s, broad, 1H), 6.25, (s, broad, 1H), 5.58 (s, weak, 1H, OH), 3.75 (s, 6H), 3.73 - 3.31 (m, 12H).

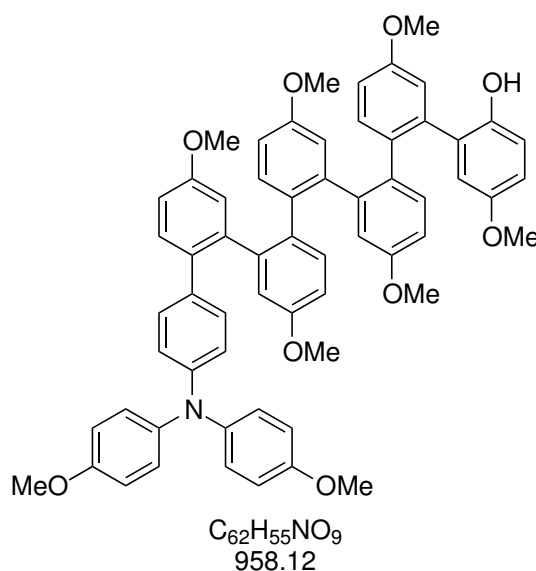
¹³C-NMR (101 MHz, acetone-*d*₆): 158.8, 156.6, 153.3, 148.6, 147.5, 142.3, 141.9, 141.3, 139.2, 134.9, 133.8, 133.6, 131.2, 130.6, 129.7, 126.9, 121.2, 117.6, 117.2, 116.9, 116.6, 115.4, 114.3, 113.4, 113.2, 55.7, 55.5, 55.4, 55.3, 55.2.

Note: Some NMR signals were broadened, complicated due to slow conformational exchange on the NMR time scale.

MS (ESI) *m/z* (relative intensities): [M-H⁺]⁻ 744.20 (100); calcd. 744.30.

Table 15: HPLC gradient used for the purification of compound TAA-(*o*-ph)₄-OH. Flow rate was 20 mL/min

time [min]	concentrations MeCN / H ₂ O [%]
0	30 / 70
10	30 / 70
60	75 / 25
61	95 / 5
70	95 / 5
75	30 / 70

Synthesis of TAA-(*o*-ph)₆-OH

Following the general procedure for TAA-(*o*-ph)_x-OH, TAA-(*o*-ph)₄-OTf (353 mg, 402 μmol, 1.00 eq.) reacted with compound **5** (206 mg, 804 μmol, 2.00 mmol) under the aid of the transition metal catalysed reaction conditions with Pd(OAc)₂ (10 mg, 40 μmol, 10mol%), SPhos (20 mg, 48 μmol, 12mol%), and K₃PO₄·H₂O (278 mg, 1.21 mmol, 3.00 eq.) in a mixture of THF (4 mL) and water (1 mL). The product was obtained after purification via flash column chromatography (toluene / EtOAc / NEt₃, 90:10:1) as a brownish solid (226 mg, 235 μmol, 59%).

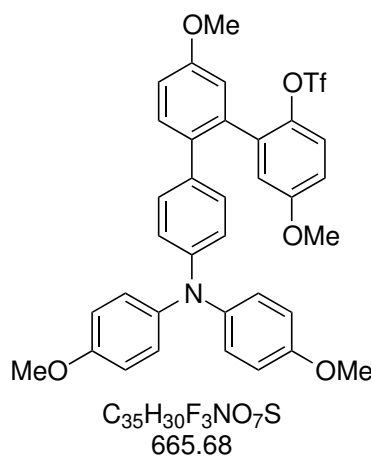
¹H-NMR (400 MHz, acetone-*d*₆): δ(ppm) = 8.13 - 5.40 (m, 31H), 3.94 - 2.87 (m, 24H).

¹³C-NMR (101 MHz, acetone-*d*₆): 160.3, 156.7, 154.1, 148.8, 142.0, 141.8, 141.0, 138.4, 134.8, 133.3, 129.8, 129.7, 129.0, 126.9, 126.1, 122.4, 120.8, 117.7, 116.4, 115.9, 115.4, 114.7,

114.0, 113.1, 55.9, 55.7, 55.4.

Note: Some NMR signals were broadened, complicated due to slow conformational exchange on the NMR time scale.

MS (MALDI-TOF): $[M]^+$ 957.53; calcd. 957.39.

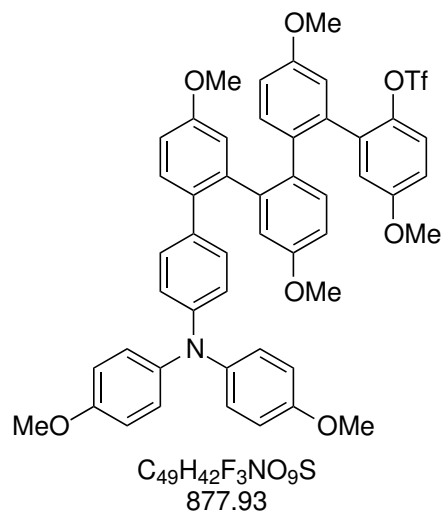
Synthesis of TAA-(*o*-ph)₂-OTf**General procedure for the triflation to form TAA-(*o*-ph)_x-OTf.**^[54]

TAA-(*o*-ph)₂-OH (246 mg, 461 μ mol, 1.00 eq.) was dissolved in dry DCM (1 mL) under an inert atmosphere and pyridine was added (1.00 mL, 1.13 mmol, 2.44 eq.). The solution was cooled to 0 °C and trifluoromethanesulfonic anhydride (238 mg, 845 μ mol, 1.83 eq.) was added at this temperature. The reaction mixture was allowed to slowly reach RT overnight. The reaction mixture was diluted with EtOAc, washed with aq. HCl-solution (1 M), water and brine. The organic phase was dried over Na₂SO₄, filtered and the solvent removed under reduced pressure. The product was obtained as a greenish foam (253 mg, 381 μ mol, 83%).

¹H-NMR (400 MHz, acetone-*d*₆): δ (ppm) = 7.39 (d, *J* = 8.5 Hz, 1H), 7.22 (d, *J* = 9.0 Hz, 1H), 7.08 (dd, *J* = 8.6, 2.7 Hz, 1H), 7.01 - 6.91 (m, 9H), 6.90 - 6.84 (m, 4H), 6.73 - 6.64 (m, 2H), 3.81 (s, 3H), 3.78 (s, 3H), 3.77 (s, 6H).

¹⁹F-NMR (376 MHz, acetone-*d*₆): δ (ppm) = 75.5.

MS (ESI) *m/z* (relative intensities): [M]⁺ 665.08 (100); calcd. 665.17.

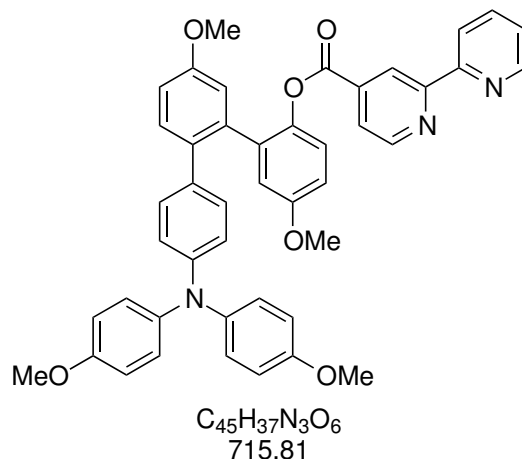
Synthesis of TAA-(*o*-ph)₄-OTf

Following the general procedure for the triflation, TAA-(*o*-ph)₄-OH (358 mg, 480 μ mol, 1.00 eq.) reacted with trifluoromethanesulfonic anhydride (203 mg, 720 μ mol, 1.50 eq.) in the presence of pyridine (0.2 mL, 2.4 mmol, 5.00 eq.) in dry DCM at 0 °C. The desired product was obtained after purification via flash column chromatography (toluene / EtOAc, 9:1) as a brownish solid (367 mg, 418 μ mol, 87%).

¹H-NMR (400 MHz, acetone-*d*₆): δ (ppm) = 7.48 - 7.29 (m, broad, 1H), 7.22 (d, $J = 7.5$ Hz, 1H), 7.19 - 7.08 (m, 3H), 7.06 - 6.13 (m, 16H), 6.01 (s, broad, 1H), 5.89 (s, broad, 1H), 5.68 (s, broad, 1H), 4.06 - 3.60 (m, 15H), 3.59 - 3.20 (m, 3H).

Note: Some NMR signals were broadened, complicated due to slow conformational exchange on the NMR time scale.

MS (ESI) m/z (relative intensities): $[M+Na]^+$ 900.15 (34); calcd. 900.24, $[M]^+$ 877.25 (100); calcd. 877.25.

Synthesis of TAA-(*o*-ph)₂-bpy

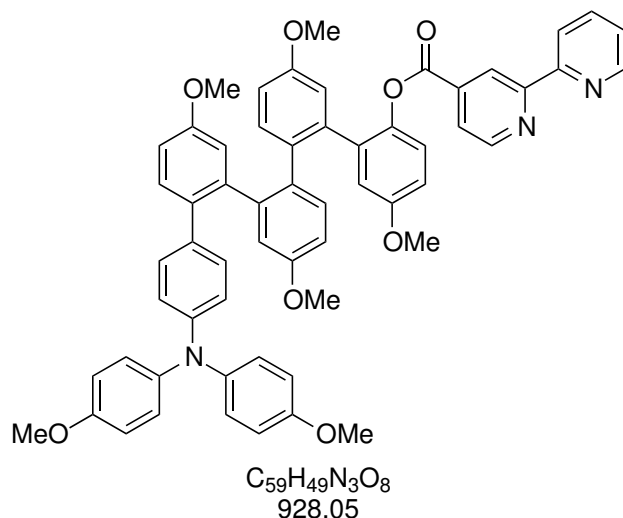
The procedure follows a literature procedure which was slightly adapted.^[121]

General procedure for the esterification with the bipyridine.

Compound **10** (29 mg, 133 μmol , 1.00 eq.) was dissolved in ice-cold DCM (0.5 mL) under an inert atmosphere. N^tBu₄Cl (1 mg, 4.4 μmol , 3mol%) was dissolved in DCM (0.1 mL) in a separate vial. A separate solution of TAA-(*o*-ph)₂-OH (71 mg, 133 μmol , 1.00 eq.) in aq. NaOH (10%, 0.5 mL) was prepared. Once all solutions were cooled to 0 °C, they were mixed at once and vigorously stirred for 5 min at this temperature. The reaction mixture was poured on ice (2 mL) and extracted twice with diethyl ether. The organic phase was washed with brine, dried over Na₂SO₄ and the solvent removed under reduced pressure. After purification via flash column chromatography (dry load, pentane / EtOAc, 9:1 → pentane / EtOAc, 5:1 → pentane / EtOAc, 3:1) the desired product was obtained as a brownish solid (18 mg, 25 μmol , 19%).

¹H-NMR (400 MHz, acetone-*d*₆): δ (ppm) = 8.89 (dd, J = 1.7, 0.9 Hz, 1H), 8.81 (dd, J = 5.0, 0.9 Hz, 1H), 8.63 (ddd, J = 4.8, 1.8, 0.9 Hz, 1H), 8.47 (dt, J = 8.0, 1.1 Hz, 1H), 7.94 (td, J = 7.7, 1.8 Hz, 1H), 7.70 (dd, J = 5.0, 1.7 Hz, 1H), 7.44 (ddd, J = 7.5, 4.7, 1.2 Hz, 1H), 7.25 (dd, J = 13.6, 8.7 Hz, 2H), 7.09 - 7.00 (m, 4H), 7.00 - 6.84 (m, 10H), 6.70 - 6.65 (m, 2H), 3.80 (d, J = 2.7 Hz, 6H), 3.76 (s, 6H).

MS (ESI) m/z (relative intensities): [M]⁺ 716.11 (100); calcd. 716.28.

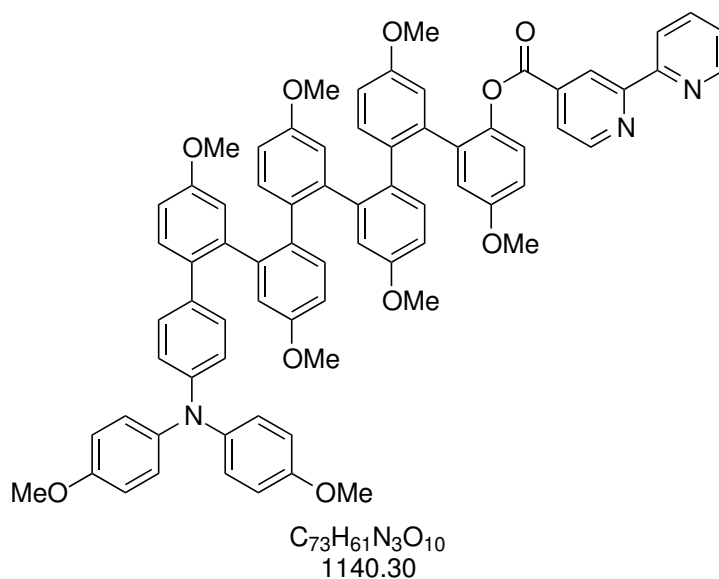
Synthesis of TAA-(*o*-ph)₄-bpy

Following the general procedure for the esterification, compound **10** (44 mg, 201 μ mol, 1.00 eq.) in DCM (1 mL) was reacted with TAA-(*o*-ph)₄-OH (150 mg, 201 μ mol, 1.00 eq.) in an aq. NaOH-solution (10%, 1 mL), and N^tBu_4Cl (6 mg, 20.1 μ mol, 10mol%) in DCM (1 mL) at 0 °C. The aq. phase was extracted twice with DCM and twice with diethyl ether. The combined organic phases were dried over Na_2SO_4 and the solvent removed under reduced pressure. The desired product was obtained after purification via flash column chromatography (dryload, toluene/EtOAc, 9:1), as a brownish solid (87.9 mg, 94.8 μ mol, 47%).

1H -NMR (400 MHz, CD_3CN): δ (ppm) = 9.00 - 8.54 (m, 3H), 8.45 (d, J = 8.0 Hz, 1H), 7.92 (t, J = 7.8 Hz, 1H), 7.70 (s, 1H), 7.41 (s, 1H), 7.31 - 7.11 (m, 7H), 7.12 - 6.66 (m, 11H), 6.60 - 6.28 (m, 5H), 6.16 (s, broad, 1H), 4.00 - 2.98 (m, 18H).

Note: Some NMR signals were broadened, complicated due to slow conformational exchange on the NMR timescale.^[54]

MS (ESI) m/z (relative intensities): $[M+Na^+]^+$ 950.26; calcd. 949.33 (21), $[M]^+$ 927.34 (100); calcd. 927.35.

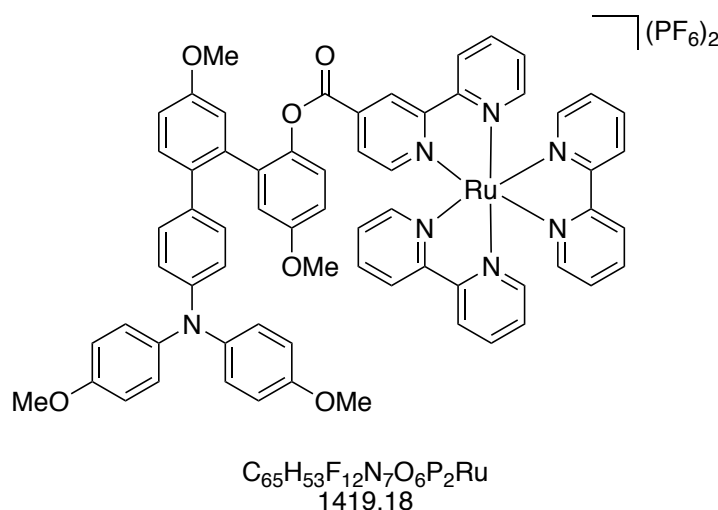
Synthesis of TAA-(*o*-ph)₆-bpy

Following the general procedure for the esterification, compound **10** (10.9 mg, 50.0 μmol , 1.20 eq.) in DCM (1 mL) was reacted with TAA-(*o*-ph)₆-OH (40.0 mg, 41.7 μmol , 1.00 eq.) in an aq. NaOH-solution (10%, 1 mL) and $N^t\text{Bu}_4\text{Cl}$ (1.30 mg, 4.70 μmol , 10mol%) in DCM (0.5 mL) at 0 °C. The aq. phase was extracted twice with DCM and twice with diethyl ether. The combined organic phases were dried over Na_2SO_4 and the solvent removed under reduced pressure. The desired product was obtained after purification via flash column chromatography (dry load, DCM \rightarrow pentane / EtOAc, 7:3) as a beige solid (16.5 mg, 14.4 μmol , 35%).

$^1\text{H-NMR}$ (400 MHz, acetone- d_6): $\delta(\text{ppm}) = 9.31 - 8.33$ (m, 6H), 8.06 - 7.92 (m, 1H), 7.68 - 5.42 (m, 30H), 4.01 - 3.20 (m, 24H).

Note: Some NMR signals were broadened, complicated due to slow conformational exchange on the NMR timescale.^[54]

MS (MALDI-TOF) m/z : $[\text{M}]^+$ 1139.58; calcd. 1139.44.

Synthesis of TAA-(*o*-ph)₂-Ru(bpy)₃(PF₆)₂

General procedure for the complexation of the functionalised bipyridine ligand with Ru(bpy)₂Cl₂·2H₂O^[122]

The ligand TAA-(*o*-ph)₂-bpy (18 mg, 25 μmol, 1.00 eq.) and Ru(bpy)₂Cl₂·2H₂O (12 mg, 25 μmol, 1.00 eq.) were dissolved in a mixture of EtOH (1 mL) and H₂O (0.5 mL) under an inert atmosphere and heated to 80 °C for 18 h. The formation of the complex was confirmed via ESI-MS. The reaction mixture was directly purified via flash column chromatography (acetone → acetone / H₂O, 9:1 → acetone / H₂O / aq. sat. KNO₃-solution, 100:10:1). The acetone of the combined fractions was removed under reduced pressure. The remaining aq. solution was mixed with sat. aq. KPF₆ solution whereupon an orange precipitate formed. The formed precipitate was dissolved upon addition of DCM. The aq. phase was extracted with DCM three times. The combined organic phases were washed with H₂O and dried over Na₂SO₄. The desired product was obtained as a red solid (20.8 mg, 14.6 μmol, 58%).

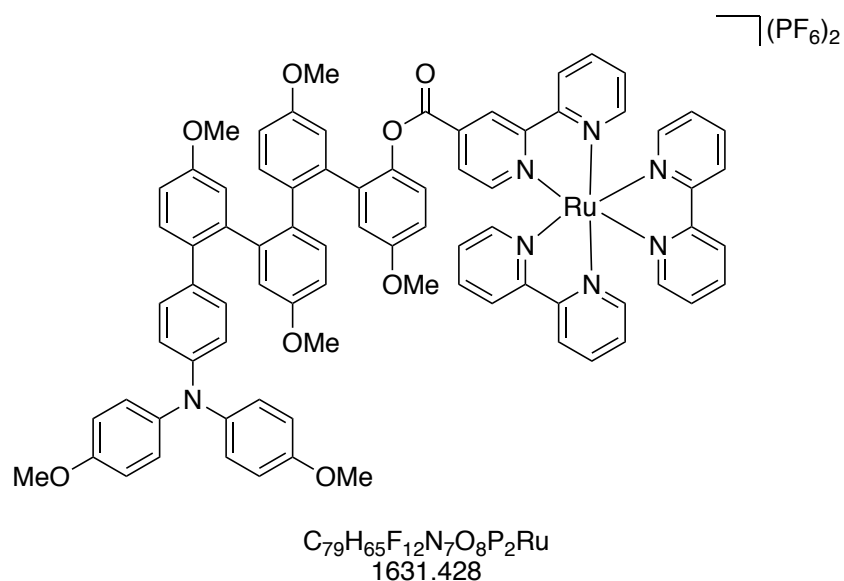
¹H-NMR (400 MHz, acetone-*d*₆): δ(ppm) = 8.89 - 8.64 (m, 6H), 8.49 - 6.40 (m, 35H), 3.88 - 3.70 (m, 12H).

Note: Due to slow conformational exchange, no ¹³C NMR spectrum has been recorded.

MS (ESI) *m/z* (relative intensities): [M-2PF₆]²⁺ 564.51 (100); calcd. 564.66.

$\text{C}_{65}\text{H}_{53}\text{N}_7\text{O}_6\text{Ru}^{2+}$ (ESI) HRMS: calculated: 564.6443
 measured: 564.6562

Elemental Analysis: found: C, 55.38; H, 4.77; N, 6.67, calcd. for C₆₅H₅₃F₁₂N₇O₆P₂Ru · C₃H₆O · 2 C₂H₆O: C, 55.10; H, 4.56; N, 6.25.

Synthesis of TAA-(*o*-ph)₄-Ru(bpy)₃(PF₆)₂

The complex was synthesised following the general procedure for the complexation of the ligand with Ru(bpy)₂Cl₂·2H₂O. TAA-(*o*-ph)₄-bpy (87 mg, 94 μmol, 1.00 eq.) and Ru(bpy)₂Cl₂·H₂O (49 mg, 94 μmol, 1.00 eq.) were dissolved in a mixture of EtOH (2 mL) and water (1 mL). The reaction mixture was then heated to 80 °C until the formation of the complex was confirmed via ESI-MS and then allowed to RT. The mixture was directly purified via flash column chromatography (acetone → acetone / H₂O, 9:1 → acetone / H₂O / sat. aq. KNO₃, 100:10:1). The acetone was removed under reduced pressure. To the remaining aq. solution, sat. aq. KPF₆ solution was added dropwise, whereupon a precipitate formed. To the suspension DCM was added and the precipitate dissolved. The aq. phase was extracted with DCM twice, the combined organic phases were washed with H₂O and dried over Na₂SO₄. The solvent was removed under reduced pressure and the desired product was obtained as a red, crystalline solid (81 mg, 50 μmol, 53%).

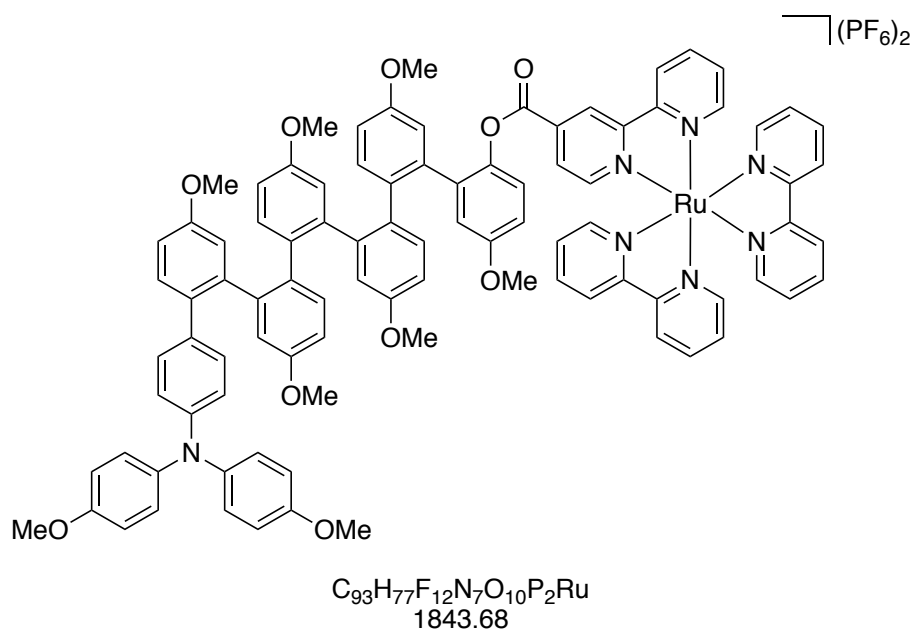
¹H-NMR (400 MHz, acetone-*d*₆): δ(ppm) = 9.03 - 5.64 (m, very broad, 47H), 3.93 - 3.27 (m, 18H).

Note: Due to slow conformational exchange, no ¹³C NMR spectrum has been recorded.

MS (MALDI-TOF) *m/z*: [M-2PF₆⁻]⁺ 1341.008; calcd. 1341.393, [M-PF₆⁻]⁺ 1486.990; calcd. 1486.357, [M]⁺ 1630.870; calcd. 1631.322.

C₇₉H₆₅N₇O₈Ru²⁺ (ESI) HRMS: calculated: 670.6974
 measured: 670.6982

Elemental Analysis: found: C, 58.02; H, 4.41; N, 6.03, calcd. for $C_{79}H_{65}F_{12}N_7O_8P_2Ru$: C, 58.16; H, 4.02; N, 6.01.

Synthesis of TAA-(*o*-ph)₆-Ru(bpy)₃(PF₆)₂

The complex was synthesised following the general procedure for the complexation of the ligand with Ru(bpy)₂Cl₂·2H₂O. TAA-(*o*-ph)₆-bpy (23.7 mg, 20.8 μmol, 1.00 eq.), Ru(bpy)₂Cl₂·2H₂O (10.8 mg, 20.8 μmol, 1.00 eq.) and AgNO₃ (7 mg, 41.6 μmol, 2.00 eq.) were reacted under the reported reaction conditions in EtOH (1 mL) and H₂O (0.25 mL). Purification via flash column chromatography (acetone → acetone / H₂O, 9:1 → acetone / H₂O / sat. aq. KNO₃ solution, 100:10:1), removing the acetone and the addition of sat. aq. KPF₆-solution yielded the desired complex after extraction with DCM, washing with H₂O, drying over Na₂SO₄ and removing the solvent under reduced pressure, as a brownish solid (14.1 mg, 7.65 μmol, 37%).

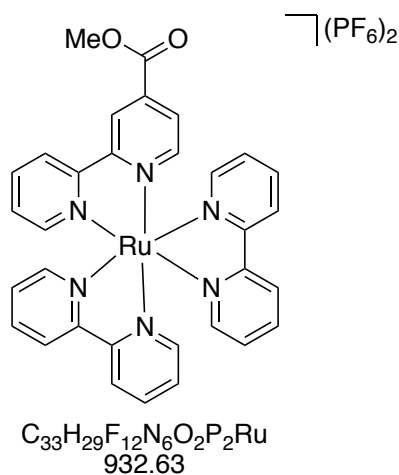
¹H-NMR (400 MHz, acetone-*d*₆): δ(ppm) = 8.96 - 5.62 (m, 53H), 4.22 - 3.06 (m, 24H).

Note: Due to slow conformational exchange, no ¹³C NMR spectrum was recorded.

MS (ESI) *m/z* (relative intensities): [M-2PF₆⁻]²⁺ 776.6 (100); calcd. 776.7.

C₉₃H₇₇N₇O₁₀Ru²⁺ (ESI) HRMS: calculated: 776.7384
 measured: 776.7396

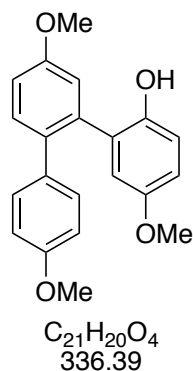
Elemental Analysis: found: C, 59.21; H, 4.34; N, 5.45, calcd. for C₉₃H₇₇F₁₂N₇O₁₀P₂Ru · 2 H₂O: C, 59.43; H, 4.34; N, 5.22.

Synthesis of Ru(bpy-4-CO₂Me)(bpy)₂(PF₆)₂

4-Methoxycarbonyl-bipyridine (70 mg, 327 μmol , 1.00 eq.) and Ru(bpy)₂Cl₂·2H₂O (170 mg, 327 μmol , 1.00) were dissolved in a mixture of EtOH (1 mL) and water (0.5 mL) under an inert atmosphere. The mixture was degassed via ultrasonification, sealed and heated to 80 °C overnight. After allowing the reaction mixture to reach RT, it was directly purified via flash column chromatography on silica (acetone → acetone / H₂O, 9:1, → acetone / H₂O / sat. aq. KNO₃ solution, 100:10:1). The acetone was removed under reduced pressure and to the remaining aq. solution, aq. sat. KPF₆-solution was added. The formed precipitate was dissolved in DCM, the aq. phase extracted with DCM three times and the combined organic layers were washed with water and then dried over Na₂SO₄. The solvent was removed and the desired complex was obtained as a red crystalline solid (22.5 mg, 24.5 μmol , 7%).

¹H-NMR (400 MHz, CD₃CN): $\delta(\text{ppm}) = 8.90$ (dd, $J = 1.8, 0.8$ Hz, 1H), 8.65 (dt, $J = 8.2, 1.2$ Hz, 1H), 8.50 (m, 4H), 8.11 - 8.03 (m, 5H), 7.92 (dd, $J = 5.9, 0.7$ Hz, 1H), 7.80 - 7.66 (m, 6H), 7.46 - 7.35 (m, 5H), 3.98 (s, 3H).

$\text{C}_{32}\text{H}_{26}\text{N}_6\text{O}_2\text{Ru}^{2+}$ (ESI) HRMS: calculated: 314.0579
measured: 314.0582

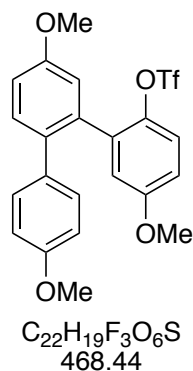
Synthesis of *o*-ph₃-OH

The compound was prepared according to a literature procedure.^[54] 4-Bromoanisole (0.78 mL, 6.24 mmol, 2.00 eq.) reacted with compound **5** (0.80 g, 3.12 mmol, 1.00 eq.) under the aid of Pd(OAc)₂ (70 mg, 0.312 mmol, 10mol%), SPhos (158 mg, 0.385 mmol, 12mol%) and K₃PO₄·H₂O (2.15 g, 9.36 mmol, 3.00 eq.) in a mixture of THF (5.00 mL) and H₂O (1.2 mL) under a N₂-atmosphere at 90 °C overnight. The reaction was allowed to reach RT and then diluted with diethyl ether. The organic phase was washed with H₂O and brine, dried over Na₂SO₄, and the solvent removed under reduced pressure. The crude product was purified via flash column chromatography on silica (pentane / DCM, 9:1 → DCM 100%) and obtained as a yellowish foam (580 mg, 1.72 mmol, 55% [Lit.^[54]: 65%]).

¹H-NMR (400 MHz, CDCl₃): δ(ppm) = 7.39 (dd, *J* = 8.6, 2.1 Hz, 1H), 7.14 - 7.04 (m, 2H), 7.01 (dd, *J* = 8.2, 2.9 Hz, 1H), 6.95 - 6.89 (m, 1H), 6.79 - 6.65 (m, 5H), 3.86 (s, 3H), 3.76 (s, 3H), 3.70 (s, 3H).

¹³C-NMR (101 MHz, CDCl₃): δ(ppm) = 159.0, 158.5, 153.4, 146.3, 136.2, 133.4, 131.7, 130.1, 128.7, 116.6, 116.2, 115.8, 114.7, 114.6, 113.6, 77.3, 77.0, 76.7, 55.7, 55.5, 55.2.

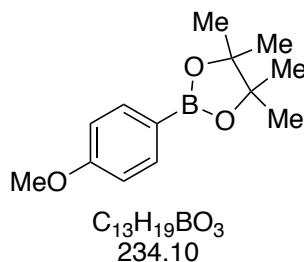
MS (ESI) *m/z* (relative intensities): [M-H]⁺ 335.06 (100); calcd. 335.13.

Synthesis of *o*-ph₃-OTf

The compound was prepared according to a literature procedure.^[54] Compound **12** (625 mg, 1.86 mmol, 1.00 eq.) was dissolved in dry DCM under a N₂-atmosphere. The solution was cooled down to 0 °C and pyridine (0.3 mL, 3.72 mmol, 2.00eq.) was added. To this mixture trifluoromethane sulfonic anhydride (1 M in dry DCM, 2 mL, 1.08 eq.) was added dropwise. The solution was slowly allowed to reach RT overnight. The mixture was diluted with EtOAc and subsequently washed with aq. 1M HCl-solution, water and brine. The organic phase was dried over Na₂SO₄, and the solvent removed under reduced pressure. The product was obtained after purification via flash column chromatography (pentane / EtOAc, 7:3) as a brownish solid (830 mg, 1.77 mmol, 95% [Lit.^[54]: 88%]).

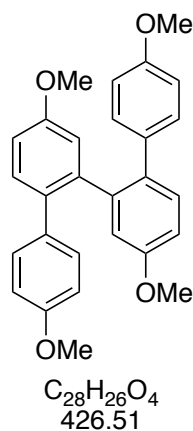
¹H-NMR (400 MHz, CDCl₃): δ(ppm) = 7.34 (d, *J* = 8.5 Hz, 1H), 7.07 - 6.98 (m, 4H), 6.94 (d, *J* = 2.7 Hz, 1H), 6.84 - 6.77 (m, 2H), 6.76 - 6.70 (m, 2H), 3.86 (s, 3H), 3.77 (s, 3H), 3.72 (s, 3H).

MS (ESI) *m/z* (relative intensities): [M+H⁺]⁺ 468.99; calcd. 469.09.

Synthesis of 4-methoxyphenylboronic acid pinacol ester (14)

The synthesis follows a former published protocol.^[123] 4-Bromoanisole (181 mg, 968 μ mol, 1.00 eq.) reacted with bis(pinacolato)diboron (310 mg, 1.22 mmol, 1.26 eq.) under the aid of Pd(dppf)₂Cl₂·CH₂Cl₂ and KOAc (310 mg, 3.16 mmol, 3.10 eq.) in dry DMF under a N₂-atmosphere. The mixture was heated to 156 °C for 65 min and the solution allowed to reach RT. Subsequently the solvent was removed under reduced pressure and dried on high vacuum. The remaining solid was suspended in Et₂O and filtered over celite. The solvent was removed under reduced pressure and the brown, crude product (219 mg) was used without further purification in the next step.

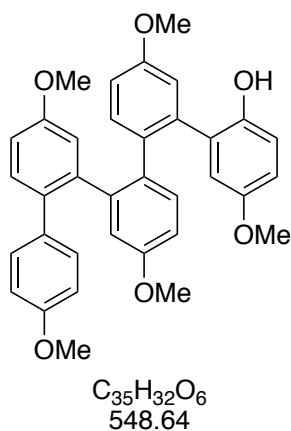
¹H-NMR (400 MHz, CDCl₃): δ (ppm) = 7.82 - 7.71 (m, 2H), 6.93 - 6.86 (m, 2H), 3.83 (s, 3H), 1.33 (s, 12H).

Synthesis of *o-ph*₄

The compound was prepared according to a literature procedure.^[54] ***o-ph*₃-OTf** (240 mg, 0.51 mmol, 1.00 eq.) reacted with **14** (238 mg, 1.02 mmol, 2.00 eq.) under the aid of Pd(OAc)₂ (11.2 mg, 0.05 mmol, 10mol%), SPhos (24.6 mg, 0.06 mmol, 12mol%) and K₃PO₄·H₂O (352 mg, 1.53 mmol, 3.00 eq.) in a mixture of THF (3 mL) and H₂O (0.25 mL) under a N₂-atmosphere. The reaction was sealed and heated to 90 °C overnight. The reaction mixture was allowed to reach RT, diluted with Et₂O, and the organic phase washed with H₂O, brine and acidified with aq. 1 M HCl-solution. Subsequently the organic phase was dried over Na₂SO₄ and the solvent removed under reduced pressure. The desired compound was obtained after purification via flash column chromatography on silica (pentane / EtOAc, 17:3 → pentane / EtOAc, 3:1) as a white solid (73.7 mg, 173 μmol, 34% [Lit.^[54]: 70%]).

¹H-NMR (400 MHz, CDCl₃): δ(ppm) = 7.10 (d, *J* = 8.4 Hz, 2H), 6.97 (d, *J* = 2.7 Hz, 2H), 6.89 (dd, *J* = 8.5, 2.8 Hz, 2H), 6.59 (m, 8H), 3.83 (s, 6H), 3.76 (s, 6H).

¹³C-NMR (101 MHz, CDCl₃): δ(ppm) = 158.3, 157.8, 141.1, 133.5, 133.4, 131.0, 130.1, 116.6, 113.3, 112.9, 55.4, 55.2.

Synthesis of *o*-ph₅-OH

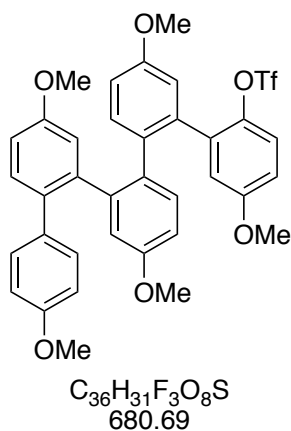
The compound was prepared according to a literature procedure.^[54]

***o*-ph₃-OTf** (232 mg, 495 μ mol, 1.00 eq.) reacted with compound **5** (507 mg, 1.98 mmol, 4.00 eq.) under the aid of Pd(OAc)₂ (22 mg, 99 μ mol, 20mol%), SPhos (49 mg, 120 μ mol, 24mol%) and K₃PO₄·H₂O in a mixture of THF (2 mL) and H₂O (0.5 mL) at 90 °C, overnight under a N₂-atmosphere. The product was obtained after purification via flash column chromatography on silica (pentane / EtOAc, 9:1, pentane / EtOAc, 3:1) as a yellowish foam (167 mg, 304 μ mol, 69% [Lit.^[54]: 78%]).

¹H-NMR (400 MHz, CDCl₃): δ (ppm) = 7.24 - 6.36 (m, 13H), 6.17 - 5.72 (m, 3H), 3.94 - 3.32 (m, 15H).

Note: The NMR signals were broadened, complicated due to slow conformational exchange on the NMR time scale and no carbon spectrum was recorded.

MS (ESI) *m/z* (relative intensities): [M-H⁺]⁻ 547.13; calcd. 547.21.

Synthesis of *o*-ph₅-OTf

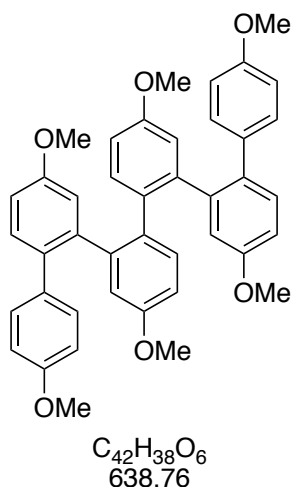
The compound was prepared according to a literature procedure.^[54]

***o*-ph₅-OH** (167 mg, 304 μ mol, 1.00 eq.) was treated with trifluoromethane sulfonic anhydride (78 μ L, 456 μ mol, 1.50 eq.) and pyridine (49 μ L, 608 μ mol, 2.00 eq.) in dry DCM (1 mL) at 0 °C. The product was obtained after purification via flash column chromatography on silica (toluene / EtOAc, 9:1) as a yellowish solid (151 mg, 223 μ mol, 73% [Lit.^[54]: 76%]).

¹H-NMR (400 MHz, CDCl₃): δ (ppm) = 7.22 - 5.39 (m, 16H), 3.94 - 3.28 (m, 15H).

Note: The NMR signals were broadened, complicated due to slow conformational exchange on the NMR time scale and no carbon spectrum was recorded.

MS (ESI) m/z (relative intensities): [M+H⁺]⁺ 681.09 (100); calcd. 681.18.

Synthesis of *o-ph*₆

The compound was prepared according to a literature procedure.^[54] ***o-ph*₅-OTf** (151 mg, 223 μ mol, 1.00 eq.) reacted with 4-methoxyphenylboronic acid pinacol ester (104 mg, 447 μ mol, 2.00 eq.) under the aid of Pd(OAc)₂ (5 mg, 22.3 μ mol, 10mol%), SPhos (11 mg, 26.8 μ mol, 12mol%) and K₃PO₄·H₂O (154 mg, 669 μ mol, 3.00 eq.) in a mixture of THF (2 mL) and H₂O (0.5 mL) under a N₂ atmosphere at 90 °C overnight. After purification via flash column chromatography on silica (toluene / EtOAc, 9:1) the desired product was obtained as a white solid (99 mg, 155 μ mol, 70% [Lit.^[54]: 75%]).

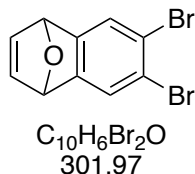
¹H-NMR (400 MHz, CDCl₃): δ (ppm) = 7.55 - 5.59 (m, 24H), 4.02 - 3.16 (m, 18H).

Note: Some NMR signals were broadened, complicated due to slow conformational exchange on the NMR time scale and no carbon spectrum was recorded.

MS (MALDI-TOF) m/z : [M]⁺ 638.620; calcd. 638.266.

7.2 Synthesis of the Nickel-(2,3-bis-diphenylphosphino naphthalene) complex

Synthesis of 6,7-dibromo-1,4-dihydronaphthalene-1,4-epoxide

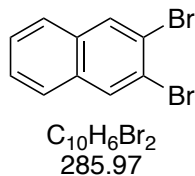


The compound was prepared according to a literature procedure.^[83,84] 1,2,4,5-*tetra*-bromobenzene (7.87 g, 20.0 mmol, 1.00 eq.) and furan (10 mL, 138 mmol, 6.90 eq.) were suspended in dry toluene and cooled to -23 °C. *n*-BuLi (1.6 M, 14 mL) was diluted with dry hexane (200 mL) and then added drop wise over a time of 95 min. The mixture was allowed to warm to RT in 1 h. 1 mL MeOH was then added, the reaction mixture washed with H₂O and the aq. phase extracted with Et₂O. The combined organic phases were then dried over Na₂SO₄, filtered and the solvent removed under reduced pressure. This yielded the desired compound as a beige solid (6.02 g, 20 mmol, quant. [Lit.^[83]: 99%]).

¹H-NMR (400 MHz, CDCl₃): δ (ppm) = 7.47 (s, 2H), 7.00 (t, $J = 1.8, 1.1$ Hz, 2H), 5.67 (s, 2H).

¹³C-NMR (101 MHz, CDCl₃): δ (ppm) = 150.2, 142.7, 125.5, 120.7, 81.8.

Synthesis of 2,3-dibromonaphthalene



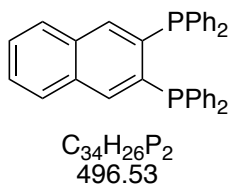
The compound was prepared according to a literature procedure.^[83] Zn-dust (10.77 g, 165 mmol, 9.20 eq.) was suspended in dry THF (300 mL) and cooled down to 0 °C and subsequently TiCl₄ (10.7 mL, 97.6 mmol, 5.45 eq.) was added drop wise. After complete addition, the mixture was heated to reflux for 5 min and then cooled down to 0 °C again. 6,7-Dibromo-1,4-dihydronaphthalene-1,4-epoxide (5.40 g, 17.9 mmol, 1.00 eq.) was dissolved in dry THF (120 mL) and slowly added to the reaction mixture. After completed addition, the mixture was refluxed for 22 h, then allowed to reach RT over 2 h. The mixture was cooled down to 0 °C and an aq. HCl-solution (10%) was added slowly. Afterwards the aq.

phase was extracted with DCM three times and the combined organic phases were dried over Na_2SO_4 , filtered and the solvent removed under reduced pressure. This afforded the desired product as a brownish solid (5.12 g, 17.9 mmol, quant. [Lit.^[83]: 100%]).

$^1\text{H-NMR}$ (400 MHz, CDCl_3): $\delta(\text{ppm}) = 8.13$ (s, 2H), 7.72 (dd, $J = 3.3, 2.8$ Hz, 2H), 7.51 (dd, $J = 3.3, 2.9$ Hz, 2H).

$^{13}\text{C-NMR}$ (101 MHz, CDCl_3): $\delta(\text{ppm}) = 133.0, 132.2, 127.2, 126.9, 122.0$.

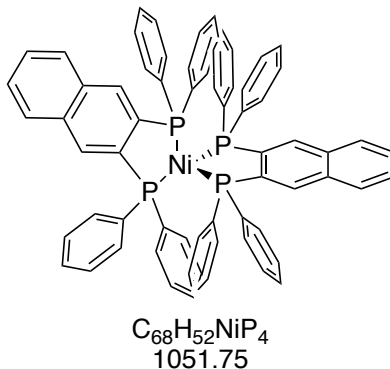
Synthesis of 2,3-bis-diphenylphosphino-naphthalene



2,3-Dibromo-naphthalene (1.00 g, 3.50 mmol, 1.00 eq.) was dissolved in dry THF (3.5 mL). The solution was degassed via bubbling Ar through the solution for 15 min. KPPH_2 -solution (0.5 M in THF, 21 mL, 10.5 mmol, 3.00 eq.) was added to the solution dropwise at RT. The reaction was stirred for 2 days at 60 °C, allowed to reach RT and subsequently diluted with degassed H_2O . The aq. phase was extracted with EtOAc three times, the combined organic phases were dried over Na_2SO_4 , filtered, and the solvent removed under reduced pressure. The crude product was then dryloaded on silica and purified via flash column chromatography (EtOAc / cyclohexane, 5:1). The first fractions were checked with MALDI and to the combined fractions MeCN was added, whereupon a precipitate formed. This precipitate could then be filtered and dried. This yielded the desired ligand as white solid (124 mg, 250 μmol , 7%).

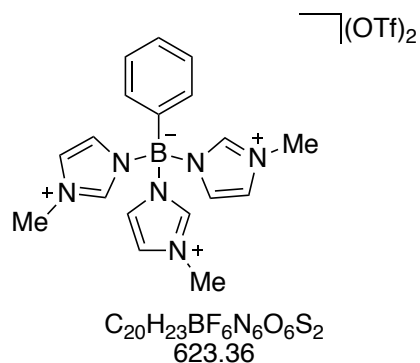
$^1\text{H-NMR}$ (400 MHz, CDCl_3): $\delta(\text{ppm}) = 7.76 - 7.70$ (m, 2H), 7.60 (dd, $J = 3.3, 2.8$ Hz, 2H), 7.49 - 7.45 (m, 2H), 7.44 - 7.39 (m, 2H), 7.37 - 7.33 (m, 2H), 7.32 - 7.15 (m, 16H).

Synthesis of the Nickel-(2,3-bis-diphenylphosphino naphthalene) complex



2,3-Bis-diphenylphosphino-naphthalene (30 mg, 60.4 μ mol, 2.00 eq.) was suspended in THF (0.5 mL). A stock solution of Ni(COD)₂ in THF (0.1 M, 0.3 mL, 30.2 μ M, 1.00 eq.) was added dropwise, whereupon the solution turned red. The solution was stirred under exclusion of light overnight at RT. The solvent was then removed under reduced pressure. The yield of the obtained dark violet crystalline solid was not determined due to the high air-sensitivity of the compound. The same applies for the missing NMR-spectrum.

MS (MALDI-TOF): [M]⁺ 1050.394; calcd. 1050.237.

7.3 Synthesis of the [Ti(MeIm₃)₂](OTf)₂ -complexSynthesis of PhB(MeIm₃)(OTf)₂ (MeIm₃)

1-Methylimidazole (3.10 mL, 39.0 mmol, 3.1 eq.) was added to a stirring solution of PhBCl₂ (1.7 mL, 12.6 mmol, 1.0 eq.) in dry toluene (35 mL) under an Ar-atmosphere. After 5 min of stirring, TMSOTf (4.8 mL, 26.0 mmol, 2.1 eq.) was added dropwise and the reaction mixture was heated to 100 °C for 24 h. The reaction mixture was then allowed to RT, the solvent was decanted and DCM (50 mL) was added to the residual suspension. The solution was refluxed until all solids were nearly completely dissolved. The DCM was concentrated to ~30 mL and then cooled to -25 °C. The formed precipitate was filtered and washed with Et₂O (10 mL) and dried under reduced pressure. The desired product was obtained as a white solid (7.98 g, 12.6 mmol, quant. [Lit.^[113]: 90% (for the *tert*-butyl derivative)]).

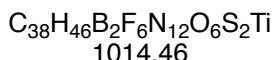
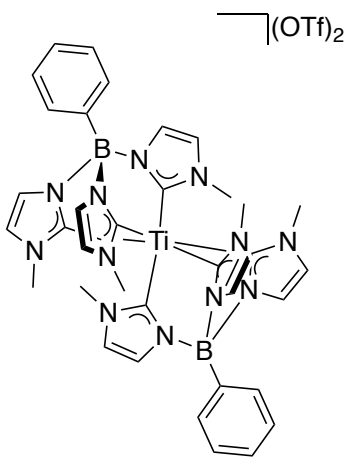
¹H-NMR (400 MHz, CD₃CN): δ(ppm) = 8.09 (s, 3H), 7.50 - 7.41 (m, 6H), 7.19 - 7.15 (m, 2H), 7.14 (t, *J* = 1.8 Hz, 3H), 3.82 (s, 9H).

¹H-NMR (400 MHz, acetone-*d*₆): δ(ppm) = 8.63 (s, 3H), 7.75 (t, *J* = 1.7 Hz, 3H), 7.48 (t, *J* = 1.8 Hz, 3H), 7.45 - 7.38 (m, 3H), 7.32 - 7.28 (m, 2H), 3.99 (s, 9).

¹H-NMR (400 MHz, DMSO-*d*₆): δ(ppm) = 8.55 (s, 3H), 7.80 (t, *J* = 1.7 Hz, 3H), 7.48 - 7.40 (m, 3H), 7.38 (t, *J* = 1.7 Hz, 3H), 7.12 - 7.09 (m, 2H), 3.84 (s, 9H).

¹³C-NMR (101 MHz, DMSO-*d*₆): δ(ppm) = 139.4, 132.6, 128.9, 128.4, 124.5, 123.9, 122.2, 119.0, 35.5.

C₁₉H₂₃BN₆F₃O₃S (ESI) HRMS: calculated: 483.1592
 measured: 483.1597

Synthesis of $[\text{Ti}(\text{MeIm}_3)_2](\text{OTf})_2$ 

PhB(MeIm₃)(OTf)₂ (503 mg, 0.79 mmol, 2.00 eq.) was suspended in dry THF (4.2 mL) under an Ar-atmosphere and cooled down to -78 °C. LDA (2 M in THF, 2.38 mL, 4.76 mmol, 6.02 eq.) was then added dropwise. The resulting solution was stirred at this temperature for 45 min and then brought slowly to RT. TiCl₄ (43 μL, 395 μmol, 1.00 eq.) was added drop wise and the reaction mixture further stirred for 24 h at RT. The mixture was then filtered under inert conditions and the solvent removed under reduced pressure. This approach yielded a red crystalline solid (127 mg, 0.19 mmol, 48%).

¹H-NMR (400 MHz, CD₃CN): δ(ppm) = 8.10 (s, 3H), 7.48 - 7.42 (m, 8H), 7.31 - 7.12 (m, 14), 6.98 (s, 2H), 6.90 (s, 1H), 3.82 (s, 9H), 3.65 - 3.64 (m, 9H).

The assignment was only done tentatively. The splitting of the signals is most probably attributed to the perturbed symmetry of the complex.

8 References

- [1] Barack Obama on climate change, <https://www.weforum.org/agenda/2015/11/15-quotes-on-climate-change-by-world-leaders/>, Accessed: 2018-04-11.
- [2] N. S. Lewis, D. G. Nocera, *Proceedings of the National Academy of Sciences* **2006**, *103*, 15729–15735.
- [3] P. Nejat, F. Jomehzadeh, M. M. Taheri, M. Gohari, M. Z. Muhd, *Renewable and Sustainable Energy Reviews* **2015**, *43*, 843–862.
- [4] O. Ellabban, H. Abu-Rub, F. Blaabjerg, *Renewable and Sustainable Energy Reviews* **2014**, *39*, 748–764.
- [5] J. Barber, *Quarterly Reviews of Biophysics* **2003**, *36*, 71–89.
- [6] D. Wöhrle, M. W. Tausch, W.-D. Stohrer, *Photochemie*, Wiley-VCH Verlag GmbH & Co. KGaA, Weinheim, FRG, **1998**.
- [7] C. Tommos, G. T. Babcock, *Accounts of Chemical Research* **1998**, *31*, 18–25.
- [8] J. Nield, O. Kruse, J. Ruprecht, P. Fonseca, C. Büchel, *The Journal of Biological Chemistry* **2000**, *275*, 27940–27946.
- [9] A. Zouni, H. T. Witt, J. Kern, P. Fromme, N. Krauss, W. Saenger, P. Orth, *Nature* **2001**, *409*, 739–743.
- [10] Y. Umena, K. Kawakami, J. R. Shen, N. Kamiya, *Nature* **2011**, *473*, 55–60.
- [11] B. Kok, B. Forbush, M. McGloin, *Photochemistry and Photobiology* **1970**, *11*, 457–475.
- [12] H. Dau, M. Haumann, *Coordination Chemistry Reviews* **2008**, *252*, 273–295.
- [13] K. N. Ferreira, T. M. Iverson, K. Maghlaoui, J. Barber, S. Iwata, *Science* **2004**, *303*, 1831–1838.
- [14] A. Arrigo, A. Santoro, F. Puntoriero, P. P. Lainé, S. Campagna, *Coordination Chemistry Reviews* **2015**, *304-305*, 109–116.
- [15] G. N. Lim, C. O. Obondi, F. D’Souza, *Angewandte Chemie - International Edition* **2016**, *55*, 11517–11521.
- [16] R. Schroot, T. Schlotthauer, B. Dietzek, M. Jäger, U. S. Schubert, *Chemistry - A European Journal* **2017**, *23*, 16484–16490.
- [17] S. Fukuzumi, *Physical Chemistry Chemical Physics* **2008**, *10*, 2283–2297.
- [18] E. A. Weiss, M. J. Ahrens, L. E. Sinks, A. V. Gusev, M. A. Ratner, M. R. Wasielewski, *Journal of the American Chemical Society* **2004**, *126*, 5577–5584.
- [19] O. S. Wenger, *Accounts of Chemical Research* **2011**, *44*, 25–35.

-
- [20] W. B. Davis, W. A. Svec, M. A. Ratner, M. R. Wasielewski, *Nature* **1998**, *396*, 60–63.
- [21] M. Bixon, J. Jortner in *Electron Transfer - from Isolated Molecules to Biomolecules*, Wiley-Blackwell, **2007**, pp. 35–202.
- [22] J. R. Winkler, H. B. Gray, *Journal of the American Chemical Society* **2014**, *136*, 2930–2939.
- [23] R. A. Marcus, *The Journal of Chemical Physics* **1956**, *24*, 966–978.
- [24] S. S. Isied, A. Vassilian, J. F. Wishart, C. Creutz, H. A. Schwarz, N. Sutin, *Journal of the American Chemical Society* **1988**, *110*, 635–637.
- [25] H. B. Gray, J. R. Winkler, *Proceedings of the National Academy of Sciences* **2005**, *102*, 3534–3539.
- [26] H. M. McConnell, *The Journal of Chemical Physics* **1961**, *35*, 508–515.
- [27] E. Zojer, J. Cornil, G. Leising, J. L. Bredas, *Physical Review B* **1999**, *59*, 7957–7968.
- [28] M. T. Indelli, C. Chiorboli, L. Flamigni, L. D. Cola, F. Scandola, *Inorg. Chem.* **2007**, *46*, 5630–5641.
- [29] A. Helms, D. Heiler, G. McLendon, *Journal of the American Chemical Society* **1992**, *114*, 6227–6238.
- [30] D. Hanss, O. S. Wenger, *Inorganic Chemistry* **2008**, *47*, 9081–9084.
- [31] D. Hanss, O. S. Wenger, *European Journal of Inorganic Chemistry* **2009**, 3778–3790.
- [32] D. Hanss, M. E. Walther, O. S. Wenger, *Coordination Chemistry Reviews* **2010**, *254*, 2584–2592.
- [33] H. C. Schmidt, C. B. Larsen, O. S. Wenger, *Angewandte Chemie - International Edition* **2018**, *57*, 6696–6700.
- [34] C. Atienza-Castellanos, M. Wielopolski, D. M. Guldi, C. van der Pol, M. R. Bryce, S. Filippone, N. Martín, *Chemical Communications* **2007**, *0*, 5164.
- [35] R. H. Goldsmith, L. E. Sinks, R. F. Kelley, L. J. Betzen, W. Liu, E. A. Weiss, M. A. Ratner, M. R. Wasielewski, *Proceedings of the National Academy of Sciences* **2005**, *102*, 3540–3545.
- [36] M. Natali, S. Campagna, F. Scandola, *Chemical Society Reviews* **2014**, *43*, 4005–4018.
- [37] V. Lloveras, J. Vidal-Gancedo, T. M. Figueira-Duarte, J. F. Nierengarten, J. J. Novoa, F. Mota, N. Ventosa, C. Rovira, J. Veciana, *Journal of the American Chemical Society* **2011**, *133*, 5818–5833.
- [38] J. Sukegawa, C. Schubert, X. Zhu, H. Tsuji, D. M. Guldi, E. Nakamura, *Nature Chemistry* **2014**, *6*, 899–905.

-
- [39] K. E. Linton, M. A. Fox, L. O. Pålsson, M. R. Bryce, *Chemistry - A European Journal* **2014**, *21*, 3997–4007.
- [40] B. a. G. Hammer, K. Müllen, *Chemical Reviews* **2016**, *116*, 2103–2140.
- [41] S. M. Mathew, C. S. Hartley, *Macromolecules* **2011**, *44*, 8425–8432.
- [42] A. Muraoka, *Chemical Physics Letters* **2013**, *582*, 44–48.
- [43] J. He, J. L. Crase, S. H. Wadumethrige, K. Thakur, L. Dai, S. Zou, R. Rathore, C. S. Hartley, *Journal of the American Chemical Society* **2010**, *132*, 13848–13857.
- [44] Y. Mizukoshi, K. Mikami, M. Uchiyama, *Journal of the American Chemical Society* **2015**, *137*, 74–77.
- [45] S. Ito, K. Takahashi, K. Nozaki, *Journal of the American Chemical Society* **2014**, *136*, 7547–7550.
- [46] C. S. Hartley, J. He, *Journal of Organic Chemistry* **2010**, *75*, 8627–8636.
- [47] J. He, S. M. Mathew, S. D. Cornett, S. C. Grundy, C. S. Hartley, *Organic & Biomolecular Chemistry* **2012**, *10*, 3398.
- [48] G. N. Vemuri, M. Chu, H. Dong, B. J. Spinello, C. S. Hartley, *Org. Biomol. Chem.* **2017**, 845–851.
- [49] V. W. W. Yam, K. M. C. Wong, *Chemical Communications* **2011**, *47*, 11579–11592.
- [50] L. A. Büldt, X. Guo, R. Vogel, A. Prescimone, O. S. Wenger, *Journal of the American Chemical Society* **2017**, *139*, 985–992.
- [51] L. A. Büldt, C. B. Larsen, O. S. Wenger, *Chemistry - A European Journal* **2017**, *23*, 8577–8580.
- [52] Y. Liu, P. Persson, V. Sundström, K. Wärnmark, *Accounts of Chemical Research* **2016**, *49*, 1477–1485.
- [53] L. Liu, T. Duchanois, T. Etienne, A. Monari, M. Beley, X. Assfeld, S. Haacke, P. C. Gros, *Physical Chemistry Chemical Physics* **2016**, *18*, 12550–12556.
- [54] J. He, J. L. Crase, S. H. Wadumethrige, K. Thakur, L. Dai, S. Zou, R. Rathore, C. S. Hartley, *Journal of the American Chemical Society* **2010**, *132*, 13848–13857.
- [55] T. Higashino, T. Yamada, M. Yamamoto, A. Furube, N. V. Tkachenko, T. Miura, Y. Kobori, R. Jono, K. Yamashita, H. Imahori, *Angewandte Chemie - International Edition* **2016**, *55*, 629–633.
- [56] S. Ando, E. Ohta, A. Kosaka, D. Hashizume, H. Koshino, T. Fukushima, T. Aida, *Journal of the American Chemical Society* **2012**, *134*, 11084–11087.
- [57] J. Hankache, M. Niemi, H. Lemmetyinen, O. S. Wenger, *Inorganic Chemistry* **2012**, *51*, 6333–6344.
-

-
- [58] K. Sreenath, T. G. Thomas, K. R. Gopidas, *Organic Letters* **2011**, *13*, 1134–1137.
- [59] A. Weller, *Zeitschrift für Physikalische Chemie Neue Folge* **1982**, *133*, 93–98.
- [60] L. G. Gagliardi, C. B. Castells, C. Ràfols, M. Rosés, E. Bosch, *Journal of Chemical and Engineering Data* **2007**, *52*, 1103–1107.
- [61] C. A. Panetta, H. J. Kumpaty, N. E. Heimer, M. C. Leavy, C. L. Hussey, *Journal of Organic Chemistry* **1999**, *64*, 1015–1021.
- [62] D. R. Striplin, S. Y. Reece, D. G. McCafferty, C. G. Wall, D. A. Friesen, B. W. Erickson, T. J. Meyer, *Journal of the American Chemical Society* **2004**, *126*, 5282–5291.
- [63] D. Hanss, O. S. Wenger, *Inorganic Chemistry* **2009**, *48*, 671–680.
- [64] C. Herrmann, J. Elmisz, *Chemical Communications* **2013**, *49*, 10456.
- [65] M. Cordes, B. Giese, *Chemical Society Reviews* **2009**, *38*, 892.
- [66] M. P. Eng, B. Albinsson, *Chemical Physics* **2009**, *357*, 132–139.
- [67] B. Albinsson, M. P. Eng, K. Pettersson, M. U. Winters, *Physical Chemistry Chemical Physics* **2007**, *9*, 5847.
- [68] S. Welter, F. Lafolet, E. Cecchetto, F. Vergeer, L. De Cola, *ChemPhysChem* **2005**, *6*, 2417–2427.
- [69] R. H. Goldsmith, O. DeLeon, T. M. Wilson, D. Finkelstein-Shapiro, M. A. Ratner, M. R. Wasielewski, *Journal of Physical Chemistry A* **2008**, *112*, 4410–4414.
- [70] M. Kuss-Petermann, O. S. Wenger, *Angewandte Chemie - International Edition* **2016**, *55*, 815–819.
- [71] M. Kuss-Petermann, O. S. Wenger, *CHIMIA International Journal for Chemistry* **2016**, *70*, 177–181.
- [72] R. A. Marcus, *The Journal of Chemical Physics* **1965**, *43*, 679–701.
- [73] D. Lotter, M. Neuburger, M. Rickhaus, D. Häüssinger, C. Sparr, *Angewandte Chemie - International Edition* **2016**, *55*, 2920–2923.
- [74] P. Lloyd-Williams, E. Giralt, *Chemical Society Reviews* **2001**, *30*, 145–157.
- [75] M. Montalti, A. Credi, L. Prodi, M. Teresa Gandolfi, *Handbook of Photochemistry, Third Edition*, CRC Press, Taylor and Francis Group, **2006**, p. 650.
- [76] E. Y. Li, Y. M. Cheng, C. C. Hsu, P. T. Chou, G. H. Lee, I. H. Lin, Y. Chi, C. S. Liu, *Inorganic Chemistry* **2006**, *45*, 8041–8051.
- [77] A. D. Becke, *The Journal of Chemical Physics* **1993**, *98*, 1372–1377.
- [78] T. Yanai, D. P. Tew, N. C. Handy, *Chemical Physics Letters* **2004**, *393*, 51–57.
-

-
- [79] M. J. Peach, T. Helgaker, P. Sałek, T. W. Keal, O. B. Lutnaes, D. J. Tozer, N. C. Handy, *Physical Chemistry Chemical Physics* **2006**, *8*, 558–562.
- [80] M. J. Frisch, J. A. Pople, J. S. Binkley, *The Journal of Chemical Physics* **1984**, *80*, 3265–3269.
- [81] W. R. Wadt, P. J. Hay, *The Journal of Chemical Physics* **1985**, *82*, 284–298.
- [82] P. J. Hay, W. R. Wadt, *The Journal of Chemical Physics* **1985**, *82*, 299–310.
- [83] A. Link, C. Fischer, C. Sparr, *Angewandte Chemie - International Edition* **2015**, *54*, 12163–12166.
- [84] H. Hart, A. Bashir-Hashemi, J. Luo, M. A. Meador, *Tetrahedron* **1986**, *42*, 1641–1654.
- [85] C. S. LeHoullier, G. W. Gribble, *Journal of Organic Chemistry* **1983**, *48*, 2364–2366.
- [86] M. T. Honaker, B. J. Sandefur, J. L. Hargett, A. L. McDaniel, R. N. Salvatore, *Tetrahedron Letters* **2003**, *44*, 8373–7377.
- [87] D. Tofan, C. C. Cummins, *Chemical Science* **2012**, *3*, 2474–2478.
- [88] F. Bayrakçeken, *Spectrochimica Acta - Part A: Molecular and Biomolecular Spectroscopy* **2008**, *71*, 603–608.
- [89] C. H. Lin, Y. Y. Chang, J. Y. Hung, C. Y. Lin, Y. Chi, M. W. Chung, C. L. Lin, P. T. Chou, G. H. Lee, C. H. Chang, W. C. Lin, *Angewandte Chemie - International Edition* **2011**, *50*, 3182–3186.
- [90] S. V. Lozovskiy, A. Y. Ivanov, A. S. Bogachenkov, A. V. Vasilyev, *ChemistrySelect* **2017**, *2*, 4505–4510.
- [91] C. K. Tseng, *Journal of Organic Chemistry* **1979**, *44*, 2793–2794.
- [92] J. P. Sauvage, J. P. Collin, J. C. Chambron, S. Guillerez, C. Coudret, V. Balzani, F. Barigelletti, L. De Cola, L. Flamigni, *Chemical Reviews* **1994**, *94*, 993–1019.
- [93] K. S. Schanze, D. Brent MacQueen, T. A. Perkins, L. A. Cabana, *Coordination Chemistry Reviews* **1993**, *122*, 63–89.
- [94] D. Stufkens, *Coordination Chemistry Reviews* **1998**, *177*, 127–179.
- [95] M. S. Lowry, S. Bernhard, *Chemistry - A European Journal* **2006**, *12*, 7970–7977.
- [96] J. Li, P. I. Djurovich, B. D. Alleyne, M. Yousufuddin, N. N. Ho, J. C. Thomas, J. C. Peters, R. Bau, M. E. Thompson, *Inorganic Chemistry* **2005**, *44*, 1713–1727.
- [97] K. N. Swanick, S. Ladouceur, E. Zysman-Colman, Z. Ding, *Angewandte Chemie - International Edition* **2012**, *51*, 11079–11082.
- [98] F. Monti, F. Kessler, M. Delgado, J. Frey, F. Bazzanini, G. Accorsi, N. Armaroli, H. J. Bolink, E. Ortí, R. Scopelliti, M. K. Nazeeruddin, E. Baranoff, *Inorganic Chemistry* **2013**, *52*, 10292–10305.
-

-
- [99] C. A. Hampel, *The Encyclopedia of the Chemical Elements*, Reinhold Book Corp., **1968**, pp. 732–738.
- [100] G. Haxel, J. Hedrick, G. Orris, *United States Geological Survey Fact Sheet* **2002**, *087*, 4.
- [101] J. K. McCusker, *Accounts of Chemical Research* **2003**, *36*, 876–887.
- [102] N. H. Damrauer, G. Cerullo, A. Yeh, T. R. Boussie, C. V. Shank, J. K. McCusker, *Science* **1997**, *275*, 54–57.
- [103] Y. Zhang, J. L. Petersen, C. Milsmann, *Journal of the American Chemical Society* **2016**, *138*, 13115–13118.
- [104] M. Kitano, S. Y. Hayashi, T. Tanaka, H. Yorimitsu, N. Aratani, A. Osuka, *Angewandte Chemie - International Edition* **2012**, *51*, 5593–5597.
- [105] K. Calderon-Kawasaki, S. Kularatne, H. L. Yue, B. C. Noll, W. R. Scheidt, D. H. Burns, *Journal of Organic Chemistry* **2007**, *72*, 9081–9087.
- [106] S. H. H. Zaidi, K. Muthukumar, S. I. Tamaru, J. S. Lindsey, *Journal of Organic Chemistry* **2004**, *69*, 8356–8365.
- [107] D. S. Sharada, A. Z. Muresan, K. Muthukumar, J. S. Lindsey, *Journal of Organic Chemistry* **2005**, *70*, 3500–3510.
- [108] X. Sheng, Y. Wang, Y. Qin, X. Wang, F. Wang, *RSC Advances* **2014**, *4*, 54043–54050.
- [109] B. J. Littler, M. A. Miller, C.-H. Hung, R. W. Wagner, D. F. O’Shea, P. D. Boyle, J. S. Lindsey, *Journal of Organic Chemistry* **1999**, *64*, 1391–1396.
- [110] J. M. Smith, *Comments on Inorganic Chemistry* **2008**, *29*, 189–233.
- [111] S. Trofimenko, *Accounts of Chemical Research* **1971**, *4*, 17–22.
- [112] S. Trofimenko, *Scorpionates: the coordination chemistry of polypyrazolborate ligands*, Imperial College Press, **1999**, p. 282.
- [113] R. E. Cowley, R. P. Bontchev, E. N. Duesler, J. M. Smith, *Inorganic Chemistry* **2006**, *45*, 9771–9779.
- [114] H. E. Gottlieb, V. Kotlyar, A. Nudelman, *Journal of Organic Chemistry* **1997**, *62*, 7512–7515.
- [115] S. Duric, C. C. Tzschucke, *Organic Letters* **2011**, *13*, 2310–2313.
- [116] L. H. Uppadine, J. E. Redman, S. W. Dent, M. G. B. Drew, P. D. Beer, *Inorganic Chemistry* **2001**, *40*, 2860–2869.
- [117] M. Ito, H. Kubo, I. Itani, K. Morimoto, T. Dohi, Y. Kita, *Journal of the American Chemical Society* **2013**, *135*, 14078–14081.
-

-
- [118] V. Jeux, D. Demeter, P. Leriche, J. Roncali, *RSC Advances* **2013**, *3*, 5811–5814.
- [119] L. G. Heinz, O. Yushchenko, M. Neuburger, E. Vauthey, O. S. Wenger, *Journal of Physical Chemistry A* **2015**, *119*, 5676–5684.
- [120] C. Lambert, G. Nöll, E. Schmälzlin, K. Meerholz, C. Bräuchle, *Chemistry - A European Journal* **1998**, *4*, 2129–2135.
- [121] A. M. Simion, I. Hashimoto, Y. Mitoma, N. Egashira, C. Simion, *Synthetic Communications* **2012**, *42*, 921–931.
- [122] J. Chen, M. Kuss-Petermann, O. S. Wenger, *Chemistry - A European Journal* **2014**, *20*, 4098–4104.
- [123] A. Schlapbach, L. Revesz, G. Koch, Heterocyclic compounds useful as MK2 inhibitors, European Patent, **2009**.

Abbreviations

A acceptor

aq. aqueous

BuLi *n*-buthyl-lithium

CS charge separation

CV cyclic voltammetry

D donor

DCM dichloromethane

DCTB *trans*-2-[3-(4-*tert*-Butylphenyl)-2-methyl-2-propenyldiene]malononitrile

DFT Density Functional Theory

ESI Electrospray Ionization

EtOH ethanol

HCl hydrochloric acid

HOMO highest occupied molecular orbital

HPLC High Performance Liquid Chromatography

ISC Intersystem Crossing

LDA lithium diisopropylamide

LHCs light harvesting complexes

LMCT ligand to metal charge transfer

LUMO lowest unoccupied molecular orbital

MALDI Matrix-assisted Laser Desorption/Ionization

MeCN acetonitrile

MLCT metal to ligand charge transfer

MMFF Merck Molecular Force Field

MS Mass Spectrometry

MeOH methanol

MV methyl viologen

mm millimeter

min minutes

MMFF Molecular Mechanics Force Field

m/z mass to charge

NaOH sodium hydroxide

NHC N-heterocyclic carbene

NADP⁺ nicotinamide adenine dinucleotide phosphate

nm nanometer

NMR Nuclear Magnetic Resonance

ns nanosecond

OEC oxygen evolving complex

Pheo pheophytin

PS photosystem

ppm parts per million

ps picosecond

RT room temperature

sat. saturated

TA transient absorption

TAA *N,N*-bis-(4-methoxyphenyl)aniline

TBAPF₆ tetra-*n*-butylammonium hexafluorophosphate

TCSPC time correlated single photon counting

THF tetrahydrofuran

TLC thin layer chromatography

Tyr tyrosine

SCE saturated calomel electrode

UV ultraviolett

A Appendix

Transient absorption spectroscopy

The dyads in the electron transfer studies from chapter 2 were not only performed in MeCN but also in DCM. The data for the temporal evolution of the rise at 750 nm for the TAA⁺-absorbance in DCM is not of sufficient quality to obtain satisfactory time constants. In the following the kinetic traces of 20 μM solutions of two dyads after excitation at 532 nm with pulses of ~ 30 ps duration in deaerated DCM are shown (Figure A.2).

For the thermal back reaction decays were recorded in deaerated 20 μM solution of all three dyads in either deaerated MeCN (detection wavelengths: 370, 510 and 750 nm) or DCM (detection wavelengths: 370 and 750 nm) after excitation at 532 nm with pulses of ~ 10 ns duration.

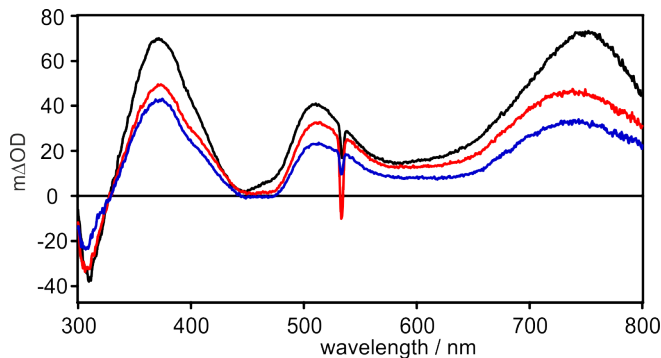


Figure A.1: Transient absorption spectra of 20 μM solutions of all three dyads recorded immediately after excitation at 532 nm with laser pulses of ~ 10 ns duration in deaerated DCM. The spectra were time integrated over an interval of 200 ns. The colour code is black: $n = 1$, red: $n = 2$, blue: $n = 3$.

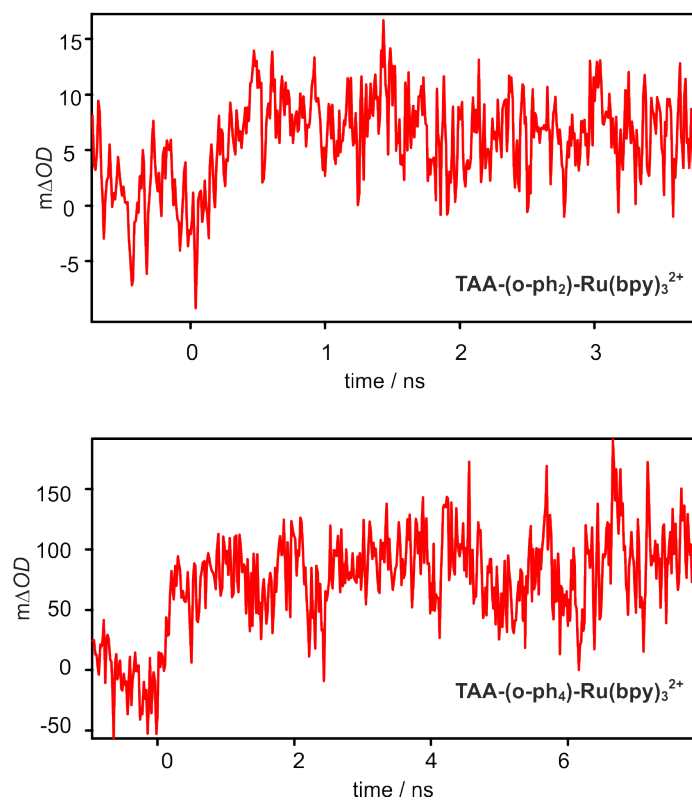


Figure A.2: Temporal evolution of the transient signal at 750 nm of the TAA^+ (red trace) after excitation at 532 nm with pulses of ~ 30 ps duration of 20 μM solutions of the two dyads. Measurements were performed at 22 $^{\circ}C$ in deaerated DCM. Data was not of sufficient quality, no fits were made.

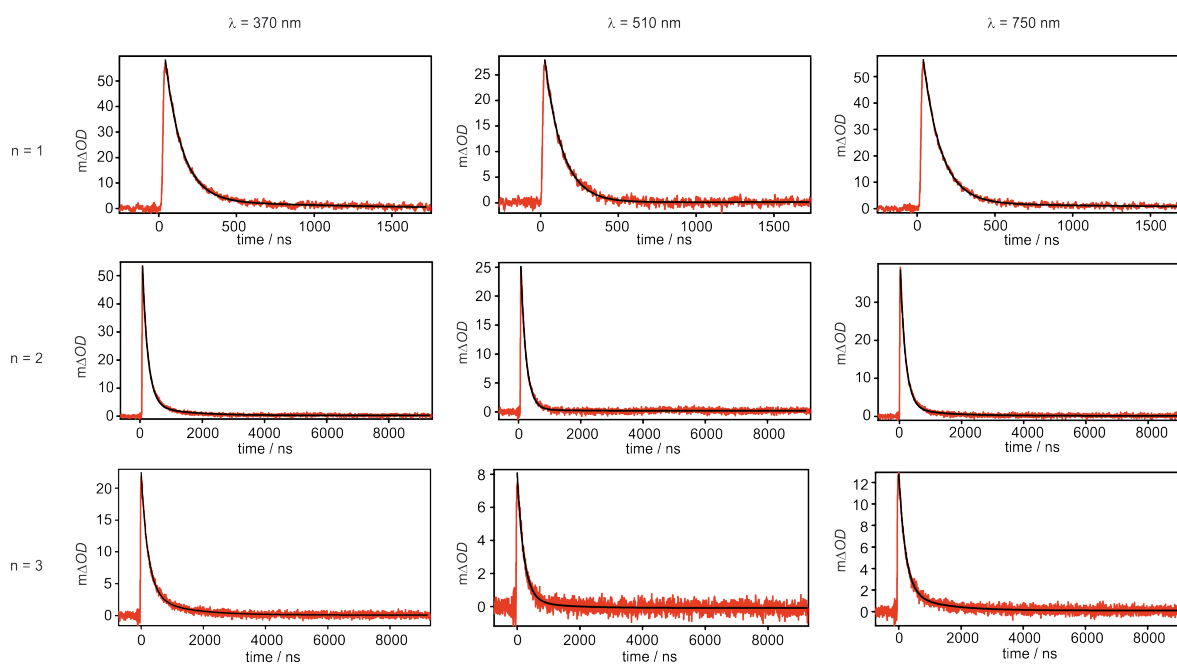


Figure A.3: Transient absorption decays (red) recorded at three different wavelengths for all three dyads recorded in deaerated MeCN at 22 °C. The sample concentrations were 20 μ M, the excitation wavelength was 532 nm and the laser pulse duration was \sim 10 ns. Exponential fits are shown in black. All time constants are given in chapter 2.5.3.

Kinetic traces from the flash quench experiments

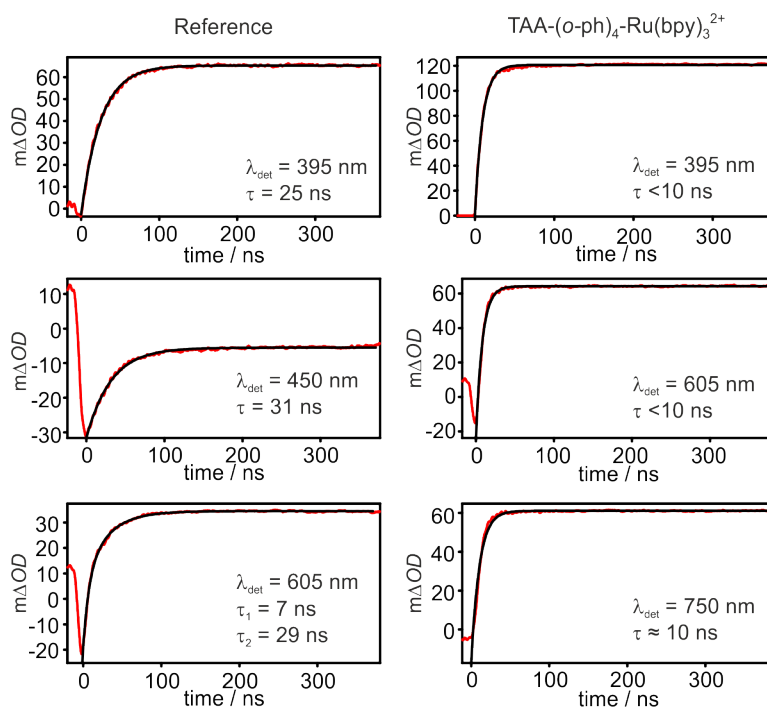


Figure A.4: Kinetic traces from the flash quench experiment described in chapter 2.6. Measurements were performed in deaerated MeCN, in 20 μM solutions of the dyads with additional 80 mM methyl viologen. Black curve depicts fit to the data. Excitation wavelength was 532 nm. Detection wavelength (λ_{det} as well as the time constants are given in the insets for the reference ruthenium complex as well as for the dyad with n = 2.)

Data for the Arrhenius plots

Here the complete data obtained from transient absorption spectroscopy for all three dyads in MeCN and DCM can be found.

Table 16: Time constants for thermal backward reaction from $\text{Ru}(\text{bpy})_3^+$ to TAA^+ at different temperatures measured in 20 μM solutions in deaerated MeCN. The decays were measured at 370 and 750 nm and the emission of the reference compound was measured at 660 nm.

T [$^{\circ}\text{C}$]	n = 1 τ_{ET} [ns]	n = 2 τ_{ET} [ns]	n = 3 τ_{ET} [ns]	Reference τ_f (660 nm) [ns]	λ [nm]
5	125	220	315	1315	370
5	125	220	310	1315	750
15	120	210	280	1250	370
15	120	200	280	1250	750
25	115	185	240	1190	370
25	110	180	240	1190	750
35	110	170	220	1130	370
35	100	160	210	1130	750
45	105	160	200	1050	370
45	100	140	180	1050	750
55	100	140	170	970	370
55	90	125	160	970	750
65	90	140	165	880	370
65	85	110	140	880	750

Table 17: Time constants for thermal backward reaction from $\text{Ru}(\text{bpy})_3^+$ to TAA^+ at different temperatures measured in 20 μM solutions in deaerated DCM. The decays were measured at 370 and 750 nm and the emission of the reference compound was measured at 660 nm.

T [$^{\circ}\text{C}$]	n = 1 τ_{ET} [ns]	n = 2 τ_{ET} [ns]	n = 3 τ_{ET} [ns]	Reference τ_f (660 nm) [ns]	λ [nm]
-5	220	300	280	2120	370
-5	210	290	260	2120	750
5	190	240	215	2000	370
5	180	240	215	2000	750
15	170	200	190	1920	370
15	165	200	180	1920	750
25	145	160	140	1790	370
25	150	160	145	1790	750

Structures of the *para*-connected systems

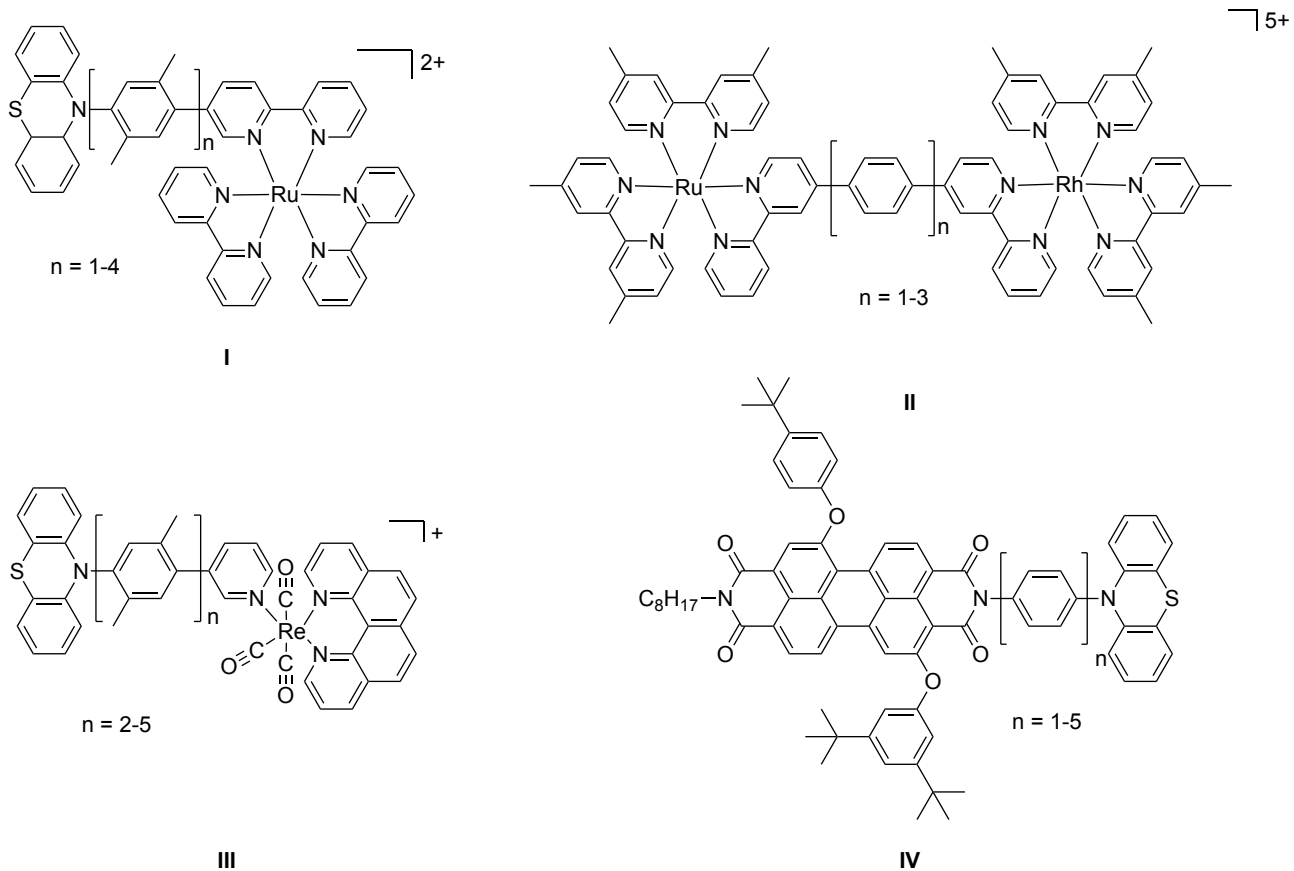


Figure A.5: Structures of the *para*-connected systems, presented in chapter 2.7. I,^[31] II,^[28] III,^[30] IV.^[18]

NMR-spectra of the dyads

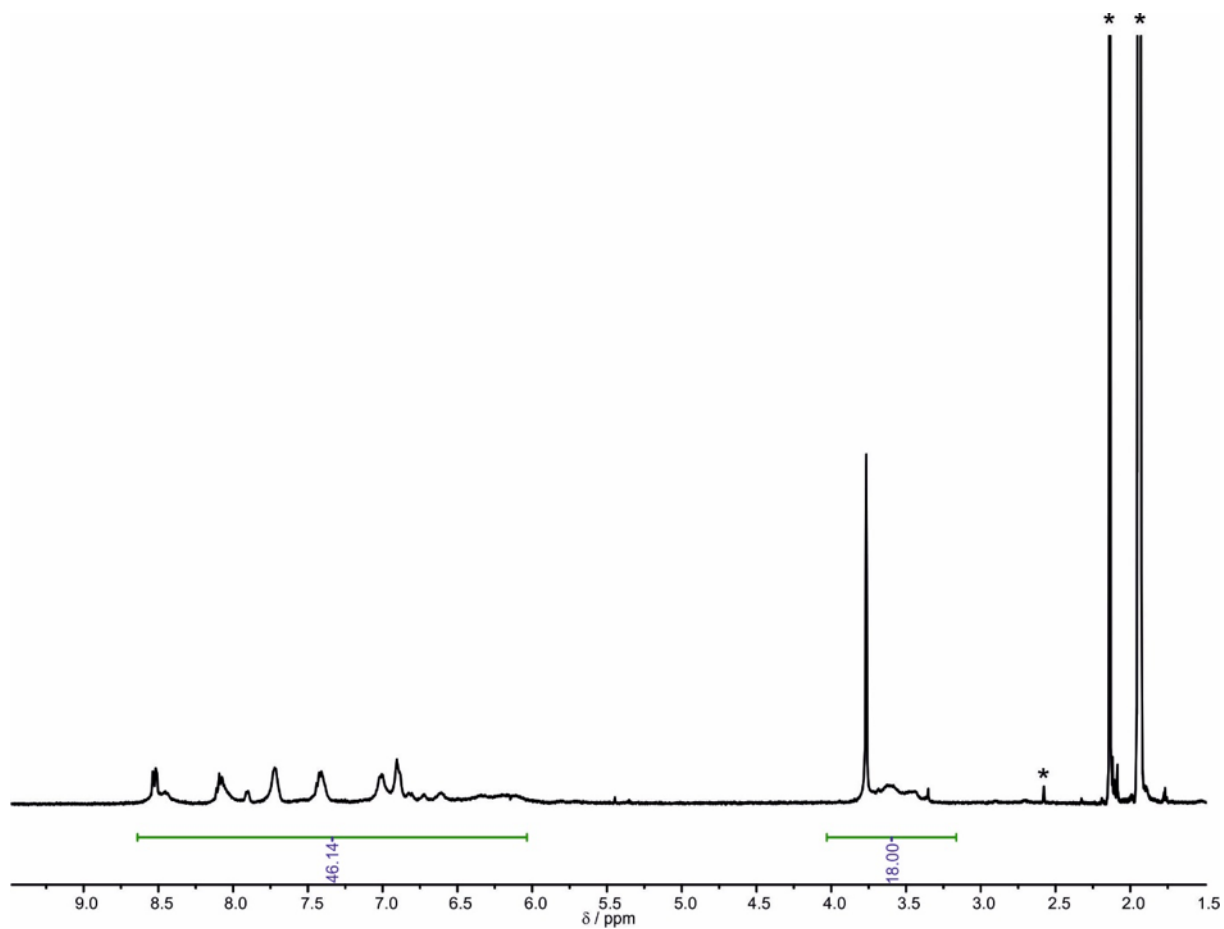


Figure A.6: $^1\text{H-NMR}$ -spectrum of $[\text{TAA-}(o\text{-ph}_4)\text{-Ru}(\text{bpy})_3^{2+}](\text{PF}_6)_2$, recorded in CD_3CN at room temperature. The signals are broad and can not directly be assigned due to interconverting conformers in solution. The residual solvent peak of CD_3CN , water from the deuterated solvent used, and a peak which could not be assigned are marked with an asterisk (*).

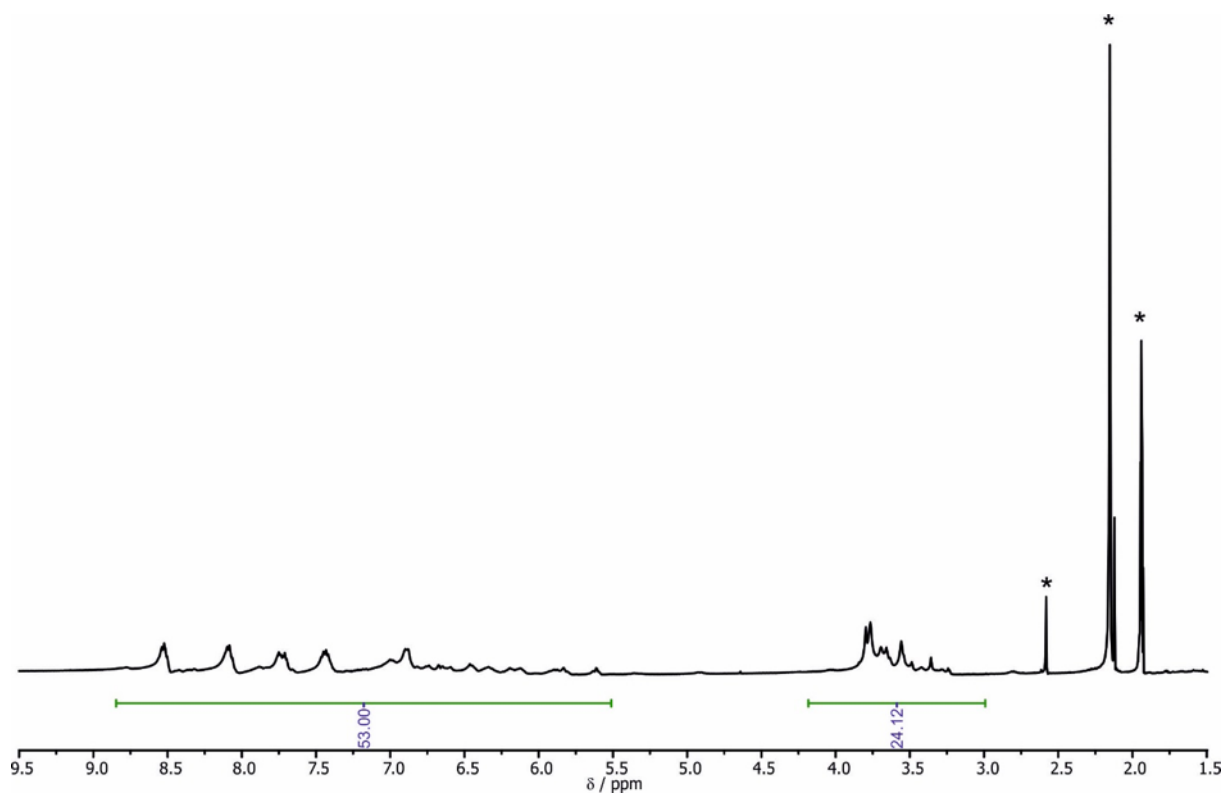


Figure A.7: ^1H -NMR-spectrum of $[\text{TAA}-(o\text{-ph}_6)\text{-Ru}(\text{bpy})_3^{2+}](\text{PF}_6)_2$, recorded in CD_3CN at room temperature. The signals are broad and can not directly be assigned due to interconverting conformers in solution. The residual solvent peak of CD_3CN , water from the deuterated solvent used and, a peak which could not be assigned are marked with an asterisk (*).

Temperature dependent NMR-measurements of $[\text{TAA}-(o\text{-ph}_4)\text{-Ru}(\text{bpy})_3^{2+}](\text{PF}_6)_2$

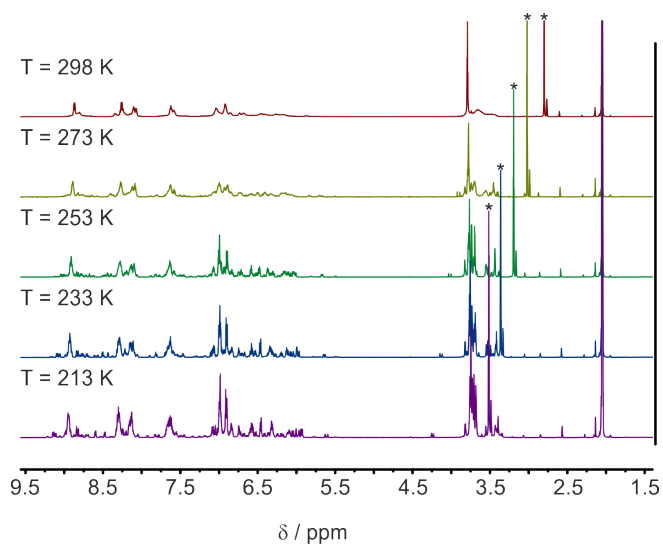


Figure A.8: Temperature dependent ^1H -NMR-spectra of $[\text{TAA}-(o\text{-ph}_4)\text{-Ru}(\text{bpy})_3^{2+}](\text{PF}_6)_2$ measured in acetone- d_6 from 213 K (bottom) to 273 K (2nd row) in 20 K intervals. On top is the spectrum at RT. The residual H_2O peak is marked with an asterisk (*).

Transient absorption decays of TAA-(*o*-naph)_{*n*}-Ru(bpy)₃²⁺

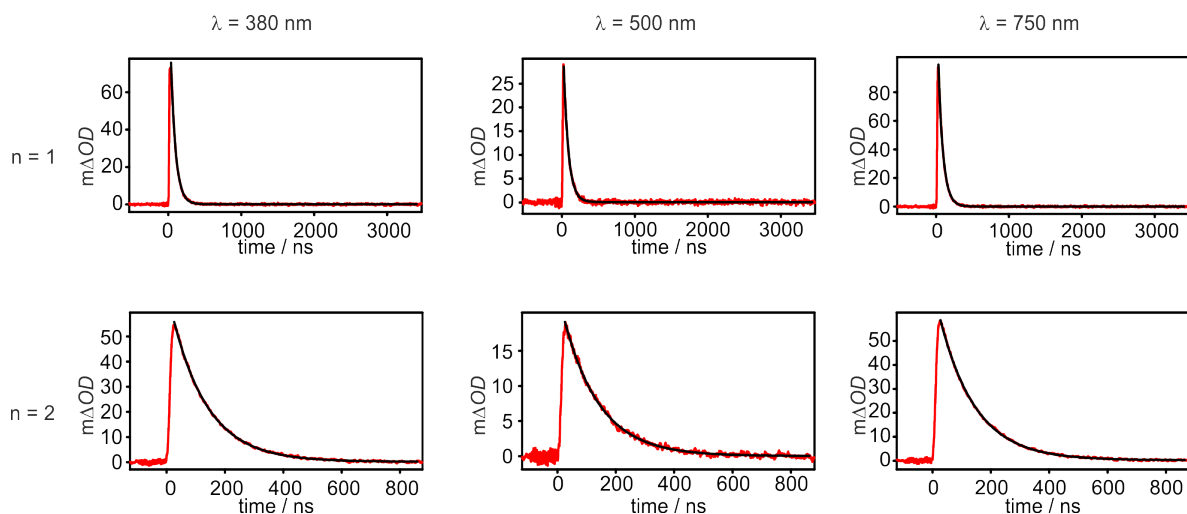


Figure A.9: Transient absorption decays (red) recorded at three different wavelengths for the two dyads recorded in deaerated MeCN at 22 °C. The sample concentrations were 20 μM, the excitation wavelength was 532 nm and the laser pulse duration was ~10 ns. Exponential fits are shown in black. All time constants are given in chapter 3.

B Acknowledgement

FIRST of all I would like to express my gratitude to Prof. Oliver S. Wenger for his support, kindness and guidance throughout the last 3.5 years. Your impact on my scientific work as well as on my personal development is without a doubt unprecedented.

Further I would like to thank Prof. Silvio Decurtins for accepting the co-examination and spending the time to travel to Basel and reading my doctoral thesis.

I would also like to thank Florian P. Seebeck for chairing the PhD defence session and for being a very pleasant neighbour before you moved to the Rosental. I mostly enjoyed the soapy bubbles!

The Werkstatt-Team is an amazing team of wizards who fix things and deal with a house of stressed PhD students, but still remain their sunny mood! I think we are very fortunate to have them and a lot of measurements would not have been there in time without this great. But it is not only the hardware which has to be fixed - moving from one country to another can sometimes bring up problems, further breaking a leg, organising exams does not make life easier. Luckily there are Brigitte Hohwald, Marina Mambelli Johnson and Beatrice Erismann, who supported me in any of these cases and I am very thankful for what they did for me.

The molecules I made became quite long - and floppy! Measuring NMR is not the easiest on these. Therefore Daniel Häussinger is thanked for his help with the analysis of NMR-data as well as carrying out temperature-dependent measurements.

Special thanks go to Martin, Laura and Hauke for proof-reading my thesis! Of course also Matthias is thanked for all his advice and helpful comments on all the snippets and sneak previews he got.

Of course I would like to thank former and current group members of the AK Wenger. It was always a very pleasant working atmosphere and I enjoyed the whole time with you guys! I loved climbing up mountains with you, racing down with sledges and running with you around the Rhein! And of course the helpful atmosphere when facing challenges in the lab. Therefore I want to thank especially Xingwei for being such a great lab-partner! I want to thank Martin and Andrea for the scientific discussions we had (and also not so scientific) which contributed a lot to this work. Further I want to thank Chris for his patience in showing me how to do proper DFT-calculations and trying to answer all my questions.

I like to thank my friends outside university who always make me smile and help me clearing my mind when needed.

For me the last 3.5 years have been an exciting journey. And I am glad I could share all the up's and down's with Matthias. Especially during the downs you really were my tailwind and support. But most important you made the up's unforgettable and I am looking forward to chase the wind with you in future together. I could not wish for a better "life-buddy".

C Curriculum Vitae

Personal Data

PLACE AND DATE OF BIRTH: Hamburg, Germany — 27 Juni 1989

ADDRESS: Kanonengasse 18, 4051 Basel, Switzerland

Education

- FEBRUARY 2015 - PRESENT PhD in the group of Prof. Oliver S. Wenger
University of Basel, Switzerland
- OCTOBER 2012 - OCTOBER 2014 Master Studies in Chemistry
Georg August University Göttingen,
Germany
- OCTOBER 2009 - OCTOBER 2012 Bachelor Studies in Chemistry
Georg August University Göttingen,
Germany
- FEBRUARY 2004 - 2008 Academic High School Sophie-Barat Schule
Hamburg, Germany

Experience abroad

- OCTOBER 2013 - APRIL 2014 Stellenbosch University,
Stellenbosch, South Africa
Internship with Prof. van Otterlo

Awards and scholarships

- MARCH 2018 Winner of the poster prize at the *Koordinationschemiker Treffen 2018* Heidelberg, Germany awarded with 200 EUR Springer-publishing group voucher.
- DECEMBER 2017 Winner of the poster prize at the *Christmas Symposium*, Basel, Switzerland awarded with CHF 50
- AUGUST 2017 Winner of the 'Runners-Up poster prize' at the *Fall Meeting 2017* of the Swiss Chemical Society Bern, Switzerland awarded with CHF 200
- FEBRUARAY 2017 to NOVEMBER 2017 antelope@novartis, competitive career program for highly qualified female students of the University of Basel, Switzerland
- MAY 2017 Nomination for the *Teaching Excellence Award* in the categories: 'Dienst an der Lehre' and 'Modern Scholarship'
- OCTOBER 2013 to APRIL 2014 PROMOS scholarship, financed through the 'Deutscher Akademische Austauschdienst' supported through the Federal Ministry of Education and Research
- 2012 - 2013 Scholarship *Deutschlandstipendium*

Honorary offices

- SEPTEMBER 2015 to SEPTEMBER 2016 Vicepresident of the *Swiss Young Chemist Association*, A division of the Swiss Chemical Society
- MAY 2015 to OCTOBER 2017 University of Basel, Board member of the *PhD Chemistry Community*, Switzerland

Journal Articles

- [Sabine Malzkuhn](#), Oliver S. Wenger, *Coord. Chem. Rev.* **2018**, *359*, 52-56.
- Fabian Geist, Andrej Jackel, Peter Irmeler, Michael Linseis, [Sabine Malzkuhn](#), Martin Kuss-Petermann, Oliver S. Wenger, Rainer F. Winter, *Inorg. Chem.* **2017**, *56*, 914-930.

Other Articles

- Lorenzo Delarue Bizzini, [Sabine Malzkuhn](#), Cedric Stress, Diana Tahchieva, Mirjam Schreier, Serena Rigo, Andrea Pannwitz, and Linda Bannwart, *Chimia* **2017**, *71*, 246-247. Conference Report
- Andrea Pannwitz, Serena Rigo, Linda Bannwart, Lorenzo Bizzini, [Sabine Malzkuhn](#), Thomas Müntener, and Charlotte Laupheimer, *Chimia* **2016**, *70*, 295. Conference Report.

Contributions to conferences

- 08/2018: Electron Donor-Acceptor Interactions Gordon Research Conference Electron Flow: From the Molecular to the Global Scale, Newport-US, Poster.
Photoinduced long-range electron transfer across ortho-oligophenylenes
- 03/2018: Koordinations-Chemie Treffen KCT 2018, Heidelberg-D, Poster.
Lichtinduzierter Elektronentransfer über ortho-Oligophenylenbrücken
- 12/2017: Christmas Symposium, Basel-CH, Poster.
Photoinduced Electron Transfer Across Oligo-ortho-phenylenes
- 08/2017: SCS Fall Meeting, Bern-CH, Poster.
Photoinduced Electron Transfer Across Oligo-ortho-phenylenes
- 07/2017: ISPPCC Oxford-UK, Poster.
Photoinduced Electron Transfer Across Oligo-ortho-phenylenes

Oral presentations

- 09/2018: Short Talk at the SCS Fallmeeting, Lausanne-CH
Photoinduced Long-Range Electron Transfer Across ortho-oligo-Phenylenes
- 05/2018: Research Seminar of the PhD Chemistry Community, Basel-CH